Three dimensional water quality modeling in a shallow lake with complex morphometry; implications for coolwater fish habitat under changing climate

A DISSERTATION
SUBMITTED TO THE FACULTY OF THE GRADUATE SCHOOL
OF THE UNIVERSITY OF MINNESOTA
BY

Shahram Missaghi

IN PARTIAL FULFILLMENT OF THE REQUIREMENTS
FOR THE DEGREE OF
DOCTOR OF PHILOSOPHY

Advisers:
Prof. Miki Hondzo
Dr. Lorin Hatch

July 2014

ACKNOWLEDGEMENTS

First, I am truly grateful to my adviser Professor Miki Hondzo for his continuous guidance, support and motivation. Thank you for giving me the confidence to complete my thesis and for the time so generously spent meeting with me and answering questions. I would like to thank my co-adviser Dr. Lorin Hatch, who first opened the door for me to have this great adventure and who was always encouraging. I also thank my committee: Professor James B. Cotner for allowing me the use of his laboratory, his guidance, and enjoyable conversations; Professor Raymond Newman for his support and making the time to listen and review my ideas; and Professor Heinz Stefan for his continuous support and kindness and for letting me share my work with his research group.

I am grateful to the people at the St. Anthony Fall Laboratory who make the lab such a great place to research, study and work. The Center for Water Research (Perth, AU) for providing the computer models ELCOM and CAEDYM, and hosting me twice at their center; the University of Minnesota Water Resources Center and Butler Jessen Water Resources Award for providing invaluable travel funds; The Minnehaha Creek Watershed District for providing the water quality data; The Minnesota Supercomputer Institute for providing the use of their computing services and technical assistance; and my colleagues and supervisors at the University of Minnesota Extension Water Resources who put up with my mysterious schedule and continuously encouraged me.

My parents, family, and friends all supported me-thank you Peyman. I am lucky that Samira, Shaghayegh, Kian, Eddie, Tajalli, and Amir have been and continue to be my unwavering army of support, source of motivations, editors, spell checkers, and my guides to stay the course. And finally I want to acknowledge my wife Michele whose contagious happiness and smile made it all possible, and watching her paint made the long days fun.

Dedication

To Naim, Nilufar, and our future grandchildren.

ABSTRACT

Morphologically complex lakes usually have a significant water quality heterogeneity and hydrodynamic gradients that require a three dimensional (3D) model to accurately capture their temporal and spatial dynamics. The objectives of this research were to evaluate and apply a 3D coupled hydrodynamic and ecological model to a morphologically complex lake and to investigate the effects of a changing climate on the lake ecosystem. The research was conducted in a series of four separate studies including modeling investigations and laboratory experiments. First, a 3D hydrodynamic model (ELCOM) coupled with an ecological model (CAEDYM) was applied to three bays of the morphologically complex Lake Minnetonka, MN, to simulate water temperature, dissolved oxygen, total phosphorus, and algal concentrations. The 3D model was calibrated and validated in two different years, and model results compared well with extensive field data. Lake hydrodynamic and ecological processes were discovered to be sensitive to mixing due to inflow and wind variability over seasonal stratification. In the second study, two sensitivity and uncertainty analysis methods were applied to the model to evaluate uncertainties in the model predictions. The contributions of predicted water temperature, dissolved oxygen, total phosphorus, and algal biomass contributed 3, 13, 26, and 58% of total model output variance, respectively. A laboratory experiment was conducted to measure the influence of fluid motion on growth and vertical distribution of *Microcystis* in a Plankton Tower bioreactor. The laboratory results indicated that a depth-averaged energy dissipation rate in the range from 3×10^{-7} to 3×10^{-6} m^2 s^{-3} facilitated *Microcystis* growth. Fourth, the applied calibrated and validated 3D model revealed the influence of local meteorological and global climate conditions on key water quality parameters and fish habitat in 3 bays of Lake Minnetonka. The research was conducted by simulating the model and analyzing the model output results under three climate scenarios of historical normal (HN), future (FU), and future extreme (FE). Water temperature (T) and dissolved oxygen (DO) concentrations were used to investigate the temporal and spatial variability of fish habitat dynamics. The epilimnetic water temperature of the FU and FE climate scenarios were up to 4 °C warmer than the HN

scenario during ice-free seasons, stratification periods were predicated to expand up to 23% (46 days), and thermocline depth to increase 49% under the FE climate scenario. In all cases hypolimnion was mostly anoxic by June 15, but started by April 15, May 1, and May 15, under the three climate scenarios of HN, FU, and FE respectively. Under future scenarios the good growth, restricted growth and lethal coolwater fish habitats that were based on T and DO thresholds changed +16%, -18%, and +85% compared to the HN scenario. A modest change (8% of total lake volume) of good growth and restricted growth into lethal habitat separated the summer good growth coolwater fish habitat by over 3 weeks. The research brought out the need for a 3D analysis in capturing the significant water quality heterogeneities and the ecological hot spots in a morphologically complex lake.

TABLE OF CONTENTS

ACKNOWLEDGEMENTS…… i
ABSTRACT…… ii
TABLE OF CONTENTS…… iv
LIST OF TABLES…… vi
LIST OF FIGURES…… ix

1. CHAPTER 1: 1

1.1. RESEARCH SIGNIFICANCE 1
1.2. OBJECTIVES 5
1.3. OVERVIEW OF DISSERTATION 5

2. CHAPTER 2 8

2.1. INTRODUCTION 10
2.2. STUDY SITE 12
2.3. METHODS 13
2.3.1. Models Description 13
2.3.2. Model Setup 13
2.3.3. Data Sources 13
2.3.4. Model Simulations 16
2.4. RESULTS AND DISCUSSION 16
2.4.1. Calibration, Sensitivity Analysis and Corroboration 16
2.4.2. Model fit 18
2.4.3. Lake Water Elevation 19
2.4.4. Simulated and measured data 20
2.4.5. Temperature Profiles 22
2.4.6. Dissolved Oxygen Profiles 24
2.4.7. Total Phosphorus Concentrations 26
2.4.8. Chla Concentrations 27
2.5. EXAMPLE OF A 3D MODEL APPLICATION FOR LAKE MINNETONKA 28
2.6. CONCLUSIONS 36

3. CHAPTER 3 38

3.1. INTRODUCTION 40
3.2. MATERIALS AND METHODS 44
3.2.1. Analysis Framework and Setup 44
3.2.2. Model calibration and confirmation 44
3.2.3. Model sensitivity and uncertainty analyses 47
3.2.4. Mean Value First-Order Reliability (MFOR) method 49
3.2.5. The Mean Square Root (MSQR) method 50
3.3. RESULTS AND DISCUSSION 52
3.3.1. Influence of model parameters on model predicted variables 52

3.3.2. Model parameter ranking *59*
3.3.3. Contributions of model predicted variables to total variance *60*
3.3.4. Spatial and temporal visualization of model uncertainty *63*
3.4. CONCLUSIONS 66

4. CHAPTER 4 69

4.1. INTRODUCTION 70
4.2. MATERIALS AND METHODS 72
4.2.1. Species and cultivation *72*
4.2.2. The Plankton Tower bioreactor *73*
4.2.3. Laboratory measurements *76*
4.2.4. Calibration of fluorescence sensor *77*
4.2.5. Turbulence generation *78*
4.2.6. Turbulence measurements and Particle Image Velocimetry *79*
4.2.7. Statistical analysis *79*
4.3. RESULTS AND DISCUSSION 80
4.3.1. Cultures *80*
4.3.2. Turbulence characteristics *80*
4.3.3. Effects of fluid motion on Microcyctis growth rate *84*
4.3.4. Effects of fluid motion on Microcyctis vertical distribution *89*
4.4. CONCLUSIONS 94

5. CHAPTER 5 97

5.1. INTRODUCTION 98
5.2. METHODS 100
5.2.1. Study site *100*
5.2.2. Field data *100*
5.2.3. Historical and future climate scenarios *101*
5.2.4. Model description *104*
5.2.5. Model setup, calibration and validation *105*
5.2.6. Model simulations for past and future climate scenarios *105*
5.2.7. Fish habitat criteria *106*
5.3. RESULTS 106
5.3.1. Model simulations for past and future climate scenarios *106*
5.3.2. Fish habitat evaluation *112*
5.4. DISCUSSION 119
5.5. FISH HABITAT EVALUATION 122

Bibliography……125

LIST OF TABLES

Table 1. Major physical, chemical and biological characteristics of the three bays in the study area. …… 12

Table 2.2. A partial list of the model parameters used in the final sensitivity and uncertainty analysis with their symbols , units, number of samples (n), minimum (min), maximum (max), mean value (ave), standard deviations derived from literature review, and their assigned or best fit values (Val.) in the model. Abbreviations are: carbon (C), oxygen (O2), ammonium (NH4), filterable reactive phosphorus, FRP (PO4), dissolved oxygen (DO), phosphorus (P), labile (L), dissolved organic carbon (DOC), particulate organic matter (POM), dissolved organic phosphorus (DOP), and dissolved organic nitrogen (DON). ..…… 12

Table 2.3. The three types of coolwater fish habitats and their associated T (C^{o}) and DO (mgL-1) criteria. ..…… 31

Table 2.4. 3D and 1D analysis of GG, RG, and UI of seasonal (May 1-Sep. 30) coolwater fish habitats average values (V/Vt) for 2000 and 2005. …… 33

Table 4.1**.** Results from the experimental conditions in the Plankton Tower where *f* is the oscillating grid frequency, k_g is the algal growth rate, $k_{gcontrol}$ is the algal growth rate in the control tower (without fluid motion), ε is the rate of energy dissipation averaged over the depth of tower with oscillating grid setup, C_f is *Microcystis* cell concentration profile, and $\bar{C}_f / \bar{C}_{f0}$ is the dimensionless time-averaged cell concentration profile ($\bar{C}_f$) normalized by the their concentration close to the air-water interface in the experimental columns ($\bar{C}_{f0}$) with the coefficient of variation (CV) listed for each of the profiles ($\bar{C}_f / \bar{C}_{f0}$). For ANOVA results: MS is mean square with a degree of freedom of 1 at 95

% probability ($p<0.05$), and * indicates F value with statistically significant difference between the groups of C_f selected during the exponential growth period from the experimental turbulent and their corresponding control conditions. …… 86

Table 5.1. The set of monthly Change Fields applied to the meteorological data of the normal climate and the extreme climate year within the climate normal period (1981-2010) to create the future and future extreme meteorological climate scenarios. ……. 102

Table 5.2. Simulated monthly averaged thermocline depth (m) under historical normal (HN), future (FU), and future extreme (FE) climate scenarios. ……..…… 111

Table 5.3. The annual total (percent of the lake volume, %) of good growth, restricted growth, and lethal fish habitats evaluated under simulated historical normal , future, and future extreme climate scenarios in the study area. …….....…… 113

LIST OF FIGURES

Fig. 1.1. Map of Lake Minnetonka and the study area (circled), including West Upper Bay (WB), Cooks Bay (CB), Priest Bay (PB), Halsted Bay (HB), Six Mile Creek (SC), and Langdon Lake Creek (LC). The water quality heterogeneity of the lake is shown by the 10-yr (1999–2009) average of water quality indicators (pie charts) for some of the bays. Water quality indicators are from clear water (blue/white) with total phosphorus (TP) <23 mg L−1, algal biomass (Chla) <10 mg L−1, and Secchi disk (clarity) >3 m, to poor water quality (green/gray) with TP >152 mg L−1, Chla >77 mg L−1, and clarity <0.7 m; therefore, the greater the area of the blue/white the clearer the water; and b) predicted 2095 summer (brown) and winter (blue) geographical climate shift for State of Minnesota, USA. ……... 4

Fig. 2.2. Year 2000 metrological Data. ……...15

Fig. 2.3. Simulated (lines) and field data for lake water elevations above mean sea water level for year 2000 (solid) and 2005 (blank), lake runout elevation (dashed line) and average lake discharge (Q_{ave}). ..……... 20

Fig. 2.4. Comparison of selected days of simulated (line) and observed water temperature (triangle) and dissolved oxygen (circles) at West Upper Bay in 2000. …... 21

Fig. 2.5. Comparison of 2000 simulated (lines) and measured a) epilimnion and b) hypolimnion TP concentration and composite top 2 meter c) Chl*a*. ……... 22

Fig. 2.6. Comparison of West Upper Bay (WU), Cooks Bay (CB) and Halsted Bay (HB) simulated and data for a) T, b) DO, c) TP, and d) Chl*a* and their respective R^2 values for the years 2000 (calibration) and 2005 (corroboration). ……... 23

Fig. 2.7. Qualitative comparison of short term duration variations of DO concentration (with few points of interest marked by solid circles) as simulated by (a) model and (b) measured by RUSS unit at Halsted Bay in a two month period in 2000. ……... 25

Fig. 2.8. Range (max-min) of simulated surface water temperature at each model output (4 hrs.) over the entire simulation period (2000) with the average seasonal range shown in dash line and the expanded map illustrating the range (6.5 ºC) of surface water temperature at 7/23/00 13:00, model output. ……... 29

Fig. 2.9. Comparison of 3D and 1D analysis of the three coolwater fish habitats: a) GG, b) RG, and c) UI for all depth layers over time with inset showing the magnitude of short duration variations and d) is the maximum (abs) of the difference between 3D and 1D analysis of GG, RG, and UI at each depth layer and output. ……... 32

Fig. 2.10. Range (max-min) of simulated T and DO values at each depth layer and model output over the entire year 2000 season, with a lake volume plot showing the accumulative volume at each depth. ……..……... 35

Fig. 2.11. Contour plots of simulated T and DO, at WB showing their values and patterns for both year 2000 and 2005. ……... 35

Fig. 3.1. Percent of fraction of variance (FOV) contributed by the top ranking parameters within each of the four temperature (T), dissolved oxygen (DO), total phosphorus (TP), and algal biomass (Chla) model outputs as analyzed by a) Mean Value First-Order Reliability, and b) the Mean Square Root methods. ……... 52

Fig. 3.2. Simulated time series of dissolved oxygen (DO Bottom) and total phosphorus (TP Bottom) at 1 m above the sediment bed, and TP at 1 m below the water surface (TP Surface). ……... 56

Fig. 3.3. Model parameter ranking measured by the fraction of variance (FOV) contribution by each parameter (values in parenthesis) and evaluated by the Mean Value First-Order Reliability (dark line) and the Mean Square Root (gray line) methods…….60

Fig. 3.4. Comparison of the fraction of variance (FOV) contributed by each model predicted variable of temperature (T), dissolved oxygen (DO), total phosphorus (TP), and algal biomass (Chla) to the total model variance as derived by Mean Square Root (MSQR) method and model calibration process for West Upper Bay location…….61

Fig. 3.5. Contributions of model predicted variables to total model variance measured by percent fraction of variance (FOV) of each output (T, DO, TP, and Chla) to the total model variance. The contributions of model parameters within each of the model output variables also are shown. ……..……... 62

Fig. 3.6. Contour plots of spatial and temporal variabilities: a) average model output (T, TP, Chla), b) standard deviation (σ) of the model outputs from the sensitivity analysis of the 29 model parameters; and c) coefficient of variation (σ/average). ……... 64

Fig. 3.7. Comparison of the stream flow (m^3s^{-1}) with the coefficient of variation (COV) of the model output temperature (T), dissolved oxygen (DO), total phosphorus (TP), and algal biomass (Chla) in a) upper, b) middle, and c) bottom water layers where multiplication factors for the right hand side Y axis are (0.00125, 0.033, 0.05, 0.2), (0.0033, 1, 0.05, 0.1), and (0.0009, --, 0.02, 0.1), respectively. ..……... 66

Fig. 4.1. Microscopic images of *Microcystis aeruginosa* a) large colonies, b)-c) cell aggregates, and d) unicellular culture (cell diameter about ~5 µm) that was used for the experiments. ……..……... 73

Fig. 4.2. Photograph of the experimental bioreactor (Plankton Tower; 1.5 m x 0.6 m x 0.2 m) with two independent sealed columns that were used for algal growth experiments with one column used as (a) control column without fluid motion and b) turbulent column with fluid motion generated by the oscillating grid. Location of the oscillating grid along with the horizontal (x) and vertical (z) axes are also shown. ……..……... 75

Fig. 4.3. Measurements by the fluorescence sensor, Cyclops-7 of a series of a) known *Microcystis* sample concentrations that were evaluated against the measured Chl-a (diamonds, μ L^{-1}; $r^2 = 0.95$), and haemocytometer cell counts (triangle, cellsmL^{-1}; $r^2 = 0.99$) for sensor calibrations, and b) of 15 random *Microcystis* samples evaluated for sensor verification ($r^2 = 0.99$) against cell counts of the same samples obtained by using haemocytometer (cells mL^{-1}). ……...78

Fig. 4.4. Data from 2-D Particle Image Velocimetry were used to estimate a) energy dissipation rate, ε (m^2s^{-3}), contours at 2 Hz oscillating grid frequency, and b) the instantaneous 2-D velocity vectors over the marked square area (40 x 40 mm). ……..81

Fig. 4.5. Averaged energy dissipation rate, ε, profiles created by using the data generated from the 2-D Particle Image Velocimetry for 1 Hz (square), 1.5 Hz (triangle), and 2 Hz (circle) oscillating grid frequency experimental conditions. The solid lines represent the estimated ε using the power-law equation (3). ……... 83

Fig.4.6. Examples of the *Microcystis* cell concentration profiles (C_f) measured in the Plankton Tower over eight days with *t* as time, *n* as the day of sampling from the start of the experiment. a) control column (without fluid motion), b) column with oscillating grid at f = 2 Hz, and c) the vertical distribution of energy dissipation (ε) in the column with oscillating grid at f = 2 Hz. The amplitudes of the oscillating grid and stroke distance (S) within the column with oscillating grid are also shown in b). ……... 85

Fig.4.7. Semi-logarithmic plots of normalized concentrations of the *Microcystis* for the corresponding control column (f = 0, filled symbols) and the column with oscillating grid at f = 1, 1.5, 2, and 3 Hz, with $\langle C_f \rangle$ as the depth-averaged concentration and $\langle C_{\mathrm{fo}} \rangle$ as the depth-averaged concentration at the beginning (t=0) of each experiment. …… 87

Fig. 4.8. Normalized *Microcystis* growth rates, $k_g / k_{gcontrol}$ at the corresponding depth-averaged energy dissipation rates, $\langle \varepsilon \rangle$ $(m^2 s^{-3})$, in the experimental column with oscillating grid at f = 0.5, 1, 1.5, 2, and 3 Hz. The graph depicts three growth zones including the non-facilitated, facilitated, and reduced growth regions. ……..…… 89

Fig. 4.9. *Microcystis* vertical distribution of time-averaged profile concentrations ($\bar{C}_f$) from the exponential growth periods and normalized by the concentration at the initial depth ($\bar{C}_{f0}$, with z= 0) in the control column where f = 0 Hz, and in the experimental turbulent column with oscillating grid at f = 0.5, 1, 1.5, 2, and 3 Hz. …… 91

Fig. 4.10. Normalized *Microcystis* time-averaged vertical concentrations ($\bar{C}_f / \bar{C}_{f0}$) along with their depth-averaged ($\langle \mathrm{X} \rangle$, filled square) and standard deviation (σ), and the range of each $\langle \mathrm{X} \rangle \pm \sigma$ (offset bars) in the control column where f = 0 Hz, and in the experimental turbulent column with the oscillating grid operating at f = 0.5, 1, 1.5, 2, and 3 Hz. ……..……... 92

Fig. 4.11. Coefficient of variation, $\mathrm{CV} = \sigma / \langle \mathrm{X} \rangle$ where $\langle \mathrm{X} \rangle$ is depth-averaged and σ standard deviation of normalized *Microcystis* time-averaged vertical concentrations ($\bar{C}_f / \bar{C}_{f0}$), at the corresponding depth-averaged energy dissipation rates, $\langle \varepsilon \rangle$ $(m^2 s^{-3})$, in

the control column where f = 0 Hz, and in the experimental turbulent column with the oscillating grid operating at f = 0.5, 1, 1.5, 2, and 3 Hz. ……... 94

Figure 5.1. Average annual air temperature (T_a) and precipitation (P) for a) measured values for the 30 years of climate normals period (1981-2010), with intersection of axes representing the climate normals (T_a = 7.78 °C and P = 0.78 m); b) measured and MIROC3.2 bias corrected modeled historical and future scenarios; and c) the 50th percentile of annual T_a and P averages with year 2000 and 2005 (crosshair) shown as the nearest (normal) and the farthest (extreme) years from the center. Dash lines in c) show the year 2005 percentile. ……..……... 104

Fig. 5.2. Examples of measured and projected (using change fields) air temperature, wind speed, and precipitation time series used for the prediction of ecological changes in the study area as historical normal (HN, black), future (FU, dark gray), and future extreme (FE, light gray) climate scenarios. ……... 107

Fig. 5.3. Comparison of lake water levels simulated under historical normal, historical extreme (2005), future, and future extreme climate scenarios for the study area with their monthly total precipitation shown on top. ……... 108

Fig. 5.4. Comparison of modeled water temperature (°C) and dissolved oxygen (mgL^{-1}) in the study area under a) historical normal , b) future, and c) future extreme climate scenarios. Horizontal and vertical axes of contour plots represent time and depth (m), receptively.
…….……... 109

Fig. 5.5. Comparison of modeled seasonally averaged of water temperature (°C) and dissolved oxygen (mgL^{-1}) profiles at West Upper Bay of the study area under historical normal , future, and future extreme climate scenarios. …….……... 110

Fig. 5.6. Comparison of the surface T, bottom T, and start (circles), end (squares), and duration (vertical lines) of stratification at West Upper Bay modeled under historical normal , future, and future extreme climate scenarios. ……... 112

Fig. 5.7. Percentage of the total lake volume for a) good growth, b) restricted growth, and c) lethal fish habitats based on predicted model variables that are averaged daily, weekly, and monthly modeled under simulated historical normal , future, and future extreme climate scenarios in Lake Minnetonka. ……...114

Fig. 5.8. Hypsographic curves, showing the percentage of total lake volume (x axis) over depth (y axis) for the averaged good growth, restricted growth, and lethal fish habitats under simulated a) historical normal , b) future, and c) future extreme climate scenarios, with the insets showing the changes in percentage points from the historical normal. ….115

Fig. 5.9. Contour plots of good growth (GG), restricted growth (RG), and lethal (L) fish habitats based on the predicted model variables averaged weekly under simulated a) historical normal , b) future, and c) future extreme climate scenarios at the deepest point (West Upper Bay) of the study area. ……..……...117

Fig. 5.10. Comparison of the areas of the study area with good growth (black), restricted growth (gray), and lethal (light gray) coolwater fish habitats based on the predicted model variables averaged weekly for the top 5 meters of water column under simulated a) historical normal, b) future, and c) future extreme scenarios covering the entire study area with all horizontal and vertical axes as distance in km. ……... 118

CHAPTER 1:

Introduction

1.1. Research significance

Water quality models are essential tools that enable water resource researchers to study and extend the understanding of physical, chemical, and biological processes of the ecological systems (Li and Wu, 2006; Gal et al, 2009). These models enhance the interpretation of available data, and allow evaluation of potential impacts of various lake restoration alternatives (Louks and Beek, 2005). Water quality models play an increasingly larger role in water resources management (Erturk, 2010) and the results of such models are commonly integrated into a decision support system to meet water quality regulatory requirements (Lung, 2001; Romero et al., 2006; Trolle et al., 2008). Water quality and ecological models also help to form environmental policies and create consensus in managing water resources.

Water quality models could be classified, based on their dimensionality, as well mix box models considered as zero-dimension, horizontal or vertical mixing as one-dimensional (1D), lateral and longitudinal with average depth as two-dimensional (2D), and a three-dimensional (3D) models. Hydrodynamic and ecological processes of natural water bodies and reservoirs may well be captured by 1D models (Riley and Stefan, 1988; Imberger et al., 1978). However, the interactions among aquatic physical, chemical, and biological processes are nonlinear and dynamic, and far from equilibrium (Hondzo and Warnaars, 2008; Leon et al., 2011). Additionally, the impact of interactions of lake morphometry and hydrodynamics on ecological processes and their complexity is further expanded in morphologically complex lake ecosystems (Kalff, 2002; Wetzel, 2001). For example, the water quality parameters and the geochemical cycles of the morphologically complex aquatic ecosystems are influenced by spatial and temporal hydrodynamic processes that are affected by multiple flow dynamics, morphometry, and metrological

parameters that increase water quality heterogeneity. Aquatic systems reflect the effect of 3D hydrodynamic processes and therefore 3D hydrodynamic and water quality models are needed to capture spatial and temporal biogeochemical distributions within these complex systems. 3D models provide resolutions that capture individual morphological features such as bays and intra-lake circulations (Hodges et al, 2000).

Lake Minnetonka (60 km^2; 44◦54' N; 93◦41' W) with its 23 bays, 200 km of shoreline, and 24 km^2 littoral zone, is considered a very morphologically complex lake (Wetzel, 2001). The lake has been regularly sampled for various water quality parameters since 1968, with greater intensity since 2000. The available data facilitates model calibration and verification which makes the lake a good candidate for water quality modeling investigation. The lake has strong water quality heterogeneity with each bay having a specific water quality characteristic or grade as depicted in Fig. 1.1a. The grade of each bay is based on the average grades of three water quality variables of total phosphorus (mg L^{-1}), algae biomass (mg L^{-1}), and water clarity (Secchi disk, m) (MCWD, 2000–2008). Temperature measurements of surface water (top 1 m) taken in the month of June (1999-2009) showed an averaged range (maximum–minimum) of 5°C throughout the surface of the lake.

The rapidly advancing computing power and improvements in 3D water quality models in the past two decades have provided researchers opportunites to use 3D models of lakes and reservoirs. However, the sensitivity and uncertainty methods of these complex 3D models have not advanced at the same pace (Ravalico et al., 2005). To have confidence in the results, models need to be calibrated, validated, and their predicted outputs investigated by sensitivity and uncertainty analyses (Arhonditsis and Brett, 2004; Saltelli et al., 2006; Salacinska et al., 2009).

Well documented, transparent sensitivity and uncertainty analyses minimize skepticism and raise confidence among scientists and the public for the use of complex 3D

ecological models (Radcliffe et al., 2009). There is a need for more flexible sensitivity and uncertainty analyses methods for 3D ecological models.

The physical processes in 3D hydrodynamic models are generally well defined and tend to require minimal calibrations. On the other hand, the biological processes in water quality models are less defined and it is more difficult to simulate their field conditions. For example, algae biomass model predicted outputs usually contribute the largest degree of model output variance of the total model output variance and uncertainty. The influence of hydrodynamics on algae, such as lateral patchiness, vertical distributions, temporal variations (blooming), and the evolving understanding of algae biological dynamics each contribute to the uncertainty of algae predicted model output (Hipsey et al., 2006; Reynolds, 2006). In Lake Minnetonka, seasonal algae succession begins with diatoms during the Spring bloom followed by a Cryptophytes and Chlorophytes in early summer and then fully dominated by Cynobacteria for the rest of the season (PhycoTech, 2007). A greater understanding of the interaction of the hydrodynamic processes with algae and defining their regionally suited biological model parameters are needed.

Against the background of uncertainty, climate change has added more uncertainty to water quality modeling by altering the frame of reference used to evaluate the water resources (Fig. 1.1b) (Kling et al., 2003). Researching the interactions and influences of anthropogenic pollution, ecological processes, and complex morphometry, climate change requires a vast amount and diverse set of data (Argent and Houghton, 2001). Furthermore, any water quality research must adjust simultaneously to these various factors and drivers of ecosystem in temporal and spatial small scales that are useful to investigators (Power et al., 2005). Models can be used to synthesize and integrate the information needed and have been the main tool in analyzing the impact of climate change on lake ecosystems (Milly et al., 2008; Menshutkin, Rukhovets & Filatov, 2014). Three dimensional models, in particular, have been used in climate change assessment of lakes (Cline, Bennington & Kitchell, 2013). Three dimensional computer models have

the feature of reproducing the ecological processes of the lake in fine temporal and spatial scales that can enhance our understanding of the interactive feedbacks among physical, chemical, and biological processes in morphologically complex lakes.

Fig. 1.1. Map of Lake Minnetonka and the study area (circled), including West Upper Bay (WB), Cooks Bay (CB), Priest Bay (PB), Halsted Bay (HB), Six Mile Creek (SC), and Langdon Lake Creek (LC). The water quality heterogeneity of the lake is shown by the 10-yr (1999–2009) average of water quality indicators (pie charts) for some of the bays. Water quality indicators are from clear water (blue) with total phosphorus (TP) <23 mg L−1, algal biomass (Chla) <10 mg L−1, and Secchi disk (clarity) >3 m, to poor water quality (green) with TP >152 mg L−1, Chla >77 mg L−1, and clarity <0.7 m; therefore, the greater the area of the blue/white the clearer the water; and b) predicted 2095 summer (red) and winter (blue) geographical climate shift for State of Minnesota, USA.

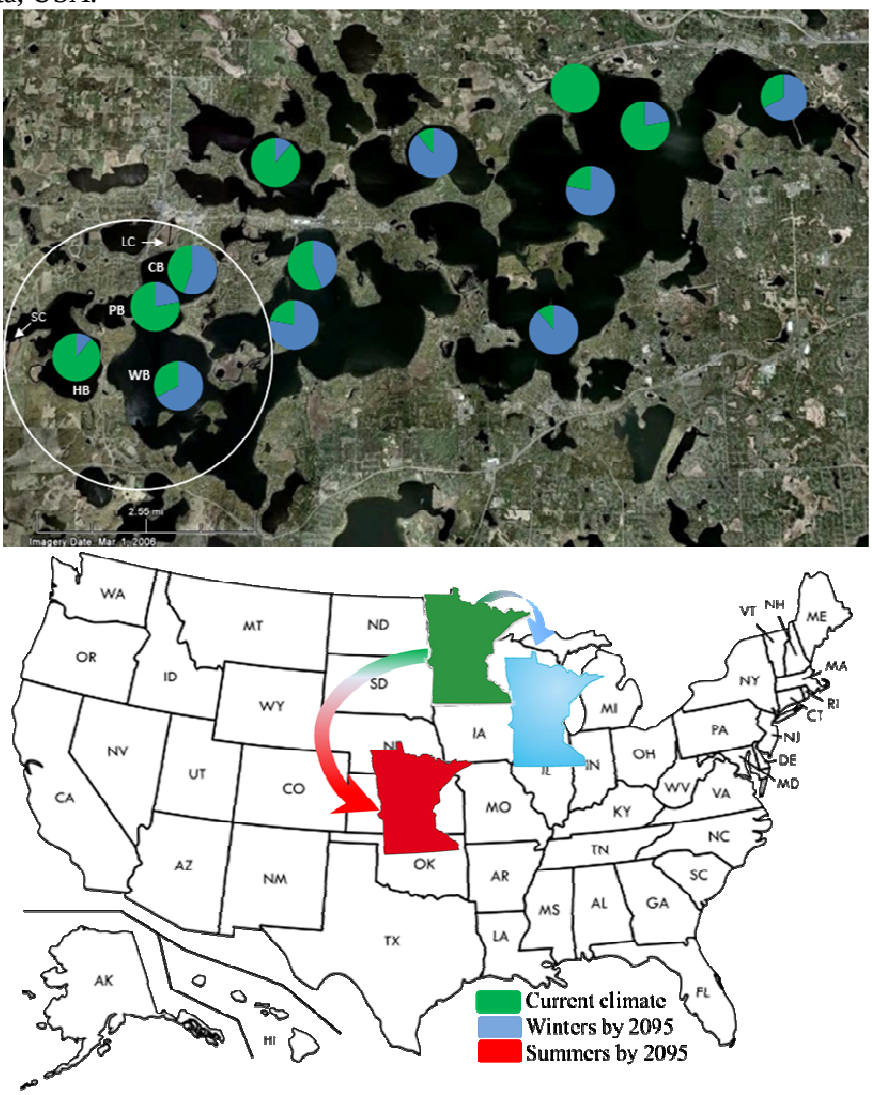

1.2. Objectives

The purpose of this research was to evaluate and apply a 3D coupled hydrodynamic and ecological model to a morphologically complex lake and to investigate the effects of a changing climate on the lake ecosystem. The research framework and approach can be summarized by four objectives:

1. Evaluation and application of a 3D model to accurately capture the spatial and temporal variability of lake water quality parameters in a shallow lake with complex morphometry;
2. Conduct a detailed sensitivity and uncertainty analysis to evaluate uncertainties in the model predictions;
3. Quantify the influence of fluid motion on spatial distribution and growth of *Microcystis* under controlled laboratory conditions, and
4. Evaluate the key water quality parameters that ultimately determine fish habitat under changing climate.

Each of the above objectives was independently researched and investigated and forms a chapter (2-5) of this thesis. Each study has been prepared as a separate manuscript that is published or prepared for publication in a specific peer-reviewed journal.

1.3. Overview of dissertation

Along with the introduction (Chapter 1), this thesis consists of four chapters that each have been prepared as independent manuscripts and submitted for publication in peer-reviewed journals. Each chapter is, therefore, in the style of a manuscript published or prepared for the specific journal. The four chapters (2-5) provide research methods and results of the investigation on the evaluation and application of the 3D model and the implications for Lake Minnetonka under a changing climate. The lake's measured data reflect a system with large spatial and temporal water quality and fish habitat heterogeneities which necessitated the use of 3D models to capture its biogeochemical changes and dynamics.

Input data sources, study area, and model description, along with model setup, configuration, parameterization, simulations, calibration, validatation, and model performance and fit are provided in Chapter 2. A strong agreement between simulated and measured lake water levels and seasonal evaporation flux suggested an accurate water balance. Comparison of 12 biweekly measured field data from three different locations within the study area against the model results agreed very well. The simulated water temperature (T) and dissolved oxygen (DO) profile concentrations compared well with that of the measured profiles. The model proved robust enough to capture the system's physical, chemical, and biological seasonal and short term (intera-seasonal) spatial and temporal variations. However, simulated algae biomass concentrations were moderately in agreement with the measured data. The modeling efforts brought out the need for a greater understanding of biological processes in the ecosystem and the need for optimization of the biological module of the model.

Chapter 3 lays out a detailed process of model parameter estimation, calibrations, and the application of two model sensitivity and uncertainty methods. The top ten influential model parameters in the simulation of the model output variables were ranked by two independent methods. The study also focused on the 3D spatial and temporal variabilities of model predictions. Model performance was most sensitive in the epilimnion and thermocline to changes in parameter values with the largest sensitivity during the streamflow events. The model outputs of T, dissolved oxygen, total phosphorus, and algae biomass contributed 3, 13, 26, and 58% to the total model variance, respectively. The analysis reiterated the need for a greater understanding of biological model parameters.

Consequently, Chapter 4 is focused on investigating the factors influencing the spatial and temporal variabilities of *Microcystis* in order to enhance the model prediction and ultimately the management of aquatic ecosystems. The study explored quantification of the influence of fluid motion on spatial distribution and growth of *Microcystis* under

controlled laboratory conditions in a Plankton Tower bioreactor. The effects of fluid motion on *Microcystis* vertical distribution and cell growth were investigated under different fluid motion (turbulence). The generated turbulence levels were measured by 2D particle image velocimetry. The results indicated that a depth-averaged energy dissipation rate in the range of 3×10^{-7} to 3×10^{-6} m^2s^{-3} generated the largest values for both vertical distribution and cell growth of *Microcystis.* The findings were quantified by fluid flow property-energy dissipation rate-that is predictable in most computational models for water quality modeling in lakes. The integration of influence of fluid motion on growth and distribution of *Microcystis* in water quality models has the potential to significantly enhance the model algae predictability.

In Chapter 5, the well calibrated and validated model is ultimately applied to test the specific and combined changes of the metrological forcing data on key water quality parameters and cool-water fish habitat under one historical and two future climatic scenarios. The climate scenarios were based on the most recent climate normal and the application of Change Fields to predict future scenarios. The modeled climate scenarios presented three hydrologically and climatically distinct years. Lake thermal structure under the future scenarios reflected the influences of a warmer air temperature that along with decreased dissolved oxygen concentration patterns controlled the boundaries of fish habitats. The lethal cool-water fish habitat had a modest increase (8 percentage points of total lake volume from historical normal) under the warmest future scenario. However, the small increase had a significant spatial and temporal pattern that squeezed feasible good growth fish habitats to the point of separation in July for over 3 weeks. Results showed that using 3D water quality model can capture important temporal and spatial consequences of changes in key water quality parameters. The findings reported in Chapters 2-5 have advanced the understanding of the interactions of hydrodynamics and ecological processes of a morphologically complex lake under a changing climate.

CHAPTER 2

Evaluation and Application of a Three-Dimensional Water Quality Model in a Shallow Lake with Complex Morphometry

Published as: Missaghi, S. and Hondzo, M., 2010. Evaluation and application of a three-dimensional water quality model in a shallow lake with complex morphometry. Ecol. Model. 221, 1512-1525.

Fundamental hydrodynamic and ecological processes of a lake or reservoir could be adequately depicted by one-dimensional (1D) numerical simulation models. Whereas, lakes with significant horizontal water quality and hydrodynamic gradients due to their complex morphometry, inflow or water level fluctuations require a three-dimensional (3D) hydrodynamics and ecological analyses to accurately simulate their temporal and spatial dynamics. In this study, we applied a 3D hydrodynamic model (ELCOM) coupled with an ecological model (CAEDYM) to simulate water quality parameters in three bays of the morphologically complex Lake Minnetonka. A considerable effort was made in setting up the model and a systematic parameterization approach was adopted to estimate the value of parameters based on their published values. Model calibration covered the entire length of the simulation periods from March 29 to Oct 20, 2000. Sensitivity analysis identified the top parameters with the largest contributions to the sensitivity of model results. The model was next verified with the same set up and parameter values for the period of April 25 to Oct 10, 2005 against field data. Spatial and temporal dynamics were well simulated and model output results of water temperature (T), dissolved oxygen (DO), total phosphorus (TP) and one group of algae (*Cyanobacteria*) represented as chlorophyll *a* (Chl*a*) compared well with an extensive field data in the bays. The results show that the use of the model along with an accurate bathymetry, a systematic calibration and corroboration (verification) process will help to analyze the hydrodynamics and geochemical processes of the morphologically complex

Lake Minnetonka. An example of an ecological application of the model for Lake Minnetonka is presented by examining the effect of spatial heterogeneity on coolwater fish habitat analysis in 3D and under a scenario where horizontal spatial heterogeneity was eliminated (1D). Both analyses captured seasonal fish habitat changes and the total seasonal averages differed moderately. However, the 1D analysis did not capture local and short duration variabilities and missed suitable fish habitat variations of as much as 20%. The experiment highlighted the need for a 3D analysis in depicting ecological hot spots such as unsuitable fish habitats in Lake Minnetonka.

2.1. Introduction

The continuous improvements in numerical water quality models and computer computing power have increased reliability and use of advanced ecological models. Ecological models extend the understanding of our systems, give meaning to our observations and enhance the interpretation of available data. The results of such models are also commonly integrated into a decision support system to meet regulatory requirements (Lung, 2001; Romero et al. 2006; Trolle et al., 2008). One approach of distinguishing ecological models, specially the water quality models, is based on their dimensionality (Henderson-Seller, 1989). With well mix box models considered as zero-dimension, horizontal or vertical mixing as one-dimensional (1D), lateral and longitudinal with average depth as two-dimensional (2D) and a system discretisized into a three- dimensional mesh with finite cells allowing for temporal and spatial analysis as three- dimensional (3D) models. Hydrodynamic and ecological processes for a number of natural water bodies and reservoirs have been well captured by 1D models such as MINLAKE (Riley and Stefan, 1988) or DYRESM (Imberger et al., 1978).
However, the impact of interaction of lake morphometry and hydrodynamics on ecological processes (Kalff, 2002; Wetzel, 2001) seems to be magnified in morphologically complex lakes. Morphometry may lead to regions of different water quality levels within a lake. This water quality heterogeneity can be further increased by the process of urban eutrophication where different streams transport varying nutrient loads into a lake reflecting the landscape and land use of their individual watersheds (Wetzel, 2001). Total phosphorus and sediment concentrations, two of the nutrient loads' components, are considered strong lake water quality metrics and their impacts on water quality is well described (Wetzel, 2001; Brett and Benjamin, 2008; Gächter and Müller, 2003; Jones and Bachmann, 1976). However, the geochemical cycles of these parameters are influenced by spatial and temporal hydrodynamic processes that are affected by flow dynamics, morphometry, and metrological parameters. The geochemical cycles are also impacted by internal factors such as sediment composition, sediment oxygen demand (SOD), entrainment by benthic boundary layers (BBL) and

other transport mechanisms that can contribute significant nutrient loadings to their systems (Søndergaard et al., 2003; Hondzo and Haider, 2004; Marti and Imberger. 2008). Collectively, these factors increase both the large and the small localized scale changes that increase water quality heterogeneity. Aquatic systems reflect the effect of 3D hydrodynamics processes and therefore a 3D hydrodynamic model is needed to capture spatial and temporal biogeochemical distributions within these systems. 3D models provide resolutions that can capture individual morphological features such as bays and intra-lake circulations (Hodges et al, 2000).

The cultural eutrophication impact on Lake Minnetonka from developments in its watershed (319 km2) has been typical of the midwestern Unites States urbanization pattern (Ramstack et al., 2003; Murchie, 1985). The hotels and resorts constructed on the lake in late 1860's were replaced by large homes and estates in the 1890's and by the 1930's most of the 175 km of the lake's shoreline was well developed followed by an increased regional urbanization after 1940's (Stein, 1978). The lake is composed of so many bays and coves that Wetzel (2001) classifies Lake Minnetonka as an extremely complex lake. Because of its complex morphometry, Lake Minnetonka has been described as a lake with three main water quality and sediment types (Murchie, 1984), 12 small and 3 large basins (Megard 1972), 16 discrete basins (Engstrom and Swain, 1986), or by 23 named bays (Hennepin, 2003). Nonetheless lake Minnetonka is currently described by 26 bays (MCWD, 2007). The lake's watershed has a precipitation average of 0.75 meter, delivering 10.8 tons (2006) of TP (MCWD, 2008) into the lake through five creeks. The lake discharges at the eastern end through a controlled outlet dam structure. The upland watershed hydrology of the lake and its discharge regime have been studied (Army Corps, 2008); however, a whole lake analysis including its internal loading, and intra lake water circulation has been lacking due to the lake's complex morphology (MCWD, 2003; MCWD, 2008). Review of water quality data collected since 1968 show areas of various degrees of water quality degradation within the lake.

The purpose of this study was to corroborate (validate) the 3D hydrodynamic model ELCOM coupled with an ecological model CAEDYM for sections of Lake Minnetonka (60 km^2), west of Minneapolis-St. Paul, MN, USA. Spatial water quality gradients and varying inflow loading distribution into Lake Minnetonka have created a mosaic of water quality areas within this morphologically complex lake. We demonstrate the application of a 3D hydrodynamic model with a detailed ecological model to accurately predict spatial and temporal variability of lake water temperature (T), dissolved oxygen (DO), total phosphorus (TP), and chlorophyll-a (Chla) concentrations in a shallow lake with complex morphometry. The results show that the lake hydrodynamic and ecological processes are sensitive to mixing due to inflow and wind variabilities over the seasonal stratification. Additionally, the results illustrate the need of 3D fish habitat ecological modeling where spatial heterogeneity and short duration temporal variations are preserved. In particular, the experiment highlighted the need for a 3D analysis in capturing ecological hot spots such as unsuitable fish habitats in Lake Minnetonka.

2.2. Study Site

West Upper Bay (WB), Cooks Bay (CB) and Halsted Bay (HB) were selected for model set-up and parameter calibrations (Fig. 1). CB is connected to HB through a smaller bay on the east and on the south end it opens into WB that leads into the lower bays of Lake Minnetonka. Six Mile Creek (SC), the largest surface water contributor to the lake, discharges into HB on the west and on the north, CB receives water from the small Langdon Lake Creek (LC). Basic physical, chemical, and biological characteristics are listed in Table 1.

Table 1. Major physical, chemical and biological characteristics of the three bays in the study area.

Bays	Area km^2	Max. Depth m.	Secchi Disk m	Chl*a* $\mu g\ L^{-1}$	TP $\mu g\ L^{-1}$
Cooks	1.465	13.1	1.6	15.3	34.1
Halsted	2.202	10	0.5	77.4	92.7
West Upper	3.557	25.6	1.8	13.1	30.6

2.3. Methods

2.3.1. Models Description

We used the 3D hydrodynamic model Estuary and Lake Computer Model (ELCOM) maintained by Centre for Water Research (CWR) of University of Western Australia. ELCOM uses hydrodynamic and thermodynamic models to simulate spatial and temporal water temperature and velocity distribution. ELCOM was dynamically coupled with Computational Aquatic Ecosystem Dynamics Model (CAEDYM), an ecological model, to simulate three dimensional biogeochemical processes. ELCOM and CAEDYM are well described by Hamilton and Schladow (1997) and Hodges (2000). Schematic representations of the modeled processes and summary of differential equations for nitrogen, phosphorous, dissolved oxygen and algal biomass in CAEDYM are also provided by Romero et al. (2004).

2.3.2. Model Setup

Lake Minnetonka topographical maps (LakeMaster, 2005) were used to manually discretize the study area (8.01 km^2) into 200 m surface grids with a uniform 0.5 m depth layer resolutions to create the 3D Cartesian mesh of computational cells used by ELCOM. Boundary conditions such as locations of tracer release, sampling stations, inflows, outflows and open water cells boundaries were identified in the bathymetry file. The time step was set to 120 seconds with output data recorded at every four hour intervals. Model output files were regularly monitored to insure that the model time step (temporal) and grid sizes (spatial) were adequately selected.

2.3.3. Data Sources

ELCOM-CAEDYM is driven by inputs from inflow, water quality parameters, initial conditions, and metrological or forcing data. An average stream flow was calculated based on the periodic stream flow data recorded. Stream field data including flow, T, DO, Chl*a*, TP and soluble reactive phosphorus (PO4) were used for inflow scalar values.

Streams were monitored biweekly at both Six Mile and Langdon Lake Creeks. No stream flows were detected and recorded for the simulation period (2000). However, an extensive hydrological study and modeling of the watershed (Army Corp, 2008) had predicted an average flow of 0.3 m^3s^{-1} in year 2000 for SC which was equivalent to some of the highest annual average flows since 1990. The large discrepancy between the modeled stream flow (0.3 m^3s^{-1}) and the recorded data (0.0 m^3s^{-1}) could not be explained and ultimately a stream flow with flow patterns matching the predicted output and with an averaged flow of 0.1 m^3s^{-1} was adopted. Stream water temperatures were estimated using available data from area streams and considering their stream water temperature patterns in a ten year period. Lake water quality records were provided by the Minnehaha Creek Watershed District organization. Samples were from three stations located at the deepest point of HB (10 m), CB (8.5 m), and WU (24 m). Each station had been sampled biweekly for T, DO, conductivity, and pH profiles (1 m interval), surface and bottom TP, PO4, total nitrogen and a composite top two meter sample for Chl*a*. Meteorological data (Fig. 2.2) included hourly readings of air temperature, relative humidity, atmospheric pressure, cloud cover, wind speed, and wind direction which were obtained from the Flying Cloud Airport (44 50 N; 93 27 W) about 14.5 km SE of the lake. Precipitation data were obtained from Mounds weather station (44 56 N; 93 39 W) 0.5 km NE of the study area. Hourly solar radiation was obtained from Rosemount Experimental Station (44 45 N; 93 04 W) 45 km SE of the lake. Air Temperature, relative humidity, wind direction and short wave solar radiations units required no unit conversions. No factors were used on any of the meteorological data and none of the values were changed or modified. Except all air temperatures of less than 7 C^o in the month of April were kept at 7 C^o to increase model stability.

Fig. 2.2. Year 2000 metrological Data

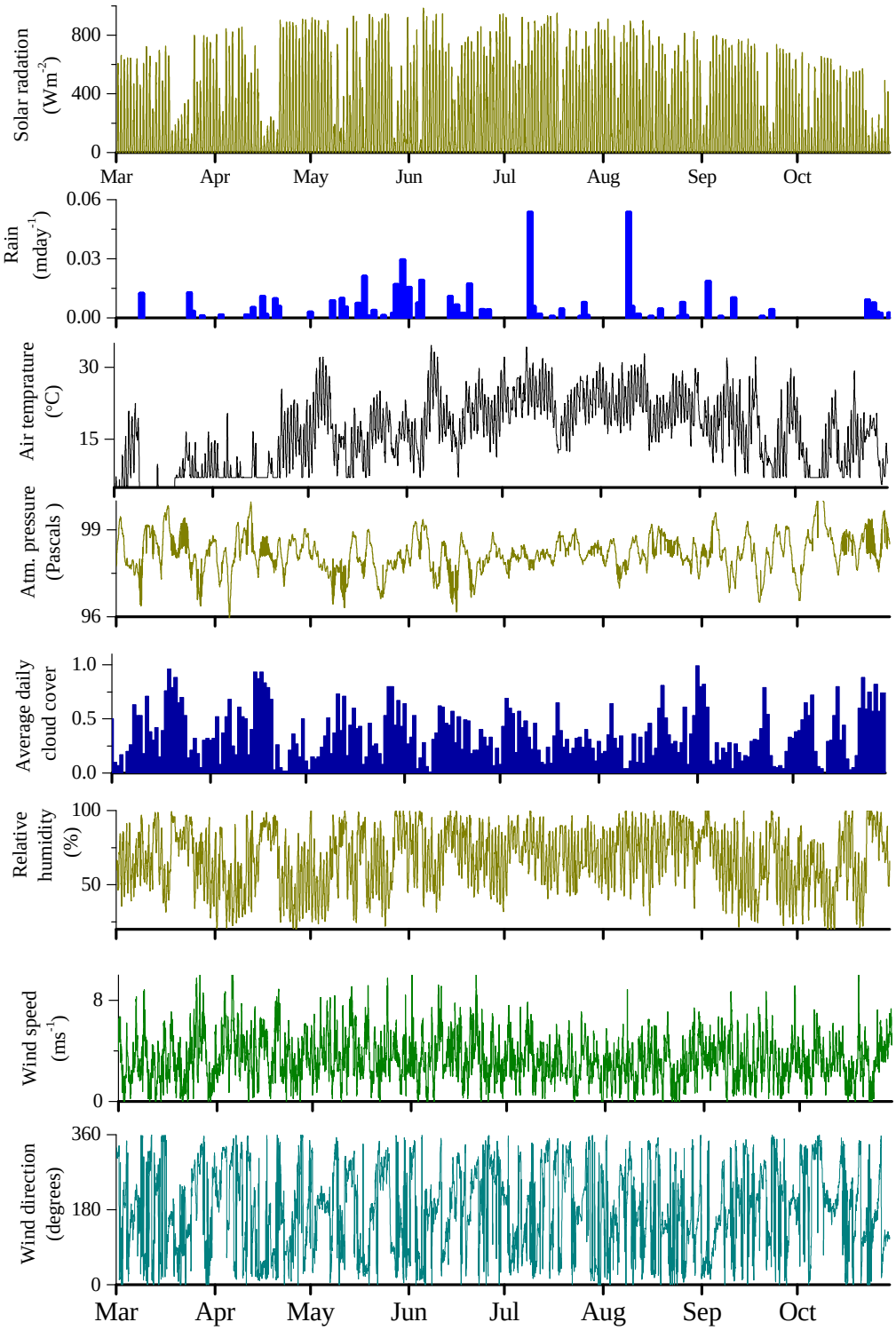

2.3.4. Model Simulations

Examination of the measured water quality data revealed that reliable measured DO was only available prior to year 2005. However, additional field measured T and DO profiles were available for most of year 2000. Therefore, the period of year 2000 was selected for model simulation and parameter calibration and year 2005 for model corroboration or verification (EPA, 2009). The 2000 simulation period included 205 days from March 29 to Oct 20, 2000. The same period was also used for CAEDYM parameters calibration. CAEDYM was configured to model phosphorus, nitrogen, pH, DO, organic carbon, and one algae group (*Cyanobacteria*). The corroboration period included 168 days from April 25 to October 10, 2005. Measured field data were used to establish the model initial conditions.

2.4. Results and Discussion

2.4.1. Calibration, Sensitivity Analysis and Corroboration

The ELCOM-CAEDYM model was calibrated for the entire simulation period where model results were compared against field data. ELCOM does not use many variable parameters and its processes are well defined (Hodges and Dallimore, 2008). ELCOM parameters used in the simulations had fixed constant values and required no calibrations. On the other hand, the complexity of CAEDYM necessitates the use of a large number of model parameters (Hipsey, 2008) which can generally be classified into biological, chemical, sediment process, and fixed parameters as listed in Table 2.

Table 2.2. A partial list of the model parameters used in model calibration and sensitivity and uncertainty analysis with their symbols , units, number of samples (n), minimum (min), maximum (max), mean value (ave), standard deviations derived from literature review, and their assigned or best fit values (Val.) in the model. Abbreviations are: carbon (C), oxygen (O_2), ammonium (NH_4), filterable reactive phosphorus, FRP (PO_4), dissolved oxygen (DO), phosphorus (P), labile (L), dissolved organic carbon (DOC), particulate organic matter (POM), dissolved organic phosphorus (DOP), and dissolved organic nitrogen (DON).

Parameters	Symbol	Units	n	Min	Max	Ave	Stdev	Val.
Biological Parameters								
Average ratio of C to chlorophyll a	Ycc	$mgC(mgChla)^{-1}$	7	0.3	90.00	31.45	30	80.00
Algal constant settling velocity	Ws	$mday^{-1}$	6	-0.1	0.3	0.04	0.16	-0.035
Fraction of respiration relative to total metabolic loss	FRML	-	6	0.14	0.80	0.33	0.250	0.50
Half saturation constant for N uptake	K_N	mgL^{-1}	17	0.00	30.0	4.9	10.8	0.07
Half saturation constant for P	K_P	mgL^{-1}	23	0.001	6	0.65	1.78	0.02
Maximum internal P concentration	IP_{max}	$mgP(mgChla)^{-1}$	12	0.08	3.00	1.18	0.87	2.40
Maximum potential growth rate of phytoplankton	P_{max}	-	29	0.70	4.66	1.98	1.00	1.20
Maximum rate of N uptake	UN_{max}	$mgN(mgChla)^{-1}day^{-1}$	14	0.12	6.48	1.93	1.82	3.50
Maximum rate of P uptake	UP_{max}	$mgP(mgChla)^{-1}day^{-1}$	12	0.08	1.00	0.37	0.29	1.00
Maximum temperature	T_{max}	C	7	28.3	39.0	35.2	3.6	28.0
Minimum internal P concentration	IP_{min}	$mgP(mgChla)^{-1}$	12	0.008	1.00	0.27	0.28	0.02
Optimum temperature	T_{opt}	C	7	23.4	30.0	26.9	2.5	21.0
Respiration mortality and excretion	Kr	day^{-1}	18	0.001	0.28	0.10	0.065	0.11
Standard growth temperature	T_{sta}	C	7	19.0	20.8	19.8	0.64	16.0
Temperature multiplier for respiration	θT_r	-	8	1.03	1.13	1.07	0.031	1.05
Temperature multiplier for phytoplankton growth.	θT_b	-	6	1.02	1.14	1.07	0.043	1.06
Chemical Parameters								
Density of POM particles	$POM_{Density}$	kgm^{-3}	9	1218	2600	1010	518	1040
Half sat constant for nitrification	KOn	mgL^{-1}	13	0.081	4.00	1.82	1.405	0.75
Half saturation constant for denitrification dependence on O_2	KN2	mgL^{-1}	9	0.01	2.00	0.57	0.562	0.44
Max mineralization of DOCL to DIC	DOC_{max}	day^{-1}	6	0.001	0.15	0.07	0.047	0.01
Max mineralization of DONL to NH4	DON_{max}	day^{-1}	14	0.003	1.00	0.12	0.263	0.08
Max mineralization of DOPL to PO4	DOP	day^{-1}	17	0.002	1.00	0.19	0.291	0.25
Max transfer of POCL to DOCL	POC_{max}	day^{-1}	6	0.001	0.07	0.03	0.032	0.07
Maximum internal N concentration	IN_{max}	$mgN(mgChla)^{-1}$	11	0.06	15.00	7.37	5.008	9.00
Nitrification rate coefficient	koNH	day^{-1}	13	0.005	0.20	0.06	0.073	0.25
Sediment Related Parameters								
Controls sediment release of PO_4 via O_2	KOxS-PO_4	gm^{-3}	5	0.05	3.00	1.32	1.55	1.00
Half saturation constant for DO sediment flux	KSOs	$mgOL^{-1}$	10	0.40	5.00	2.23	1.815	1.25
Sediment, Release rate of PO_4	$SmpPO_4$	$gm^{-2}day^{-1}$	28	0.0005	49.00	5.14	0.110	0.04
Static sediment exchange rate of O_2	rSOs	$gm^{-2}day^{-1}$	10	0.20	3.95	1.00	1.121	1.30

The model calibration began with simulating the minimum processes and state variables, and expanded gradually in a step wise process. This process proved to be very time and effort intensive. However, the process does provide a greater depth of understanding of the system (Hipsey et al., 2006). By focusing on specific parameters and processes it allowed to recognize any potential errors in the data or model setup. Through this iteratively process and using the available published parameter values (Bruce et al. 2006, Hamilton 1997, Romero et al., 2004, Hipsey et al., 2006), a reasonable range of parameter values were established. These set of parameters were used to develop a reference model simulation for the calibration process. Simulated T, DO, TP and Chl*a* were used to calibrate the model by comparing them to 12 biweekly measured data from WB water quality station using the minimum weighted sum of squares (WSS) parameter estimation procedure (Omlin et al., 2001). Phytoplankton growth rate and patterns were visually inspected and evaluated against measured data to further evaluate calibration fit (Robson and Hamilton, 2004; Bruce et al., 2006; Hipsey et al., 2006). The model was then run with the same configuration, parameter values and set up for the period of April 25 to October 10 of 2005 for corroboration. A sensitivity analysis was performed that included over 40 major of the model parameters. The mean value first-order reliability analysis method (Melching and Bauwens, 2001) was used to evaluate and rank the top dominant CAEDYM parameters. The top ranking parameters provided the most significant sources of uncertainty affecting the estimation of model output of DO and Chla. The top four ranking parameters and their fraction of the total variance of model outputs (values in parenthesis) were: DOC_{max} (45%), IP_{min} (23%), tcpy (7%) and sSOs (5%).

2.4.2. Model fit

The iterative parameter estimation and calibration process of the model yielded a base or a final set of model parameters and simulation configurations. Model outputs of calibration and corroboration periods were measured against the base model output for fitness of the model. Data from the vertical profiles of all sampling events and locations throughout the simulated period for each of T, DO, TP, and Chl*a* were plotted against

each of their corresponding model control volume point in time and place on a scatter plot with y-intercept set at zero. Model fitness was measured by evaluating the R^2 (coefficient of determination) using EzyFit toolbox in MATLAB software. Additional insights were gained by examining and evaluating profiles of each parameter against meteorological data, stream flows and other parameters. Concentration profiles for soluble reactive phosphorus (SRP) were not constructed as its epilimnion and *metalimnion* values were in general below detection levels. Corresponding model SRP output values were below 5 μgL^{-1} in the first half of the simulation period as well, indicating that the system is phosphorus limited. Furthermore, profiles of all parameters were also qualitatively examined by "eye" for patterns and times of peaks and minimums. This review was particularly valuable in evaluating the simulated algae growth.

2.4.3. Lake Water Elevation

The model calibration (2000) and corroboration periods (2005) presented two hydrologically distinct years and the model accurately simulated the lake water levels for both periods (Fig. 2.3). The mean difference of water level between the simulated and measured water levels (n=151) during the periods of March 29 to September 30 of 2000 and 2005 was 0.05 m (standard deviation = 0.06 m; range = -0.26-+0.15 m). Analyses of the modeled evaporation volumetric flux (2000) yielded an average daily and seasonal rate of 0.64 m. The seasonal evaporation rate compared well with the known area rate of 0.77 m (MCWD-2000 Hydro report). The good agreement between simulated and measured lake water levels and seasonal evaporation flux suggest an accurate water balance. However, review of the measured stream flow raises concerns about their accuracy and that the measured inflows do not appear to reflect the actual field conditions or precipitation rates

Fig. 2.3. Simulated (lines) and field data for lake water elevations above mean sea water level for year 2000 (solid) and 2005 (blank), lake runout elevation (dashed line) and average lake discharge (Q_{ave}).

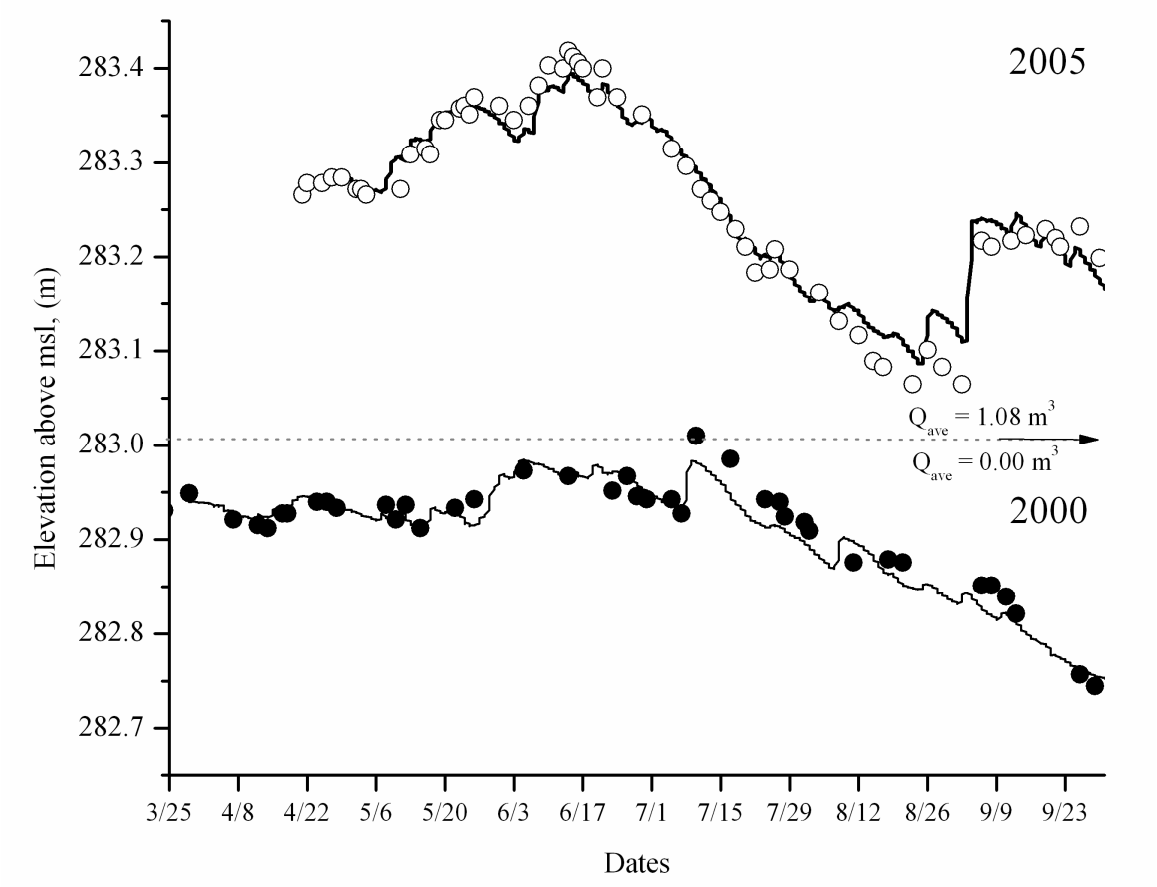

2.4.4. Simulated and measured data

Twelve biweekly measured field data from three inlake water quality monitoring stations (Fig. 1.1) were used to evaluate the model simulated T, DO, TP and Chl*a.* profiles. Water quality field samples had been collected at various times of day from 9:00 am to 8:00 pm. Simulated data matching the vertical profiles for T and DO and epliminic and hypolimnic depths for TP and Chl*a* were extracted from the model output corresponding to the specific dates of the measured data and the exact location of each of the water quality monitoring stations. Temperature and dissolved oxygen profiles compared best

with the measured data (Fig. 2.4). TP and Chl*a* were reasonably well simulated and had the same general seasonal variation patterns as the measured data (Fig. 2.5). The model managed to capture the diurnal cycle of stratifications and changes. Anoxic conditions in hypolimnion are observed starting early June and were accurately simulated at all three water quality stations in both 2000 and 2005.

Fig. 2.4. Comparison of selected days of simulated (line) and observed water temperature (triangle) and dissolved oxygen (circles) at West Upper Bay in 2000.

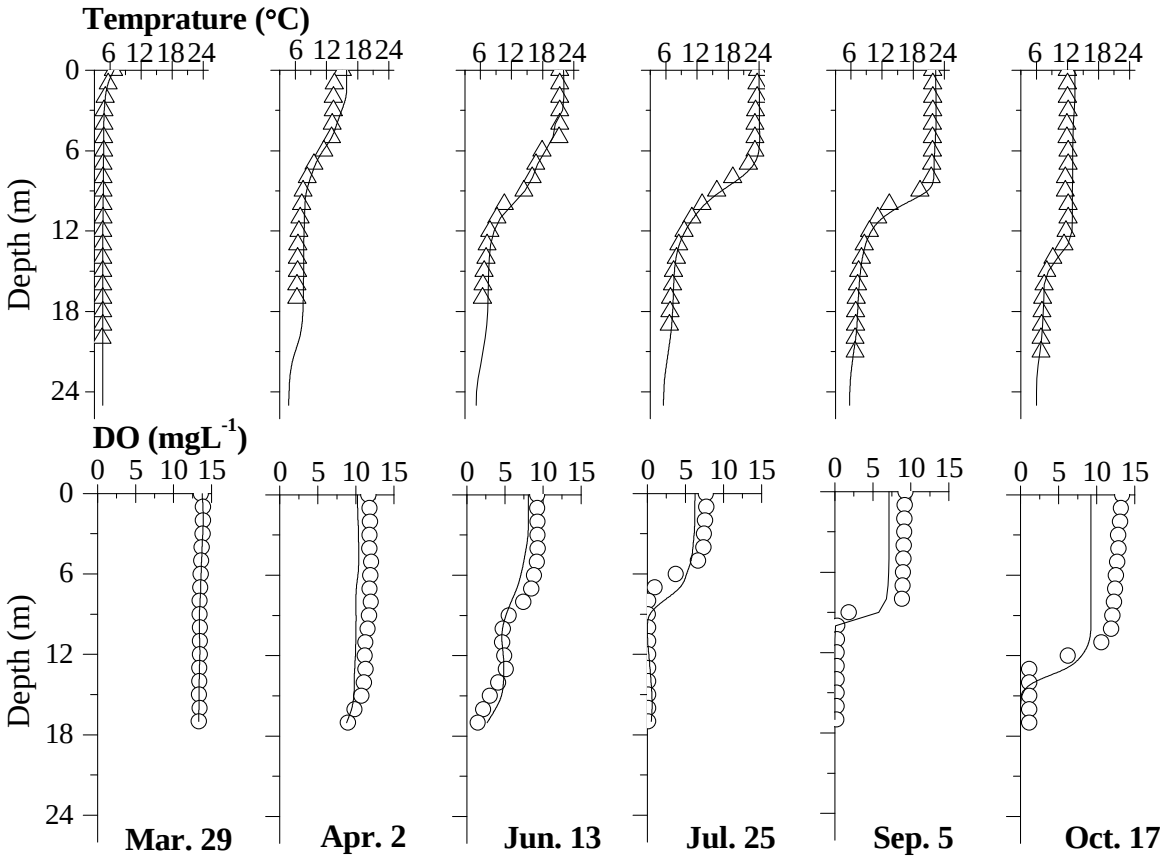

Fig. 2.5. Comparison of 2000 simulated (lines) and measured a) epilimnion and b) hypolimnion TP concentration and composite top 2 meter c) Chl*a*.

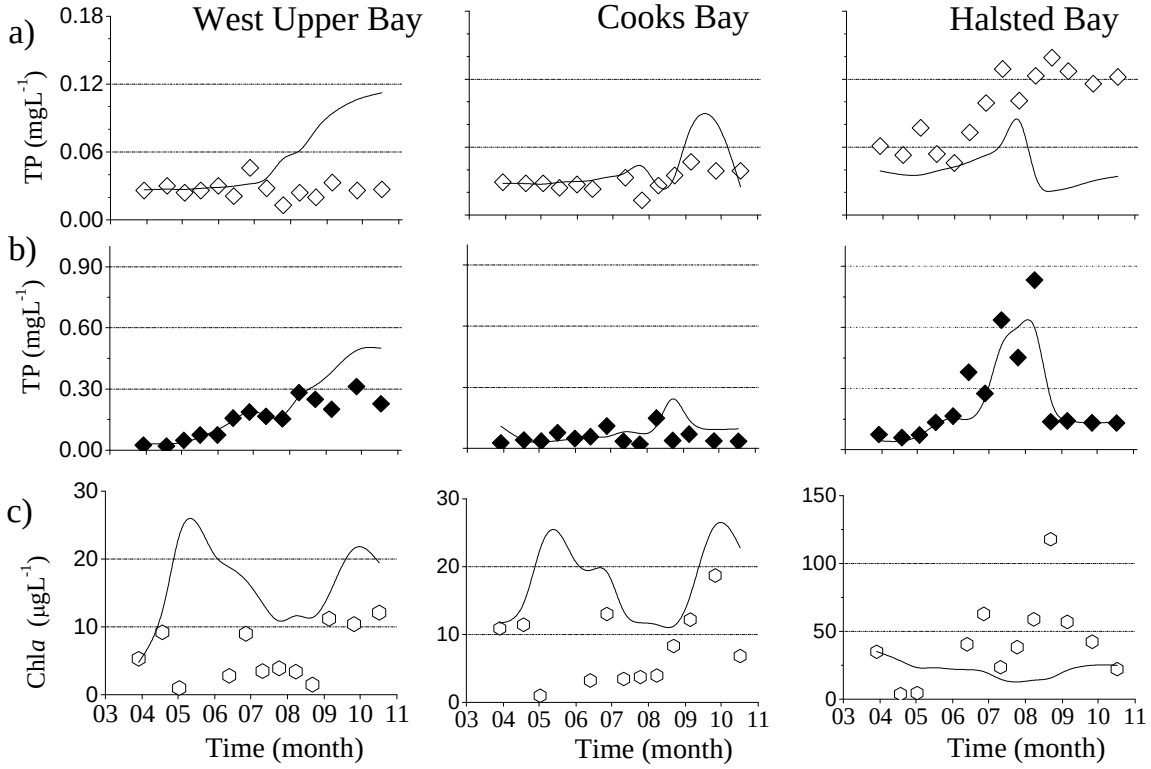

2.4.5. Temperature Profiles

Water temperature profiles had the best fit in the quantitative comparison of the model output with the measured data. Without adjusting the initial model parameters, the model was able to explain 98% of the observed temperature variability in the calibration year of 2000 (R^2 = 0.98, Fig. 2.6). The measured lake water temperature profiles from the water quality stations represented three different distinct parts (bays) of the lake. The model was successful in accurately capturing the three different mixing depths and thermoclines at each of these locations. Most lake water temperature discrepancies between the model output and the observed data occurred in the epilimnion with the maximum difference in order of 4 ºC in CB in May. Solar radiation is the major source of lake's heat budget and surface water temperatures are more directly related to weather whereas hypolimnion water temperature is impacted more by lake morphometry (Robertson and Imberger,

1994; Hondzo and Stefan, 1996a). The meteorological input data, including wind data that is used in the model to determine evaporation flux, were acquired from a weather station 14.5 km SE of the lake.

Fig. 2.6. Comparison of West Upper Bay (WU), Cooks Bay (CB) and Halsted Bay (HB) simulated and data for a) T, b) DO, c) TP, and d) Chl*a* and their respective R^2 values for the years 2000 (calibration) and 2005 (corroboration).

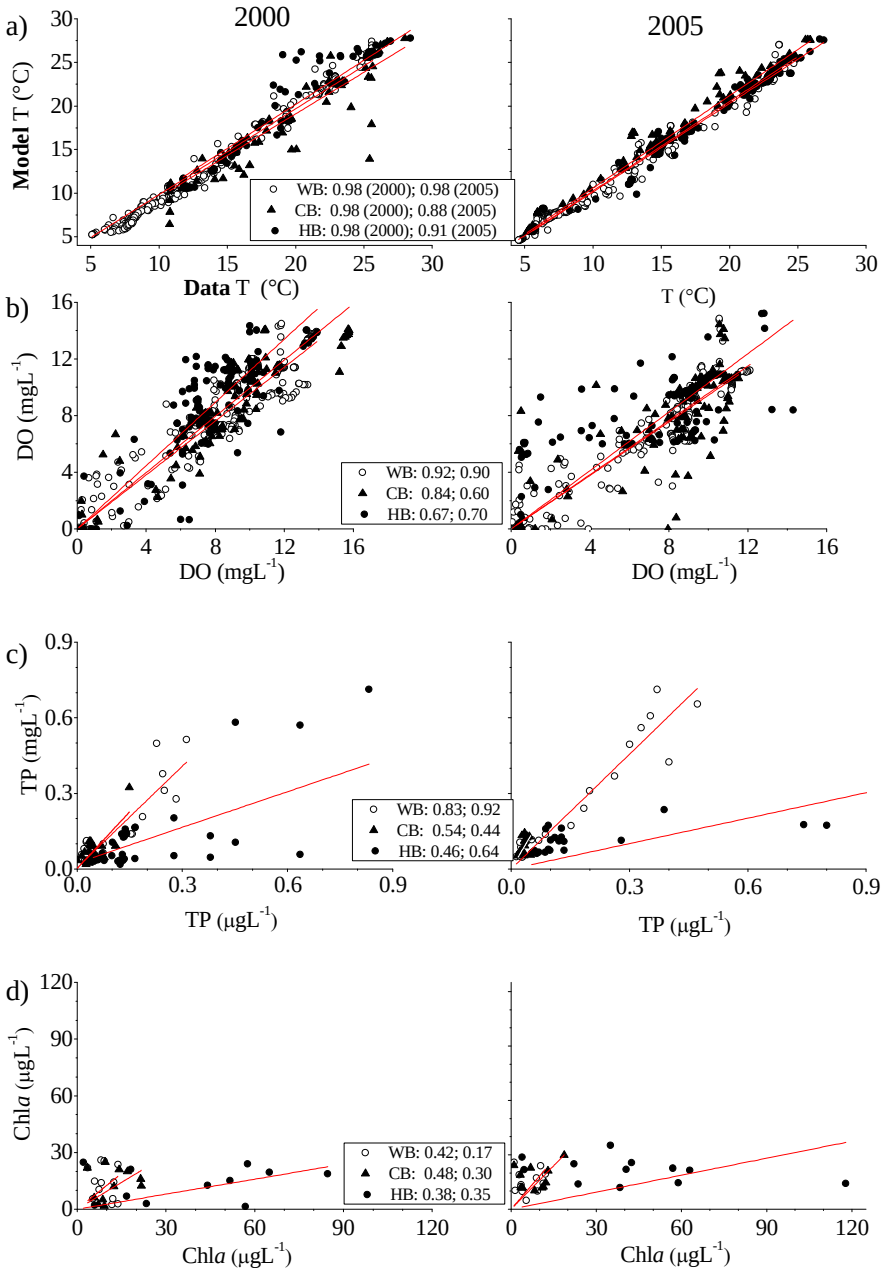

2.4.6. Dissolved Oxygen Profiles

The simulated DO profile concentrations compared well with that of the measured profiles (R^2 =0.67-0.92; Fig. 2.6). The model was able to capture the DO concentrations at the lake surface and the onset of the hypolimnion anoxic conditions at each of the water quality stations (Fig. 2.4). The hypolimnion anoxic conditions started at WB in early June followed by CB and finally HB by early July. The simulated DO, similar to the measured data, decreased sharply from the metalimnion reflecting the rapid DO depletion. A gentle metalimnic oxygen peak due to algae oxygen production (Wetzel, 2001) is observed in 2000 at the deeper WB water quality station (Fig.2.4). The model was only able to simulate this during a very short period with minimal but detectable peaks and 4 m deeper than the measured data. This was identified during the calibration process by adjusting the algae settling velocities or the oxidation processes. However, changes also altered the epilimnion algae growth peak times to an unacceptable levels which then limited the ability to calibrate the epilimnic DO concentrations. The model can simulate up to five different algae groups. To simplify the calibration and parameterization process only one algae group (Cynobacteria) was configured for this simulation. But when four algae groups were simulated, the model was able to simulate the metalimnic oxygen peak well, particularly in year 2005 which had a more pronounced peak.

The hypolimnitic DO concentration depletion rate is largely determined by sediment oxygen demand (SOD) which model simulated it well. The DO concentrations were also impacted by large storms, wind or inflow induced mixing events. Two large storm events occurred (July 18 and August 8) in-between the water quality sampling collection events during the simulation period (Fig. 2.2). Both events created a mixing that drastically changed the DO concentrations profiles, specifically throughout HB. The changes were not detected in the measured DO concentration profiles because the events lasted from few hours to less than 3 days, whereas the water quality sampling took place more than a week after these events. However, the model successfully captured these mixings and

their consequences on DO concentrations. The timing of the events corresponds well with the rain events dates. Furthermore, the findings were also verified by the additional water quality monitoring data gathered by Three Rivers Park District using a Remote Underwater Sampling Station (RUSS unit) in 2000. The RUSS unit on HB had operated for much of the 2000 with a four hour sampling intervals. The model simulated DO compared very well with the RUSS unit measured data (Fig. 2.7). The additional data confirmed the model simulations that during these storm events the water column was well mixed at HB, less at CB and with minimal mixing at WB. A similar scenario was observed in 1999 (EPA, 1999)

Fig. 2.7. Qualitative comparison of short term duration variations of DO concentration (with few points of interest marked by solid circles) as simulated by (a) model and (b) measured by RUSS unit at Halsted Bay in a two month period in 2000.

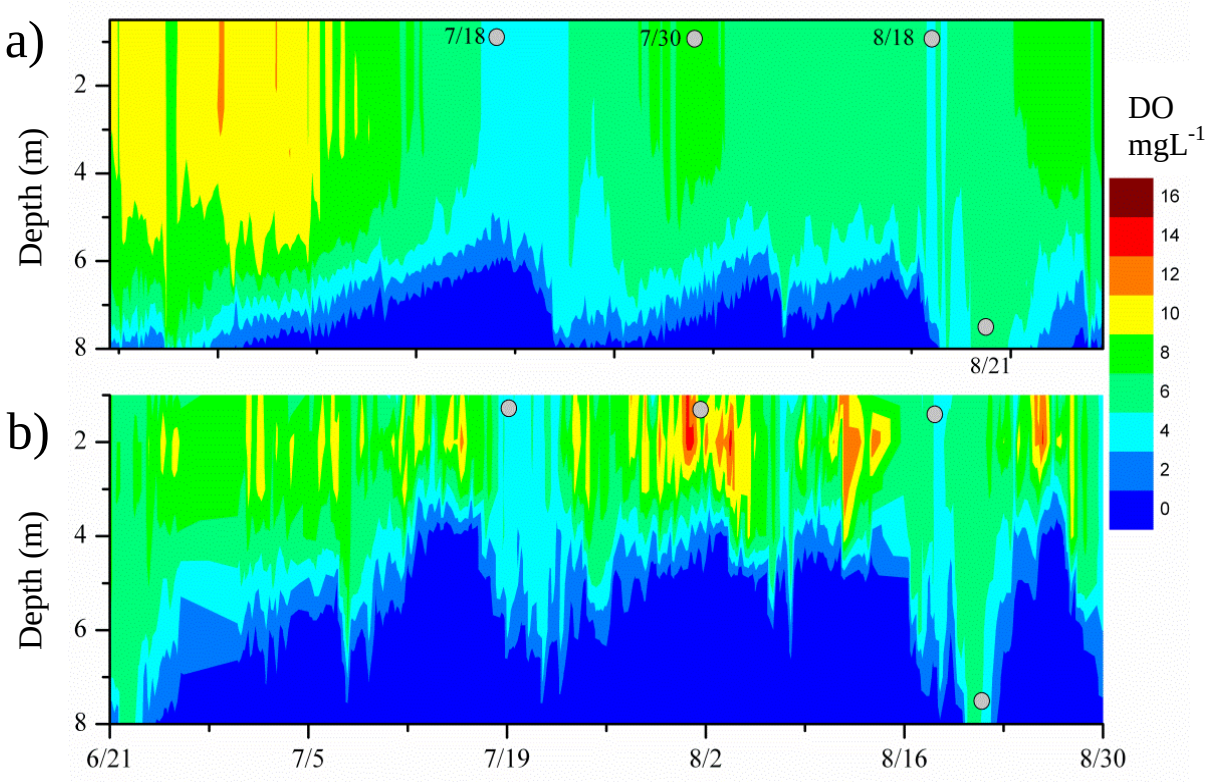

2.4.7. Total Phosphorus Concentrations

Model simulated total phosphorus concentrations were generally in good agreements with the measured data (Fig. 2.5 and Fig. 2.6). Measured TP values show that the three sampling locations have distinct localized TP concentrations indicating TP heterogeneity with HB having the largest values followed by WB and CB. Data analysis also indicated that the short duration variations of hypolimnitic TP in HB were more likely the consequences of storm events. CAEDYM allows for dynamic sediment diagenesis model configuration but it was not simulated in order to simplify the calibration process and to keep the computing time manageable. There was also a lack of measured field sediment data and associated parameters that are required by the dynamic sediment diagenesis. The static sediment model simulated TP is largely controlled by bottom T, DO, and the sediment phosphorus release rate. Given the variation in the sediment characteristics, the selection of sediment phosphorus release rate value became a balance between capturing the short term TP variations in as many locations as possible, capturing the general TP seasonal variations and keeping it within the known regional values.

Simulated eplimnic and hypolimnic TP values had a strong fit in the first half of the simulation period at all three sampling sites. The model captured many of the short term TP variations at the two shallower HB and CB, but it generally over predicted the TP values for WB site. The TP short term variations did not correspond to the measured wind data of those periods but they closely followed the inflow and precipitation events. The simulated inflows showed a clear sinking of the cooler inflows from SC through HB, suggesting that storm event mixing could have been induced by inflow plunge. Further investigation with finer bathymetry grids of 100 m successfully showed the inflow plunge and mixing. These results along with simulated and measured DO supports the notion that physical perturbations by inflows at HB and CB are causing the water column mixing and that the hydrodynamics are responsible for the spatial and temporal variations of state variables (Romero et al., 2004) . The investigation also led to discovery of a few deep isolated non-active control volumes that were eliminated by minor changes to

bathymetry. The bathymetry changes improved the model performance under both 200 and 100 meter grids configurations.

2.4.8. Chl*a* Concentrations

Simulated Chl*a* concentrations were moderately in agreement with the measured data (Fig. 2.5.C). The measured Chla data was collected as a composite sample of the top 2 meter of water column while the simulated Chl*a* values represented the average of top 2 meters. The model overestimated the Chl*a* concentrations at WU and CB, missed the early summer algae bloom but did captured the late fall bloom. The model also missed to capture any of the seasonal peaks and under predicted the Chl*a* concentrations at HB, however the values stayed within range. The general five year (1996-2000) algae growth cycle at the study area begins with a peak in late March during the turnover followed by a rapid decline after complete stratification by end of May. Summer bloom peaks in June, followed by another late season (Aug-Oct) bloom at HB and then at WB. On average in 2000, HB was 10 times more productive than the other bays and it has historically been an extremely productive basin in compare to other regional basins (Megard, 1970). The unusual high productivity at HB created a large heterogeneity that exasperated the calibration efforts.

Modeling biological biomass concentrations such as algae are inherently difficult because of their lateral patchiness, vertical distributions , temporal variations (blooming) and the still evolving understanding of algae biological dynamics (Hipsey et al., 2006; Reynolds, 2006). Typical seasonal algae dominant succession on Lake Minnetonka begins with diatoms during the Spring bloom followed by a Cryptophytes and Chlorophytes in early summer and then fully dominated by Cynobacteria for the rest of the season (PhycoTech, 2007). The difficulty of simulating the algae biomass was more likely compounded by the fact that only the dominant group of algae (Cynobacteria) was configured in the simulations. Measured Chl*a* concentration was limited to one composite sample of the top 2 meters that didn't allow creating vertical concentration profiles. However, DO profiles suggested an increase in algae biomass right below the water surface where algae

is more sheltered and a peak at metalimnion where the algae gain access to additional nutrients from hypolimnion while still exposed to limited light. The algae biomass then declines rapidly as it reaches hypolimnion. These upper and lower boundaries form an algae growth favorable layer with seasonal thickness variations reflecting nutrient and light availability, turbulence, microbial loop interactions and hydrodynamic affects (Chen, et al., 2002; Scavia and Fahnenstiel, 1987; Robson and Hamilton, 2002; Hondzo and Warnaars, 2008). Measured Chl*a* profiles would have provided a valuable opportunity to further investigate the algae growth favorable layer in the study area. There were no measured zooplanktons data for the study site. Zooplanktons were not simulated and the model did not include zooplankton grazing on phytoplankton. However, algae mortality rate was assumed to compensate for it.

2.5. Example of a 3D Model Application for Lake Minnetonka

Simulations showed that the 3D ELCOM-CAEDYM model was robust enough to capture the system's physical, chemical and biological seasonal and short term duration (intera-seasonal) spatial and temporal variations. The spatial variation of our study area requires an accurate bathymetry and a detailed 3D hydrodynamics to capture its large heterogeneity. The simulated surface water temperature for each model output shows temperature range (maximum-minimum) of 1 ºC to near 13 ºC with a seasonal average of 5 ºC (Fig. 2.8).

Fig. 2.8. Range (max-min) of simulated surface water temperature at each model output (4 hrs.) over the entire simulation period (2000) with the average seasonal range shown in dash line and the expanded map illustrating the range (6.5 ºC) of surface water temperature at 7/23/00 13:00, model output.

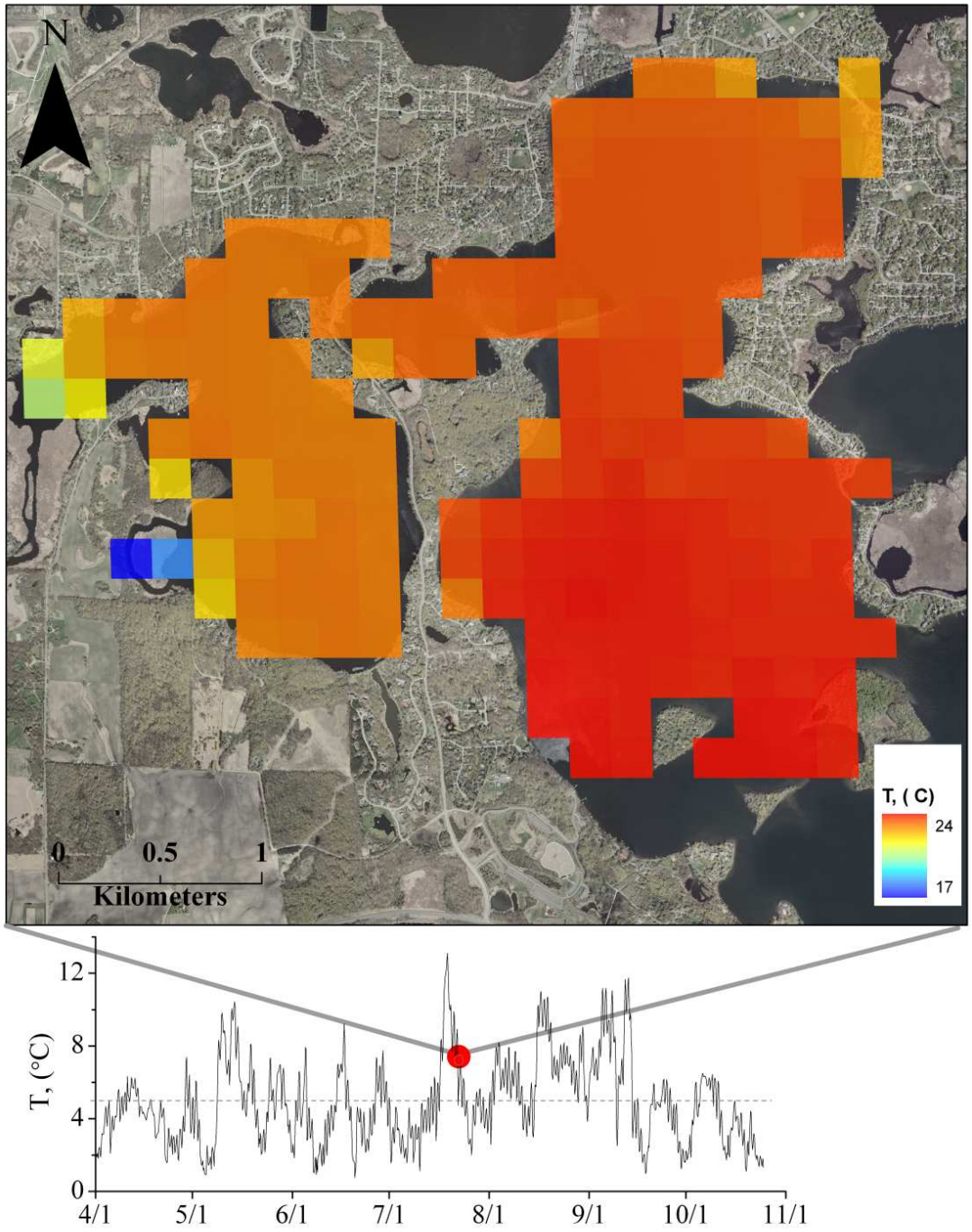

Some of the surface temperature variations are likely due to the temperature fluctuations in the shallow areas or the areas near the inflows. Nonetheless, each of the three bays still show distinct water temperature ranges. Such spatial variations may have significant impacts on ecological systems and need to be considered in any ecological modeling efforts. The question was how would the elimination of T and DO spatial heterogeneity impact the analysis of coolwater fish habitat. To illustrate this idea, we examined the variability of suitable coolwater fish habitat in our study area under two different scenarios. In the first scenario, we analyzed the fish habitats by the 3D model. In the second scenario (averaged), the spatial heterogeneity was eliminated by horizontally averaging the two state variables T and DO. The analysis can be also considered as an example of an engineering application of such a 3D ecological model for Lake Minnetonka. Fifteen fish species are found in Lake Minnetonka dominated, as defined by mass per gillnet, with northern pike (*Esox lucius)*, walleye (*Stizostedion vitreum*), and bluegill *(Lepomis macrochirus)* (MNDNR, 2007). Walleye abundance as measured by number of fish caught per gillnet, has been low, less than 4 catch per gillnet, since 1970, with a general decline since 1999. In 2007, 99% of the Walleye population was found to be sustained by annual stocking. Walleye population has remained steady regardless of increase of stocking rate as much as 100% in 2001. Walleye grow to 33.0 cm by age 3, a rate slower compared to the regional lakes. Walleye lake-wide average catch was 45.5 cm. Within the lake, the walleye catch in the two stocked bays were 43 and 45.7 cm. However, those that had migrated into the northwest bays had a catch average of 55.4 cm (MNDNR, 2007), indicating the presence of distinct fish habitats within the lake. Suitable fish habitat is determined by a large number of environmental factors. T and DO are recognized as the two most significant water quality parameters that shape fish habitat (Hondzo and Stefan, 1996b; Coutant, 1985; Christie and Regier, 1988). Different fish habitat criteria have been established using these two parameters (Stefan et al., 1995; Stefan et al., 2001). For the purpose of this analysis we adopted the mean coolwater fish thermal and dissolved oxygen criteria established by Stefan et al. 2001 (Table 2.3) which includes both walleye and northern pike.

Table 2.3. The three types of coolwater fish habitats and their associated T (C^o) and DO (mgL^{-1}) criteria.

Habitat Criteria	**Abbreviations**	**Conditions**
Good Growth	GG	(16.3 < T < 28.2) AND (DO > 3)
Restricted Growth	RG	(28.2 <T < 30.4) OR (T< 16.3 AND DO > 3)
Uninhabitable	UI	(T > 30.4) OR (DO < 3)

The model was configured to generate the simulated T and DO of 12 depth layers at 2 meter intervals (0-22 m). These outputs were then quarried for coolwater fish T and DO criteria. To represent the spatial heterogeneity minimized scenario, the T and DO values of each depth layer was first averaged horizontally (1D) for each time step and then queried same as in the 3D analysis. The number of control volumes (cells) of each type of habitat was normalized by the total volume of the lake (V/V_t). Sum of each of the three types of fish habitats were plotted at each time step for all depth layers over time and the mean integrated value (average) for each type was computed and plotted (Fig. 2.9). The process was completed for both calibration (2000) and corroboration (2005) periods which also presented an opportunity to compare the coolwater fish habitats under two different climate scenarios. The summers (Jun.-Aug.) of 2000 and 2005 were ranked the 16^{th} and the 5^{th} warmest summers on the records (NOAA, 2009) making these two seasons significantly different.

Fig. 2.9. Comparison of 3D (black lines) and 1D (red lines) analysis of the three coolwater fish habitats: a) GG, b) RG, and c) UI for all depth layers over time with inset showing the magnitude of short duration variations and d) is the maximum (abs) of the difference between 3D and 1D analysis of GG, RG, and UI at each depth layer and output.

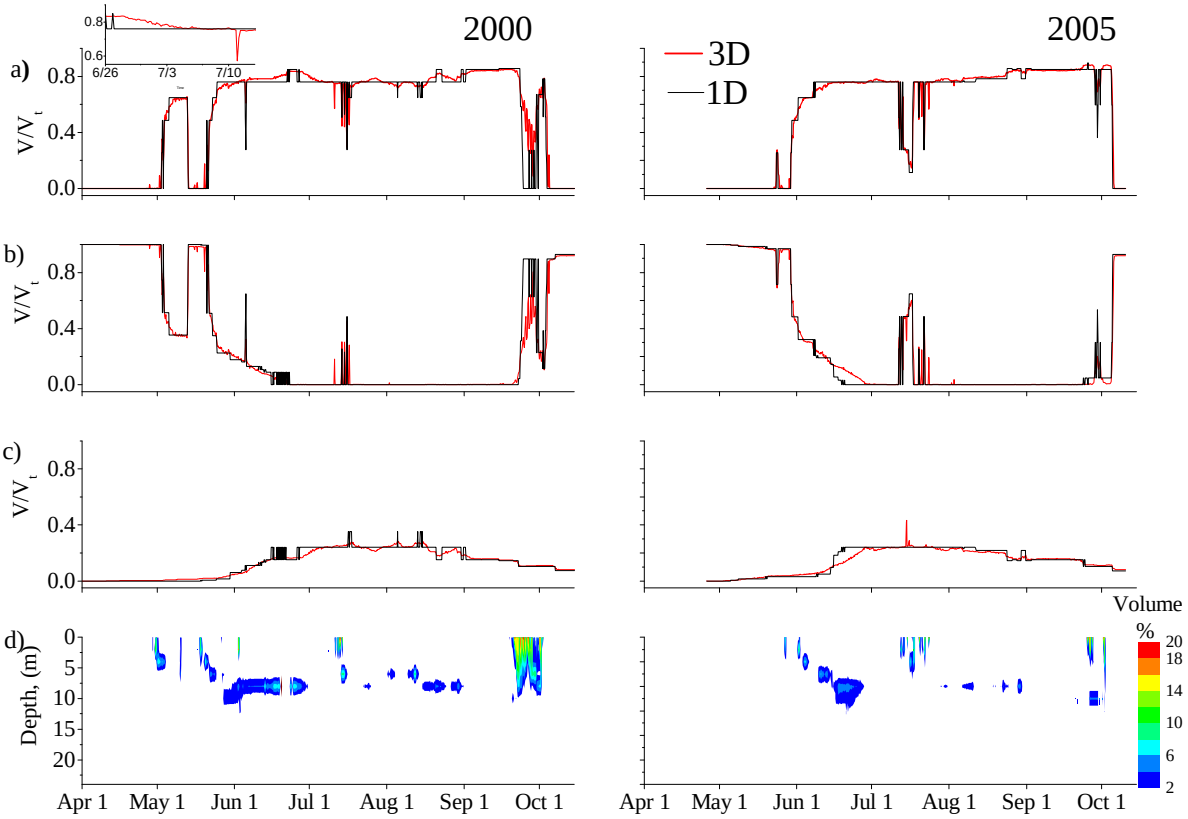

Initially, the 3D and the 1D analysis of coolwater fish habitats were conducted for the full simulation periods of 2000 and 2005. Both analyses accurately captured major seasonal changes (Fig. 2.9). Minimal changes in the fish habitats are expected early in the season with cooler water temperatures and before the water columns stratify. During this period the fish habitat is dominated by RG. This was captured in both years by both analysis as indicated by the straight lines at the start of the seasons. The GG begins to increase as the season progresses and the temperature is increased and is minimized again towards the end of season. RG and GG show large fluctuations in late Spring of 2000 which corresponds to the upper water column temperature fluctuation (Fig. 2.9.a-c), a reflection of the changing weather patterns. The air temperature was 2 ºC and the average wind

speed was 10% less in May of 2000 than in 2005. The UI increase coincides with the onset of hypolimnic anoxic conditions in both years and its small values reflect the smaller hypolimnic volume. GG showed stronger correlation with RG and less with UI. The coolwater fish habitats seasonal (May 1-Sep. 30) averages for the 3D and the 1D analyses methods were similar (Table 2.4).

Table 2.4. 3D and 1D analysis of GG, RG, and UI of seasonal (May 1-Sep. 30) coolwater fish habitats average values (V/V_t) for 2000 and 2005.

Simulation scenarios	**GG**	**RG**	**UI**
2000, 3D	0.70	0.15	0.15
2000, 1D	0.68	0.17	0.16
2005, 3D	0.61	0.25	0.14
2005, 1D	0.61	0.24	0.15

This may have been driven by the large seasonal fluctuations of the state variables and their seasonal dependencies. Percent changes from 3D to 1D analysis were grater in 2000, where the difference of RG in 3D and averaged analysis was more than 11%. The 2000 GG habitat bias (3D-averaged) showed that 3D analysis was leading and was able to capture the changes faster early in the season while temperature was generally increasing and later in the season when temperature was decreasing. The averaged analysis did not capture short term duration variations. The 2000, GG averaged analysis missed to capture variations as large as 20% in a two week period (Inset Fig. 2.9) whereas the 3D analysis exhibited greater local variability. The maximum bias (absolute values) of the three habitats (GG, RG, UI) at each depth layer and output was calculated as percent change of volume and plotted for each year (Fig. 2.9,d). The patterns are similar for both 2000 and 2005. The averaged analysis, where heterogeneity has been minimized by horizontally averaging the state variables, shows the largest differences (up to 20%) from the 3D occurring at surface layer. These changes are localized in early, mid, and late season where T and DO may be changing rapidly. Some moderate differences (2-8%) between 3D coolwater fish habitat and the averaged analysis are also

seen at 6 to 10 m depth. To demonstrate the T and DO heterogeneity in the lake, the range (max-min) of their values for each depth layer at each model output was measured and plotted for all of 2000 season (Fig. 2.10). The largest ranges of T values were detected on the surface layer and at the depth corresponding to thermocline and shallow areas (6-10 m). The largest ranges of DO values were also concentrated at these depths during the early and late season with smaller concentrations in the deepest areas. The results correspond well to our earlier findings that minimizing heterogeneity of state variables in coolwater fish habitat analysis has the greatest impact at surface layer and at 6 to 10 m depth.

The 2000 to 2005, 3D analysis compression of coolwater fish habitat, showed a 12% reduction in GG, 62% increase in RG and 5% reduction in UI. These variations could be explained in parts by marked changes of the simulated T and DO values and patterns at WB from year 2000 to 2005 (Fig. 2.11). In 2005, horizontally averaged values for water temperature in the top 10 m where temperature is more impacted by weather was about 2 ^{o}C warmer and the DO concentrations were about 1 mgL^{-1} less than 2000. Based on our defined coolwater fish habitat T and DO criteria, it would be expected that an increase in T and a decrease in DO would yield less GG and greater RG conditions as shown by the 3D analysis.

Fig. 2.10. Range (max-min) of simulated T and DO values at each depth layer and model output over the entire year 2000 season, with a lake volume plot showing the accumulative volume at each depth.

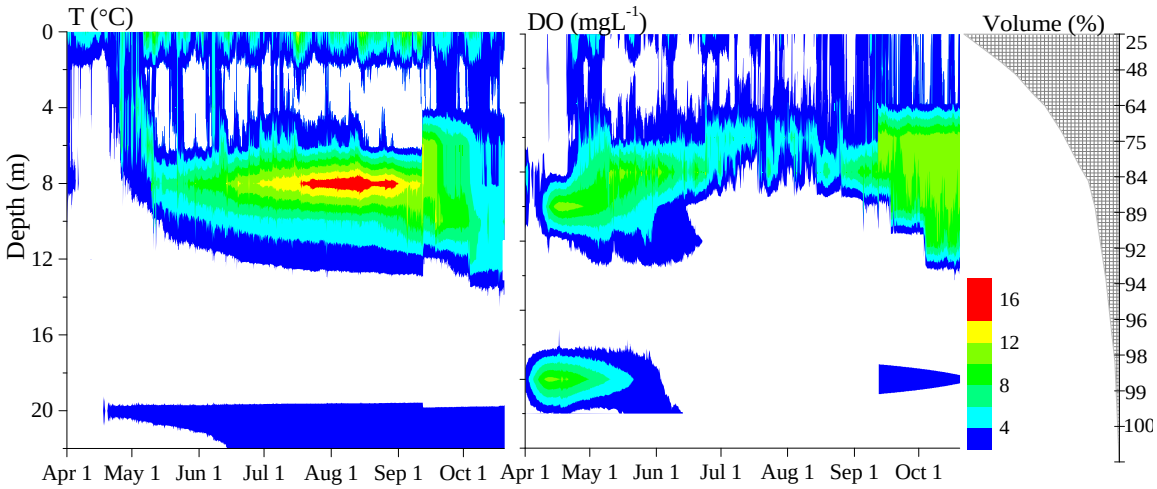

Fig. 2.11. Contour plots of simulated T and DO, at WB showing their values and patterns for both year 2000 and 2005.

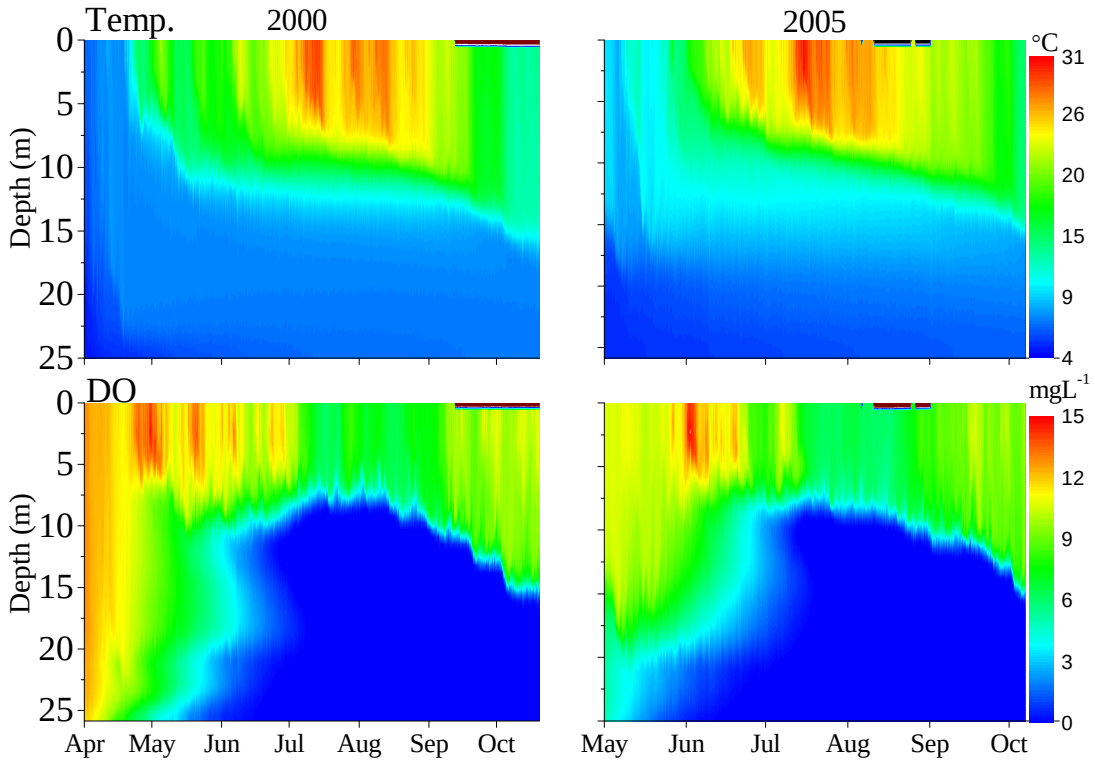

2.6. Conclusions

We successfully validated and applied a coupled 3D hydrodynamic and ecological model to a morphologically complex lake. Measured data reflect a system with large spatial and temporal water quality and fish habitat heterogeneity which necessitated the use of 3D models to capture its biogeochemical changes. ELCOM-CAEDYM models were selected and configured for this analysis through an intensive calibration and validation process. Simulated and biweekly measured data were used to evaluate model fit. T profiles had a remarkable fit ($R^2 = 0.98$) with DO profiles agreeing very well at the three water quality locations (R^2 of 0.67 to 0.92) but missing gentle metalimnic oxygen peaks. TP (R^2 of 0.44 to 0.92) and Chl*a* (R^2 of 0.3 to 0.48) agreed reasonably well. The model was able to capture the spatial and temporal biogeochemistry variations including the short duration variations that were not detected by the regular biweekly measured data. The modeling efforts brought out the need for high quality input measured data. Input data are used as boundary conditions in model configuration, in evaluation against simulated data to measure model fit and in sensitivity analysis. High integrity input data are essential in establishing reliable models. The 2000 measured stream flows proved questionable and failed to reflect field conditions. Measured Chl*a* profiles would have offered a rare opportunity to examine the algae growth favorable layer as well as aid in model calibration. The apparent large variation of sediment phosphorous flux in each bay, as indicated by their TP, also requires further investigation. The model captured the heterogeneity of the system and showed that a 3D analysis was needed to adequately gain insight into its spatial and temporal biogeochemistry distribution. An example of an ecological application is provided by examining and comparing the coolwater fish habitat analysis in 3D and under a scenario where spatial heterogeneity was eliminated by horizontally averaging T and DO. The 2000 and 2005 seasons also represented two climatologically distinct years. The seasonally-averaged GG habitat for coolwater of 3D and that of 1D analyses agreed well in both years. However, the averaged analysis failed to capture short term duration variations of as much as 20% of the lake volume during a two week period. The largest (20%) differences between 3D and 1D analysis were

located in the surface layer with a modest (2-8%) difference around thermocline depth. The simulated fish habitat changes from 2000 to 2005 were supported by a 2 ºC warmer water temperatures and 1 mgL^{-1} lower DO levels of measured data in 2005.

CHAPTER 3

Three-Dimensional Lake Water Quality Modeling: Sensitivity and Uncertainty Analyses

Published as: Missaghi, S., Hondzo, M., Melching, C., (2013) "Three-Dimensional Lake Water Quality Modeling: Sensitivity and Uncertainty Analyses"; Journal of Environmental Quality 2013 42:1684-1698.

Two sensitivity and uncertainty analysis methods are applied to a three-dimensional (3D) coupled hydrodynamic-ecological model (ELCOM-CAEDYM) of a morphologically complex lake. The primary goals of the analyses are to increase confidence in the model predictions, identify influential model parameters, quantify the uncertainty of model prediction, and explore the spatial and temporal variabilities of model predictions. The influence of model parameters on four model-predicted variables (model output) and the contributions of each of the model-predicted variables to the total variations in model output are presented. The contributions of predicted water temperature, dissolved oxygen, total phosphorus, and algal biomass contributed 3, 13, 26, and 58% of total model output variance, respectively. The fraction of variance resulting from model parameter uncertainty was calculated by two methods and used for evaluation and ranking of the most influential model parameters. Nine out of the top ten parameters identified by each method agreed, but their ranks were different. Spatial and temporal changes of model uncertainty were investigated and visualized. Model uncertainty appeared to be concentrated around specific water depths and dates that corresponded to significant storm events. The results suggest that spatial and temporal variations in the predicted water quality variables are sensitive to the hydrodynamics of physical perturbations such as those caused by stream inflows generated by storm events. The sensitivity and uncertainty analyses identified the mineralization of dissolved organic

carbon, sediment phosphorus release rate, algal metabolic loss rate, internal phosphorus concentration, and phosphorus uptake rate as the most influential model parameters.

3.1. Introduction

Water quality in lakes and reservoirs is subject to the temporal and spatial variabilities of climatic and hydrologic processes which, in conjunction with the lake morphometry and aquatic basin setting in the watershed, drive water currents. The resulting water currents, temperature (T), dissolved oxygen (DO), algal biomass (Chla), and nutrient concentrations, such as phosphorus (P) and nitrogen (N) have inherent spatial and temporal variabilities over the lake basin. Interactions and interactive feedback among physical, chemical, and biological processes are nonlinear, dynamic, and far from equilibrium (Shigesada and Okubo, 1981; Hondzo and Warnaars, 2008; Sejnohova, 2008; Leon et al., 2011; Makler-Pick et al., 2011). Thus, an advanced three-dimensional (3D) representation of physical, chemical, and biological processes of ecosystems is needed to capture ecological heterogeneity of ecosystems such as lakes and reservoirs, particularly those with complex morphometery (Hodges et al., 2000; Power et al., 2005).

The concept of 3D hydrodynamic modeling implies that the fundamental description of physical processes would minimize the calibration process. 3D water temperature prediction models of lakes and reservoirs have successfully proven this concept in a variety of water bodies and associated climatic and hydrologic conditions (Hodges, 2000; Hodges et al., 2000; Romero and Imberger, 2003; Romero et al., 2004; Komatsu et al., 2006; Spillman et al., 2007; Leon et al., 2011) and have become an essential tool in research and resource management (Li and Wu, 2006). Aquatic environments include multiple, complex processes that depend on numerous dependent and independent variables across a wide range of scales. This multi-level scale variability engenders a greater variability in the numerical 3D modeling of aquatic systems. On the one hand, 3D models are needed to capture the complex and interconnected physical, chemical, and biological processes in the aquatic systems (Arhonditsis and Brett, 2005), and on the other hand, the 3D depiction and corresponding prediction of state variables such as DO, N, P, and Chla generate a substantial number of calibration parameters needed to accurately describe the ecological processes of the simulated system. Additionally, some

of these models use appropriate calibration parameters to address subgrid processes that are not necessarily resolved or captured at the larger, required computational grid scale (Passalacqua et al., 2006), which further increases the complexity of the models and their dependence on more parameters. Therefore, the predictive ability of these models may depend upon numerous calibration parameters which work against the fundamental concept of minimal calibration needed by 3D modeling.

The purpose of sensitivity and uncertainty analyses of a complex, nonlinear, temporally and spatially variable and configurable ecological model is to gain insight about the impact of the model parameters on model output and to find a reasonable or best fit set of parameters that best respond to available data (Brun et al., 2001). Sensitivity and uncertainty analyses are the appropriate tools for such an exercise and can also be used as screening tools to set up the initial simulations where information on model parameter values is limited (Arhonditsis and Brett, 2005). Furthermore, well-designed sensitivity and uncertainty analyses of complex models can yield important information about the key processes of the systems under study (Mooij et al., 2009: Makler-Pick et al., 2011) and about their spatial and temporal variations. Sensitivity and uncertainty analyses of water quality prediction models have been effectively used to quantify how sensitive the prediction variables are to changes in corresponding calibration parameters and how uncertain the model prediction is due to the variability of the calibration parameters (Melching and Bauwens, 2001; Saltelli, 2002; Cacuci, 2003; Arhonditsis and Brett, 2004; Saltelli et al., 2006; Manache and Melching, 2008). The results of sensitivity analysis enhance the understanding of the model, increase model reliability, identify influential model parameters, and confirm if the model resembles the system under study (Saltelli et al., 2000; Saloranta and Andersen, 2007; Zhang and Arhonditsis, 2009). Sensitivity and uncertainty analyses guide which model input requires further investigation in order to reduce the uncertainty in model prediction and to set the stage for future research and model improvement (Beck, 1987; Burs and Jansen, 2004; Miao et al., 2004; Loucks and

van Beek, 2005; Saltelli et al., 2006; Munoz-Carpena, et al., 2010; Salacinska et al., 2010).

Sensitivity and uncertainty analysis are considered essential components of model evaluations (Gaber et al., 2009; Schmolke et al., 2010), but were reported in less than half of the modeling investigations published in the 1990 to 2002 (Arhonditsis and Brett, 2004). However, many strides have been made in the past two decades in conducting of sensitivity and uncertainty analyses for 1D, 2D, and a few other complex ecological models. They have included new definitions and calculation processes (Turley and Ford, 2009) and in depth description of uncertainty and sensitivity analyses for a multi-year simulation model (Saloranta and Andersen, 2007). Janse et al. (2010), analyzed uncertainties of the phosphorus loading parameter influencing the clear and turbid equilibrium state in shallow lakes, and Makler-Pick et al. (2011) have conducted a detailed sensitivity analyses and have proposed a new approach to screen subsets of significance parameters. A good list of models and the status of their sensitivity and uncertainly analyses is provided by Mooij et al. (2010), including static, minimal, and complex dynamic lake ecosystem models. Nonetheless, many of the methods used in these investigations are not readily applicable to 3D models due to the intense computational cost of ecologically complex 3D models. Whereas, the increased computing power and improvements in numerical models have advanced and increased the use of complex 3D ecological models, the sensitivity and uncertainty methods have not kept up with that pace (Ravalico et al., 2005). There is a need for more flexible sensitivity and uncertainty analyses methods for 3D ecological models where these methods can become an integral part of models and are readily available to modelers. Finally, transparent sensitivity and uncertainty analyses can minimize skepticism and raise confidence among scientists and the public for the use of complex 3D ecological models (Radcliffe et al., 2009).

Sensitivity analysis is generally classified into global and local analyses. In global sensitivity analysis, model parameters are changed within a particular region (space) and their influence on the model output variability is analyzed. In local sensitivity analysis, the changes in model parameter values are limited to a fixed point in space. Depending on the study's approach and available data, the fixed point in space can be the first statistical moment (mean) from the available literature parameter values, creating a reasonable "operating point" (Brun et al., 2001), or from a "best fit" set of parameters obtained from the best calibrated model fit against measured data. In either case, a one-factor-at-a-time (OAT) approach is employed by changing the value of one parameter while the values of all other parameters are kept at their central or best fit values and the model output is evaluated against that of the baseline simulations (Van Griensven et al., 2006; Gaber, 2009).

A detailed application of two local sensitivity and uncertainty analyses methods is explored in this paper. Both methods employ the OAT approach and have been applied to a coupled 3D hydrodynamic and ecological model simulating a morphologically complex lake. The results of each method are discussed along with a comparison of the two methods. The model predictions were compared to the measured seasonal patterns of the predicted variables in the study area. Special attention is given to model performance during physical perturbations caused by stream inflows generated by storm events. The primary goals of the analyses were to improve the understanding of the complex 3D model, gain insight into the ecological processes of the simulated system, increase confidence in the model predictions, identify influential model parameters, quantify the uncertainty of the model prediction, and explore spatial and temporal model output variabilities.

3.2. Materials and Methods

3.2.1. Analysis Framework and Setup

The application of the 3D coupled ELCOM-CAEDYM ecological modeling for Lake Minnetonka consisted of many steps. A detailed description of modeling evaluation and application of ELCOM-CAEDYM to Lake Minnetonka including model description, configuration, set up is provided by Missaghi and Hondzo (2010) and as described in chapter one. The analyses presented in this chapter include the implementation of: a) parameterization, calibration, confirmation, and model performance (fit), b) sensitivity and uncertainty analyses by two different methods, and c) the process of model parameter ranking by importance and their influence on the model prediction.

Sensitivity analysis could be conducted for any set of the model inputs, such as the model boundary conditions (Trolle et al., 2008), meteorological (Hondzo and Stefan, 1992; Arhonditsis and Brett, 2005; Leon et al., 2005), hydrodynamic (Romero et al., 2004; Hurtado, 2007), and field measured data. In previous work, the boundary conditions used for this study were carefully reviewed, corrected with few modifications, and proved accurate. However, the predicted biological variables proved to have the greatest spatial and temporal variabilities similar to the field measured data and representative of the system. The objectives of sensitivity and uncertainty analyses conducted in this study were focused on the variability of model parameters, the parameters' influence on model output variance, and ranking the influence of the most significant parameters on model predictions.

3.2.2. Model calibration and confirmation

Over 750 values of 80 model parameters were obtained from their published values (Hamilton and Schladow, 1997; Schladow and Hamilton, 1997; Romero et al., 2004; Bruce et al., 2006; Hipsey et al., 2006; Hipsey, 2008; Gal et al., 2009). Minimum, maximum, mean, number of samples (n), and standard deviation (σ) of published values

of each of the parameters were determined (Table 2.2). The averaged values of each of the 80 model parameters, or the most appropriate values used in similar studies, were used to form a reasonable operating set of parameter values as a starting point for model parameterization and calibration.

The entire simulation period from Mar. 29 to Oct. 20, 2000, (205 days) was used for model calibration. The model calibration process began with the minimal number of model processes and model state variables simulated. Gradually and iteratively, additional model processes and predicted variables were included in model simulations. This step wise approach proved very time and effort intensive. But, by focusing on specific parameters and processes the approach made clear any potential errors in the data and model setup as well as provided a greater depth of understanding of the system (Hipsey et al., 2006).

At the end of each simulation, 12 biweekly measured field data of T, DO, TP, and Chla from the vertical profiles of the deepest sampling location (WB) were evaluated against their corresponding model control volume point in time and space. The weighted square sum (WSS) parameter estimation procedure, described by Omlin et al. (2001), was used for model parameter calibration. The WSS is the sum of the squares of the residuals divided by a scale:

$$\mathrm{WSS}(\theta)= \sum_{k=1}^{y} \sum_{j=1}^{t} \sum^{Zy_k} \left(y_{meas.k}, j, i - y_k(t_j, z_{yk_i}, \theta) \Big/ \sigma_{meas.y_k} \right)^2 \qquad (1)$$

where the index i represents the spatial (vertical) locations from 1 to the total number $\left(Z_{y_k}\right)$ of depth field sampling locations for model predicted variables $\left(y_k\right)$ where k represents T, DO, TP, and Chla model outputs. The total vertical profile points represented by Z_{y_k} is not the same number for all model predicted variables, as some variables are sampled at different water depth intervals. Index j is time (t_j) from 1 to the total number of dates (t) where measured profiles were used. Model predicted variables calculated with the parameter value (θ) are represented by $y_k\left(Z_{y_{k_i}}, t_j, \theta\right)$ and

corresponds to the same location and time of the measured data $(y_{meas.k}, j, i)$. Different scale factors, or the standard deviation of the measured variable $(\sigma_{y_{meas.k}})$ with the same units as the model output, can be used to make WSS dimensionless and to give all model predicted variables similar influence in the parameter estimation. The WSS was used to assign optimal estimates of the 80 model parameters. These sets of parameters were used to create the assigned values for the best fit set of parameters (Table 2.2) and to develop a reference model output used for calibration and confirmation.

From this set of parameters, the calibrated parameters with the smallest values of WSS were selected for the sensitivity and uncertainty analyses. To strengthen the analyses, all simulations of evaluated parameters with less than five prior data points (i.e. *n* in Table 2.2) were excluded from consideration in the sensitivity and uncertainty analyses. A total of 29 parameters remained that are listed in Table 2.2. The values for the biological parameters of standard (T_{sta}), maximum (T_{max}), and optimum (T_{opt}) temperature representations were assigned considering regional climate conditions and field data. The published values reported for these three parameters associated with CAEDYM are from studies conducted in relatively much warmer climate and water temperature than the current study area. Consequently the assigned values for T_{sta}, T_{max}, and T_{opt} parameters are lower than their reported ranges. Particularly, T_{opt} was set at a lower value to initiate early season Cyanobacteria growth and to capture the smaller portion of diatom growth, i.e. the algal group that grows first in the early season but were not included in the model.

The agreement between prediction and measurement was quantified by using the coefficient of determination (R^2) as computed by the Ezyfit Toolbox in Matlab software (The MathWorks, Inc., R2008b). The measured data of T, DO, TP, and Chla from the vertical profiles of the three different sampling locations (bays) within the study area were plotted against each of their corresponding model control volume point in time and space on a scatter plot and their R^2 computed. Additional insights were gained by examining and evaluating profiles of each model prediction against meteorological data

and stream inflows to the lake. The profiles of all variables were also qualitatively examined by eye for patterns and times of maximum and minimum. This review was particularly valuable in evaluating the simulated algal growth (Robson and Hamilton, 2004; Bruce et al., 2006; Hipsey et al., 2006). The model was then run with the same configuration, parameter values, and setup for 168 days of confirmation period (Apr. 25-Oct. 10, 2005). Evaluation of agreement (goodness of fit) between model predictions and field measured data as measured by R^2 for both the calibration and confirmation periods from all three water quality stations are listed in (Fig. 2.6).

The model accurately simulated lake water level under the two hydrologically distinct periods of calibration (2000) and confirmation (2005) years. The mean difference of water level between the simulated and measured water levels (n = 151) for both years was 0.05 m with a standard deviation of 0.06 m and a range of -0.26 to +0.15 m. The simulated (2000) seasonal average of evaporation volumetric flux (0.64 m) agreed very well with the reported field value (0.77 m) (MCWD-2008). Both results indicated an accurate modeled water balance.

The model reference simulation, $g(\theta_m)$, for the calibration period, predicted the spatial and temporal variabilities of T, DO, TP, and Chla. Temperature predictions were excellent (R^2 =0.98). DO profiles agreed well at all of the three measuring locations (0.67–0.92) but missed gentle metalimnic oxygen peaks. TP (0.46–0.83) and Chla (0.38–0.48) agreed reasonably well (Fig. 2.6). The model was able to capture the spatial and temporal variations of the physical, chemical, and biological processes of the system. Specifically, the model was able to capture the drastic short duration (less than 1 week) variations of the system that were not detected by the regular biweekly measured data but were well documented by simulated DO changes in HB.

3.2.3. Model sensitivity and uncertainty analyses

The 3D hydrodynamic model, ELCOM, uses physical processes that are well defined (Hodges and Dallimore, 2008) and it requires minimal calibration with most of its model parameters set at fixed values. However, the focus of this study was to evaluate the model output sensitivity to model parameters of the ecological model, CAEDYM, which relies on numerous model parameters (Hipsey, 2008), depending on model configuration and model processes invoked during the model setup. The large number of parameters and the simulation computation cost (24 h per simulation for the full calibration period, using 2526 Mhz X86-based PC) were also a few of the major criteria for selection of the sensitivity analysis methods and only a few methods could realistically be considered (Melching and Bauwens, 2001; Ravalico et al., 2005; Van Griensven et al., 2006; Van Griensven and Meixner, 2007; Salacinska et al., 2010). The Mean Value First-Order Reliability (MFOR) method described by Melching and Bauwens (2001), and the Mean Square Root (MSQR) method described by Omlin et al. (2001) were selected to address the research objectives. Both methods assume linear correlation between the changes in model parameters and model predictions, use differential and correlation analyses, and the OAT approach (local sensitivity) to measure the effect of variability in the model parameters on the uncertainty of the model prediction (Brun et al., 2001; Melching and Bauwens, 2001; Omlin et al., 2001).

Initially, the top 40 calibrated parameters with the least values of WSS were selected and a total of 40 model simulation runs, $g(\theta_i)$, were conducted for the sensitivity and uncertainty analyses. However, 11 simulation results were excluded due to lack of sufficient prior parameter data points or unreliable simulation results. All further sensitivity and parameter ranking evaluations and analysis are based on the remaining 29 parameters (Table 2.2). No other modifications were made to the data.

Although 29 parameters were included in these analyses, only a few were expected to contribute significantly to the uncertainty in the model prediction. It is clear for example, that if 5 parameters out of a list of 100 parameters were to contribute more than 50% of

the total model variance, then the average individual contribution of all of the remaining parameters would be drastically less (Saltelli, 2008).

3.2.4. Mean Value First-Order Reliability (MFOR) method

The MFOR method (Burges and Lettenmaier, 1975; Scavia et al., 1981a, b; Chadderton et al., 1982; Melching and Bauwens, 2001) relies on the statistical moments of the estimated model parameters (θ) and the model sensitivity to yield the variance of model prediction variables (model outputs, y_k). The model sensitivity is evaluated about the best fit values of model parameters (θ_m) and is represented by $\frac{\partial g(\theta_\iota)}{\partial \theta_\iota}$ where $g(\square)$ is the function representing the model prediction variables and is computed by the forward difference numerical approach $\left(\frac{g(\theta_\iota)-g(\theta_m)}{\theta_\iota-\theta_m}\right)$ with θ_ι as the "i^{th}" parameter. All parameters are perturbed uniformly using a $\Delta\theta$ of 10%, $(\theta_\iota=\theta_m+\Delta\theta_m)$, except for parameters of the temperature multipliers where a $\Delta\theta$ of 1% was used instead.

The MFOR method implies (Melching and Bauwens, 2001) a first-order truncated Taylor series expansion of y_k:

$$y_k = g(\theta_m)+\sum_{\iota=1}^{p}(\theta_\iota-\theta_m)\left(\frac{\partial g(\theta_\iota)}{\partial \theta_\iota}\right)_{\theta_m} \qquad (2)$$

where the ι index represents the number of model parameters (θ) from 1 to p, and the expected (mean) value (E) and variance ($\sigma_{y_k}^{\,2}$), given the case of statistically independent model parameters, can be approximated by:

$$E(y_k)\approx g(\theta_m) \qquad (3)$$

And

$$var(y_k)=\sigma_{y_k}^{\,2}\approx\sum_{\iota=1}^{p}\left(\left(\frac{\partial g(\theta_\iota)}{\partial \theta_\iota}\right)_{\theta_m}\sigma_\iota\right)\left(\left(\frac{\partial g(\theta_\iota)}{\partial \theta_\iota}\right)_{\theta_m}\sigma_\iota\right)=\sum_{\iota=1}^{p}\left(\left(\frac{\partial g(\theta_\iota)}{\partial \theta_\iota}\right)_{\theta_m}\sigma_\iota\right)^2 \qquad (4)$$

where σ_{y_k} is the standard deviation of y_k, and σ_t is that of model parameters θ_t (derived from literature values, Table 2.2).

The fraction of variance resulting from each parameter for each model prediction variable $FOV_{\theta_t}(y_k)$ was calculated by dividing the variance contributed by that parameter, $var(y_k)_{\theta_t}$ by the total variance contributed by all parameters, $var(y_k)$:

$$FOV_{\theta_t}(y_k) = \frac{\left(\left(\frac{\partial g(\theta_t)}{\partial \theta_t}\right)_{\theta_m} \sigma_t\right)^2}{var(y_k)} \qquad (5)$$

The dimensionless $FOV_{\theta_t}(y_k)$ was used to evaluate the influence of each parameter (θ_t) within each of the model outputs y_k (T, DO, TP, and Chla). The average of the $FOV_{\theta_t}(y_k)_m$ of all four model outputs was calculated for each parameter and used in ranking the influence of model parameters on model predictions.

3.2.5. The Mean Square Root (MSQR) method

The MSQR method (Omlin et al., 2001) is based on the concept developed by Brun et al. (2001) stating that the uncertainty (variance) contributed by a model parameter (θ) is defined as:

$$\delta_{\theta_t}^{msqr}(\theta) = \frac{1}{\sqrt{n}} S_t(\theta) \qquad (6)$$

where *n* is the number of total sampled data, $\|S_t(\theta)\|$ is the norm (positive values) of the dimensionless sensitivity measure $S_t(\theta)$, defined as:

$$s_{\{j,k,i\},t}(\theta) = \frac{\sigma\theta_t}{\sigma y_k} \frac{\partial g(\theta_t)}{\partial \theta_t} \quad (t_j, \quad Z_{y_{k_i}}, \quad \theta) \qquad (7)$$

The uncertainty (σ) contribution of each parameter (θ_t) to the uncertainty results of the simulated model predicted variable $y_{k\,siml}$ is expressed as:

$$\sigma_{y_{k\,siml},\,\theta_t} = \sigma_{\theta_t} \frac{\partial g(\theta_t)}{\partial \theta_t}(z,t) \qquad (8)$$

and is made dimensionless by division with the standard deviation of the measured variable (σ_{y_k}). This allows a measure of sensitivity of $y_{k\,siml}$ as influenced by θ_t, by averaging the squares of the dimensionless error contributions of all corresponding model state and measured variables for all points in time and all sampling locations:

$$\delta_{\theta_t}^{msqr}(\theta) = \sqrt{\frac{1}{n}\sum_{k=1}^{y}\sum_{j=1}^{t}\sum_{i=1}^{Z_{yk}}\left(\frac{\sigma\theta_t}{\sigma y_k}\frac{\partial g(\theta_t)}{\partial \theta_t}\left(t_j,\, Z_{y_{k_i}},\, \theta\right)\right)^2} \qquad (9)$$

The $FOV_{\theta_t}(y_k)$, $\dfrac{\delta_{\theta_t}^{msqr}}{\sum_1^p \delta_{\theta_t}^{msqr}}$, was used to evaluate the influence of each parameter (θ_t) within each of the model outputs, y_k (T, DO, TP, and Chla). The sum of $FOV_{\theta_t}(y_k)$ of the four model outputs (T, DO, TP, and Chla) was computed for each parameter and used in ranking the influence of model parameters on model predictions. The dimensionless $\delta_{\theta_t}^{msqr}(\theta)$ is a global sensitivity (across all model outputs) of total model outputs to each model parameter. This made it possible to calculate the *FOV* contributed by each model output (y_k) to the total model variance, by:

$$FOV_{y_k} = \frac{\sum_t^p \delta_{\theta_t}^{msqr}}{\sum_{k=1}^{y}\sum_{t=1}^{p}\delta_{\theta_t}^{msqr}} \qquad (10)$$

The FOV_{y_k} was used to compare the influence of each model output to the total model variance and to identify the most influential model output.

3.3. Results and discussion

3.3.1. Influence of model parameters on model predicted variables

The FOV_{θ_t} in each individual model output (T, DO, TP, and Chla) were computed by the MFOR and MSQR methods and the most influential parameters for each model output were selected for analysis (Fig. 3.1).

Fig. 3.1. Percent of fraction of variance (FOV) contributed by the top ranking parameters within each of the four temperature (T), dissolved oxygen (DO), total phosphorus (TP), and algal biomass (Chla) model outputs as analyzed by a) Mean Value First-Order Reliability, and b) the Mean Square Root methods.

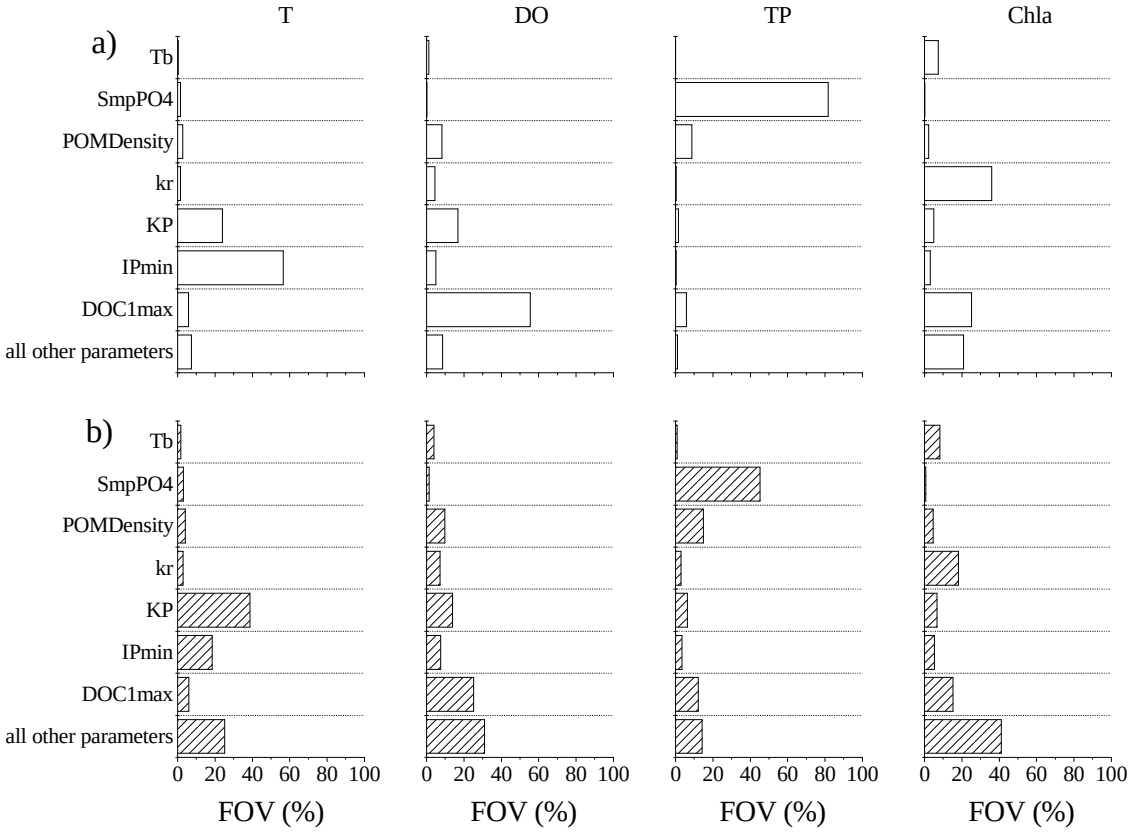

Modeled temperature output

The three biological model parameters – minimum internal P concentration (IP_{min}), half saturation constant for phosphorus (K_P), and maximum mineralization of dissolved organic carbon to dissolved inorganic carbon (DOC_{max}) – were rated as the highly influential parameters but ranked differently by the two methods. Cumulatively, IP_{min} (38%-average of the two methods), K_P (31%), and DOC_{max} (6%) together explained 75% of the total variance of model temperature output contributed by the 29 tested parameters (Fig. 3.1). In the CAEDYM model temperature prediction is impacted by light (I, μmol photons m^{-2} s^{-1}) attenuation that penetrates into the water according to Beer's Law

$$I_{(\eta_{PAR}, z)} = f_{PAR}\ I_0\ e^{\eta_{PAR} Z} \tag{12}$$

where in the case of the photosynthetically active radiation (PAR) fraction, $I_{(\eta_{PAR}, Z)}$ is the intensity of PAR at depth Z, and I_0 is the incident shortwave intensity. $I_{(\eta_{PAR}, Z)}$ is influenced by the PAR extinction coefficient (η_{PAR}) which in turn is dynamically calculated at each time step depending on concentrations of algal biomass (A_a), suspended particle concentration (SS_S), particulate organic carbon (POC), and dissolved organic carbon (DOC) concentration.

$$\eta_{PAR} = \eta_w + \sum_a \eta_A\ A_a + \sum_S \eta_{SS}\ SS_S + \sum_{POC} \eta_{POC}\ POC + \sum_{DOC} \eta_{DOC}\ DOC \tag{13}$$

The higher ranking parameters of IP_{min} and K_P influence algal biomass where *Microcystis* relies on the stored internal P to grow when the available P becomes scarce in the water column. Therefore, in a P limited system, *Microcyctis* growth is influenced by the level of the minimum internal P concentration and its biomass ultimately influences the extinction coefficient (Eq. 13). The sensitivity of the extinction coefficient variability to IP_{min} reflects a P limited system. Similarly, the DOC_{max} influences the dissolved organic carbon (DOC) concentration in the water column which impacts the extinction coefficient. All three parameters ultimately influence temperature.

Modeled dissolved oxygen output

The oxygen rate equation in the DO module as configured in CAEDYM included atmospheric flux (*ATM*), algal group photosynthetic oxygen production (*PHY*) and respiration consumption (R), oxidation through nitrification (*OXD*), sediment oxygen demand (*SED*), and oxygen uptake through organic matter decomposition (*BOD*).

$$\frac{\partial DO}{\partial t} = f_{O_2}^{ATM} + f_{O_2}^{PHY} - f_{O_2}^{R} - f_{O_2}^{OXY} - f_{O_2}^{SED} - f_{O_2}^{BOD} \quad (14)$$

The sensitivity analyses showed that the three parameters of DOC_{max}, K_P, and density of particulate organic matter particles ($POM_{Density}$) were most influential and they were ranked in the same order by both methods (Fig. 3.1). The three parameters explained about 65% of the total variance observed in DO model output. The DOC_{max} parameter is most dominant in the BOD processes and specifically in the utilization (U_{DOC}) of oxygen through mineralization of organic matter (Eq. 15)

$$U_{DOC} = DOC_{max}\, f(DO)\, f(T)\, DOC\, Y_{O_2:C} \quad (15)$$

where $Y_{O_2:C}$ is the conversion of carbon to DO. The rate of the dissolved inorganic (DI) nutrients (C, N, and P) that is available to algae controls algal biomass and in turn the DO production. Bacteria, responsible for mineralization of dissolved organic carbon to dissolved inorganic carbon, were not simulated; however, their nutrient uptake was considered as part of the DOC_{max} parameter. Similarly, Chen et al. (2002) demonstrated that the maximum dissolved organic P uptake rate by bacteria in Lake Michigan was the top ranking parameter in the sensitivity analysis. The model parameter K_P is used by CAEDYM to model the algae internal phosphorus dynamics, which directly impacts algal growth and, consequently, DO concentrations. The $POM_{Density}$ determines the availability and the rate of dissolved organic matter mineralization where heavier particulate organic matter would settle faster and minimize their availability for mineralization. Bruce et al. (2006) suggested $POM_{Density}$ as the parameter to which CAEDYM was most sensitive in the prediction of DO dynamics in Lake Kinneret, Israel, and Romero et al. (2004) identified particle settling and resuspension parameters as essential in improving the algal growth component of the model.

Modeled total phosphorus output

The phosphorus rate equation in CAEDYM as configured includes PO_4, as simulated in the model and reported as the filterable (soluble) reactive phosphorus (*FRP*), dissolved organic phosphorus (*DOP*), and particulate organic phosphorus (*POP*).

$$\text{Total Phosphorus, } TP = FRP + DOP + POP \quad (16)$$

The model parameters of the sediment release rate of phosphorus ($SmpPO_4$), $POM_{Density}$, and DOC_{max} explained about 85% of the variance for TP model output. The FOV of $SmpPO_4$ calculated by the MFOR method (82%) was near twice as large as that estimated by the MSQR method (45%). However, all three parameters were ranked in the same order by the two methods (Fig. 3.1). The parameters $SmpPO_4$ along with the parameter of the sensitivity of PO_4 flux to the overlaying concentration of DO ($KOxS\text{-}PO_4$) are used in the CAEDYM static sediment model to determine the release of FRP from sediment

$$f_{FRP} = \text{SmpPO}_4 \, f\left(DO\right) f\left(T\right) \left({}^{1}\!/\!_{\text{Z}_{\text{bot}}} \right) \quad (17)$$

where Z_{bot} is the layer above the sediment-water interface and $f\left(\text{DO}\right)$ is defined as:

$$f\left(\text{DO}\right) = \frac{\left(\text{KOxS} - \text{PO4}\right)}{\left(\text{KOxS} - \text{PO4}\right) + \text{DO}_{\text{bot}}} \quad (18)$$

The hypoliminic TP concentrations are negatively correlated (R^2= -0.86) with the depletion of overlaying DO concentrations that become anoxic early in the season (Fig. 3.2). Therefore, $SmpPO_4$ becomes an influential parameter as it regulates the release rate of PO_4 from sediment into the water column (internal loading) where it is readily taken up by algae and directly impacts biological components and geochemical cycles (Christophoridis and Fytianos, 2006; Belmont et al., 2009; Radcliffe et al., 2009). The timing and the degree of hypoliminic anoxic condition determines the magnititute of the internal loading and its consequences on water quality.

Fig. 3.2. Simulated time series of dissolved oxygen (DO Bottom) and total phosphorus (TP Bottom) at 1 m above the sediment bed, and TP at 1 m below the water surface (TP Surface).

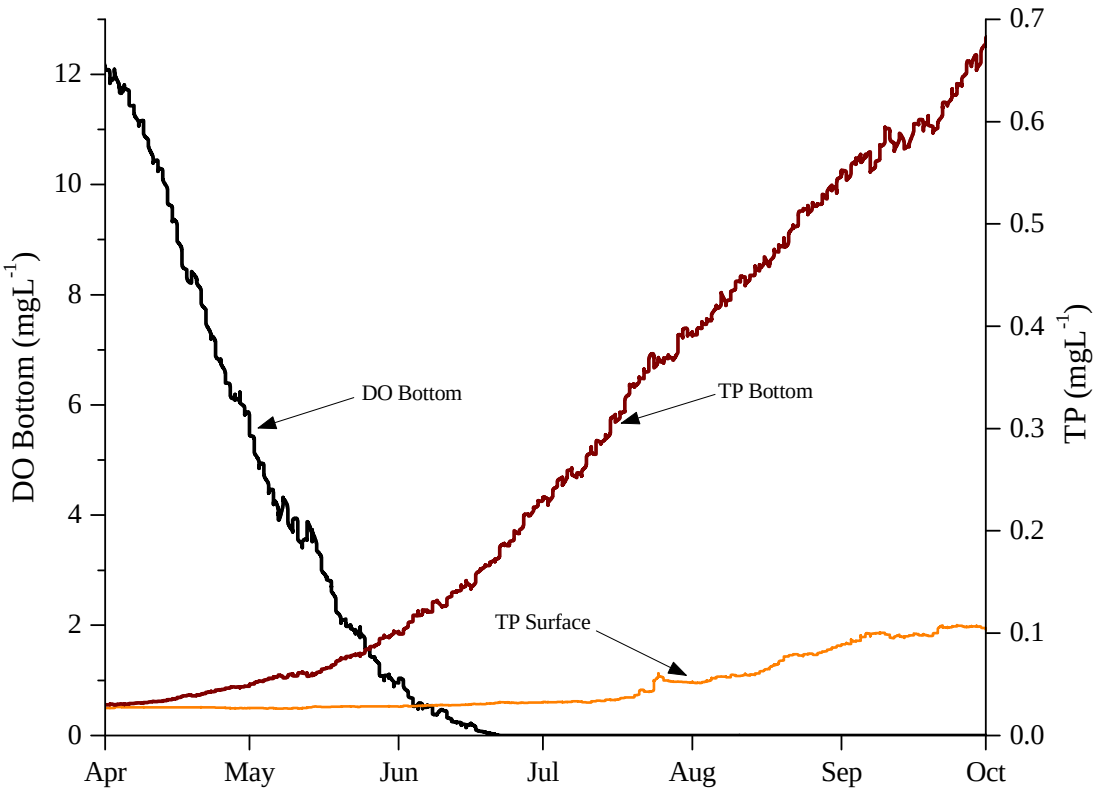

Modeled algal biomass output

The three most influential model parameters $DOC_{max,}$, the respiration rate coefficient (respiration and metabolic loss, kr), and the temperature multiplier function (θT_b) explained 55% of the observed variance within the model predicted Chla. The high ranking of the DOC_{max} parameter represents the cycle of mineralization of DOC to dissolved inorganic carbon (DIC) and eventual biological uptake and it relates to bacteria responsible for mineralization of DOC to DIC. $POM_{Density}$ regulates the availability of DOC mineralization and is essential in providing nutrients in the algal growth model.

The respiration rate coefficient influences the photosynthetic oxygen production:

$$f_{O_2}^{PHY} = (P_{max}\, f(\mathrm{T}) \min\left[f(\mathrm{N}), f(\mathrm{P}), P(I) \right] - \mathrm{kr})\; Y_{O_2:C}\; Y_{C:Chla}\; A \qquad (19)$$

where $Y_{C:Chla}$, is the stoichiometric factor that converts chlorophyll *a* to carbon. The respiration rate coefficient (kr), also influences the general loss term (*L*) used in the model

$$L = \mathrm{kr}\theta \mathrm{T}_r^{\mathrm{T}-20} + \mathrm{k}_{\mathrm{rp}}\mu_g \qquad (20)$$

where μ_g is algal growth rate, g represents Cyanobacteria, the phytoplankton group configured in the simulations, and k_{rp} is the fraction of production lost during photosynthesis. Together, the components of the total loss term include the constant loss fractions such as respiration, excretion, particulate matter (detritus), and settling. Loss rate is then multiplied by the dynamic internal nutrient concentrations to determine metabolic loss due to mortality and exudation. The $\mathrm{IP}_{\mathrm{min}}$ parameter itself did not rank as high as expected but it does influence the loss term which was ranked high. Grazing by zooplankton was not specifically configured in the model, but was lumped into the loss term kr. The sensitivity of the model to the loss term is important because it shows that predation could be an important factor and necessitates the modeling of zooplankton which may also better highlight the influence of $\mathrm{IP}_{\mathrm{min}}$ on algal biomass.

Algal growth depends on availability and rate of mineralization ($\mathrm{DOC}_{\mathrm{max}}$) and its magnitude is determined by $\theta \mathrm{T}_{\mathrm{b}}$ where μ_g is modeled by maximum potential growth rate (P_{max}) at 20 °C multiplied by θT_b, and the minimum value of expressions for limitation by light, phosphorus, and nitrogen.

$$\mu_g = P_{max} \min\left[f(\mathrm{I}), f(\mathrm{N}), F(\mathrm{P}) \right] f(\mathrm{T}) \qquad (21)$$

The maximum growth is achieved at the optimum temperature ($\mathrm{T}_{\mathrm{opt}}$) with zero growth over the maximum temperature ($\mathrm{T}_{\mathrm{max}}$).

It is worth mentioning that the other temperature related parameters, $\mathrm{T}_{\mathrm{max}}$ and $\mathrm{T}_{\mathrm{sta}}$ were ranked as the 11$^{\mathrm{th}}$ and 12$^{\mathrm{th}}$ highest ranking parameters by both methods (not shown). The

model sets the growth rate to zero for any temperature above T_{max}, and for any temperature below T_{sta}, it follows an exponential relation similar to the loss term with temperature multipliers determining the slope of the growth rate. The sensitivity of the model outputs to algae temperature related parameters are a consequence of the dependencies of algal biomass on temperature. This is important because the study area has a large horizontal (spatial) temperature heterogeneity that may lead to increased algal biomass within different bays with similar geochemical concentrations; therefore, algal spatial distribution has significant ecological importance (Robson and Hamilton, 2004; Salacinska et al., 2010; Wu et al., 2010).

The total influence of the three highest ranking model parameters on the total model variance is less for Chla than for the other model outputs. This result indicates that model predicted Chla sensitivity is spread over a larger number of biological model parameters. A process that further exacerbates the problem is the model configuration setup where different sets of model routines or groups of phytoplankton can be configured simultaneously, leading to an increased need for an additional number of parameters and expanded parameter intra-dependency. Up to seven groups of phytoplankton may be configured in CAEDYM, and each group has its own set of biological model parameters which multiplies the number of total model parameters. There is also a large interdependence between the different functional groups (Mieleitner and Reichert, 2008) which compounds the complexity. The biological parameter identifiability also involves neighboring parameter sets where the value of one parameter depends on and can influence the values of other parameters and different sets of values of parameters may lead to similar simulation results (Beck, 1987; Mieleitner and Reichert, 2008). Therefore, a universal set of best parameter values may not be identified. For that reason, the Cyanobacteria group was the only algae group configured in the simulations in order to keep the number of parameters manageable. Furthermore, the Cyanobacteria group constitutes of nearly 80% of the total algae in the system.

3.3.2. Model parameter ranking

The fraction of variance of every parameter (FOV_{θ_i}) was calculated by the MFOR and MSQR methods and used for evaluation and ranking of the most influential model parameters. The results of the two methods agreed very well (Fig. 3.3). On average, the MFOR ranking method had a 30% larger slope (faster accumulation of the proportion of the total variance for the highest ranking parameters) than for the MSQR method. In the MFOR method the first four highly ranked parameters (DOC_{max}, $SmpPO_4$, IP_{min}, and K_P) explained over 70% of the total variance of model predictions. However, the MSQR method required the contribution of seven parameters (DOC_{max}, $SmpPO_4$, kr, K_P, $POM_{Density}$, θT_b, and IP_{min}) to reach the same level. The ranking of the first and second most influential parameters (DOC_{max}, $SmpPO_4$) were the same for both methods, but the ranking order of the other top ranked parameters were different. Nonetheless, nine out of the top ten parameters were identified by both methods (Fig. 3.3). The four parameters related to sediment nutrient and DO flux ($SmpPO_4$, sSOs, KOxS-PO_4, and KSOs) were all in the top 10 ranking model parameters (Fig.3.3), a fact that reflects the system's potential sensitivity to internal loading.

Fig. 3.3. Model parameter ranking measured by the fraction of variance (FOV) contribution by each parameter (values in parenthesis) and evaluated by the Mean Value First-Order Reliability (dark line) and the Mean Square Root (gray line) methods.

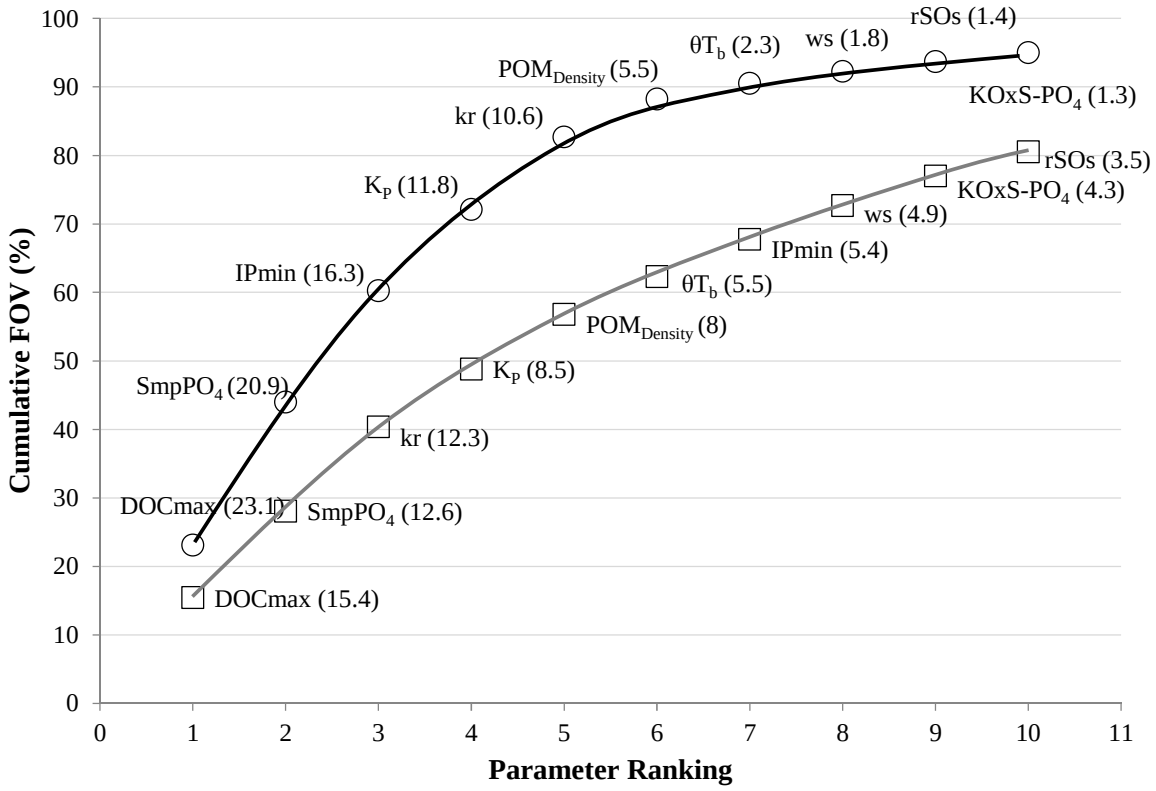

3.3.3. Contributions of model predicted variables to total variance

The dimensionless sensitivity measure, $\delta_{\theta_i}^{msqr}(\theta)$, derived by the MSQR sensitivity and uncertainty method created a gauge for the global sensitivity of total model outputs to each model parameter (Omlin et al., 2001) that made it possible to calculate the contributions of each of the model predicted variables (FOV_{y_k}) to the total model output variation. The results showed that the model predicted biological component (Chla) had the greatest contribution to the total model variance followed by TP, DO, and T output with FOV contributions of 58, 26, 13, and 3%, respectively. This corresponds well with

the results of the model goodness of fit (R^2) from the model calibration process where T had the best fit and the biological component of the model (Chla) had the poorest fit between the measured data and simulated model predicted variable (Fig. 2.6). In this case, the *FOV* of each model output was defined as their contributed variability ($1-R^2$) divided by the total of the four model output variabilities. The FOV of model predicted variables derived from calibration process correlated very well with those derived from the MSQR method (Fig. 3.4).

Fig. 3.4. Comparison of the fraction of variance (FOV) contributed by each model predicted variable of temperature (T), dissolved oxygen (DO), total phosphorus (TP), and algal biomass (Chla) to the total model variance as derived by Mean Square Root (MSQR) method and model calibration process for West Upper Bay location.

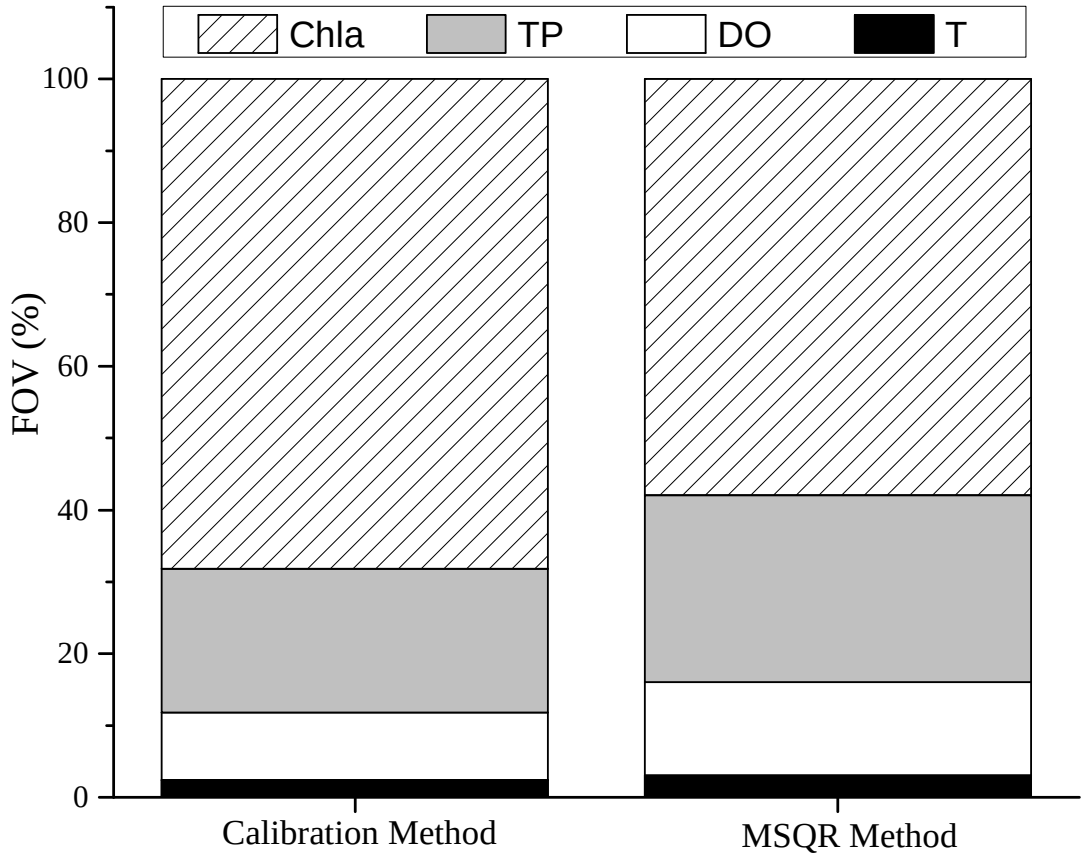

The relative parameter contributions to each model predicted variable and the relative variability contributed by each model predicted variable to total model variability is shown in Figure 3.5. The analysis confirms the earlier observation that Chla output sensitivity is spread over a larger number of parameters, with almost 40% of the variance depending on all other lower ranking parameters. The results show that there are model outputs (T, DO, TP, Chla) of specific influential parameters which reflect the design of rate equations and their sensitivity to these parameters. However, there are also parameters that influence multiple model predicted variables reflecting the interaction of various processes. The analyses of these parameters and their related processes have yielded a greater understanding of ecological processes of the system (Makler-Pick et al., 2011).

Fig. 3.5. Contributions of model predicted variables to total model variance measured by percent fraction of variance (FOV) of each output (T, DO, TP, and Chla) to the total model variance. The contributions of model parameters within each of the model output variables also are shown.

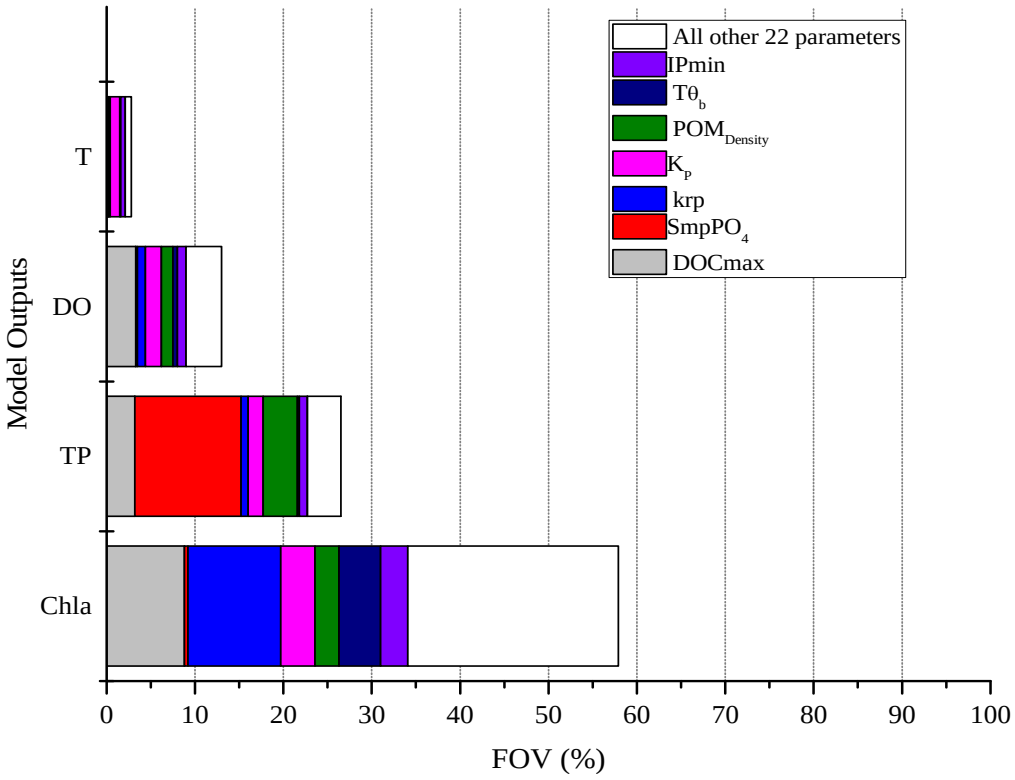

3.3.4. Spatial and temporal visualization of model uncertainty

The average model predicted variables (model outputs) along with their standard deviation (σ) and coefficient of variation (COV) were plotted on contour maps to visualize the spatial and temporal variabilities of model uncertainty (variances) (Fig. 3.6). Starting mid-June, the concentration of DO is rapidly depleted at depths below 9 m and its value in the control volume approaches zero. This creates a situation where the COV (σ/average) becomes infinity; therefore, the DO plots were not included in the analyses.

The impact of seasonal meteorological forces on the model outputs are readily observed (Fig. 3.6). The water temperature gradually increases from 4 °C at the start of the season in April to 26 °C in July, and gradually decreases down to 14 °C at the end of the simulation period in October. Whereas, for the same periods, DO (not shown) starts at about 14 mgL^{-1}, then gradually declines to 5 mgL^{-1}, and gradually rises again to about 10 mgL^{-1}. On the other hand, TP stays below 0.03 mgL^{-1} until July 7th (the largest rainstorm and stream inflow event), and then steadily increases to near 0.12 mgL^{-1}. The influence of Chla on DO and TP concentrations also is evident. In the hypolimnion, a steady increase of TP, initiated by anoxia, is observed as well.

Model uncertainty appeared to be concentrated around certain depths and dates (e.g., April 26; July 6-22; and August 12-17) (Fig. 3.6). An analysis of these dates revealed that they closely corresponded to stream inflow into the lake generated from rainstorm events. Previous investigations of lake model results had indicated that the lake hydrodynamic and ecological processes area are sensitive to mixing due to inflow and wind variabilities as observed in similar investigations (Scavia and Fahnenstiel, 1987; Asaeda, et al., 2001; Chen et al., 2002; Robson and Hamilton, 2004; Hondzo and Warnaars, 2008). It was also observed that periods with extreme, sudden, and short term duration of varying DO concentrations in the water column were driven by stream inflow events

Fig. 3.6. Contour plots of spatial and temporal variabilities: a) average model output (T, TP, Chla), b) standard deviation (σ) of the model outputs from the sensitivity analysis of the 29 model parameters; and c) coefficient of variation (σ/average).

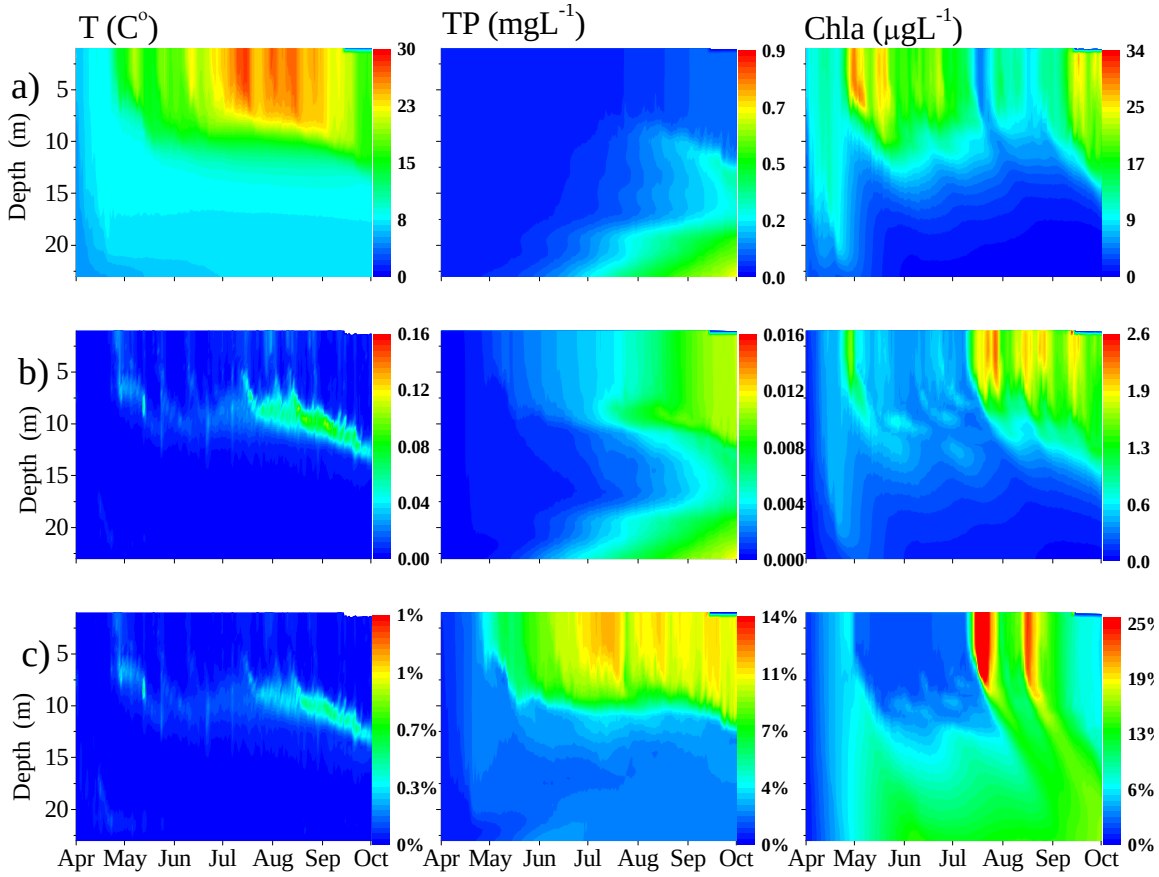

The spatial and temporal model uncertainties were further evaluated by analyzing the COV of model outputs at three different fixed water column layers. These values were plotted against the flow of a major stream (Six Mile Creek) that contributes 25% of the total inflow to the lake. The COV in each of three depth averaged layers of top (top 8 m,), middle (8.5-10 m), and bottom (10.5-25 m) showed a distinct pattern and behavior. The impacts of spring and late season water column mixing, summer stratification, and stream event inflows on model outputs are readily observed (Fig. 3.7). In the top layer, DO correlated best (R^2 values in parenthesis) with Chla (0.88) and TP (0.52) outputs. The rapid rise of the COV (greater model output uncertainty) for both DO and Chla are preceded by the largest streamflow event. In the middle layer the COV of T correlated

best with that of Chla (0.77) and DO (0.41), followed by correlation between Chla and TP (0.32). Rapid COV fluctuations of DO are focused in periods of the largest inflows. The largest COV values of Chla are observed later in the season in the same period of the largest streamflow events and the largest COV values of T are during the spring streamflow events. In the bottom layer, the COV of Chla correlated best with T (0.7) and TP (0.61) followed by the correlation between T and TP (0.45).

Generally, the largest values of COV coincide with the stream inflow to the lake generated from rainstorm events in the top and middle layers and it appears that model performance is most sensitive to changes of parameter values during these periods. These findings are supported by the authors' previous findings that the greatest range (max-min) of model output values in each control volume were near the thermocline and on the surface (Missaghi and Hondzo, 2010). The results suggest that spatial and temporal variations of the model outputs are sensitive to the hydrodynamics of physical perturbations such as stream inflows.

Fig. 3.7. Comparison of the stream flow (m^3s^{-1}) with the coefficient of variation (COV) of the model output temperature (T), dissolved oxygen (DO), total phosphorus (TP), and algal biomass (Chla) in a) upper, b) middle, and c) bottom water layers where multiplication factors for the right hand side Y axis are (0.00125, 0.033, 0.05, 0.2), (0.0033, 1, 0.05, 0.1), and (0.0009, --, 0.02, 0.1), respectively.

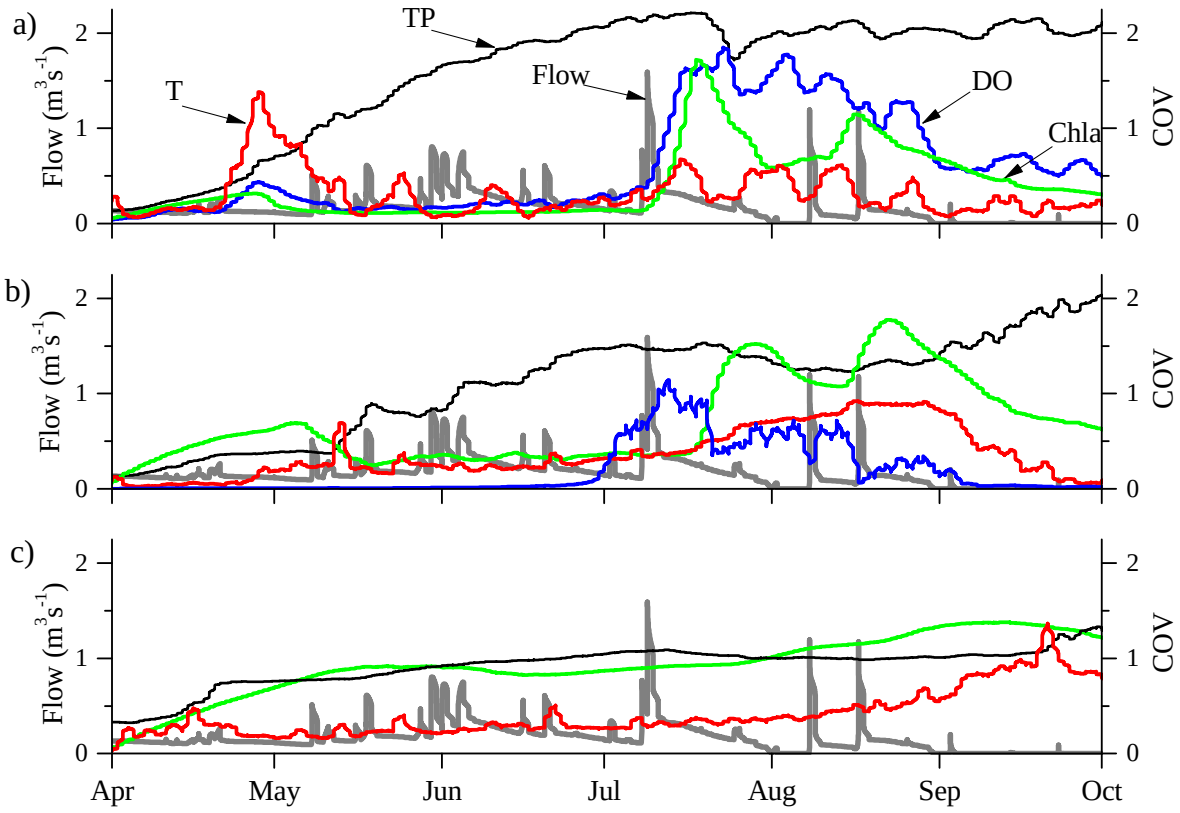

3.4. Conclusions

A 3D coupled hydrodynamic and ecologic model was applied in a morphologically complex shallow lake. The model parameter estimation, sensitivity and uncertainty analyses by two methods, and parameter sensitivity ranking were presented. The most influential model parameters in the simulation of model output variables T, DO, TP, and Chla were successfully ranked by the MFOR and MSQR methods and the results agreed very well. Seventy percent of the total model output uncertainty (variance) was

explained by the four highest ranked model parameters (DOC_{max}, $SmpPO_4$, IP_{min}, and K_P) using the MFOR method and the seven highest ranked parameters (DOC_{max}, $SmpPO_4$, kr, K_P, $POM_{Density}$, θT_b, and IP_{min}) using the MSQR method. However, the parameters influenced the variance of each model output differently based on model equations and the ecological processes of the system.

The three model parameters of IP_{min}, K_P, and DOC_{max} explained 75% of model predicted T variance. DOC_{max}, K_P, and $POM_{Density}$ contributed 65% of the variance observed in DO model output with DOC_{max} as the most prominent parameter. $SmpPO_4$, $POM_{Density}$, and DOC_{max} explained 85% of the variance of model predicted TP variable. Model simulations suggest that the lake is strongly sensitive to internal loading, a fact that should be considered in any future management schemes.

The model outputs of T, DO, TP, and Chla contributed 3, 13, 26, and 58% to the total model variance, respectively. This corresponded with the model performance (fit) (Fig. 2.6). The Chla output sensitivity was spread over a larger number of parameters, with almost 40% of the variance depending on all other lower ranking parameters. The analysis highlighted the need for a greater understanding and number of field measurements of biological model parameters and inclusion of zooplankton in the model. The sensitivity and uncertainty analyses were limited to model predictions at only one location in the study area. Future work should evaluate model sensitivity at more than one location (bays) to aid in establishing a stronger set of best fit model parameter values with greater transferability (universality).

Contour maps of COV of the model predictions showed that COV values were the greatest around specific depths and time periods. In the epilimnion and thermocline the largest values of COV coincided with streamflow events where model performance is most sensitive to changes in parameter values. Therefore, simulation periods selected for 3D sensitivity and uncertainty analyses must include periods with appreciable rainstorm

events and corresponding inflows to the lake. Such an approach may also improve the water quality monitoring plans and regimes to better capture the system processes that happen at different scales and during the growing season, and to reveal any needs for additional field data. The application of the two sensitivity and uncertainty analyses have expanded the understanding of a 3D coupled hydrodynamic and ecological model sensitivity to its parameters and the interaction of various ecological processes within a morphologically complex system.

CHAPTER 4

Influence of fluid motion on growth and vertical distribution of Cyanobacterium *Microcystis aeruginosa*

Microcystis aeruginosa (*Microcystis)* is rapidly becoming one of the dominant alga in lakes surrounded by urban and agriculture dominated landscapes. We conducted laboratory study by measuring the population growth and vertical distribution of *Microcystis* in a Plankton Tower bioreactor. An oscillating grid was installed on the top of one of the columns in the Plankton Tower and operated at selected frequencies of 0.5, 1, 1.5, 2, and 3 Hz to generate turbulence with negligible time-averaged fluid flow. The effects of fluid motion on *Microcystis* growth rate and vertical variations were evident by a 32% and 246% increase in growth rate and vertical cell concentration corresponding to a depth-averaged energy dissipation rate ($\langle\varepsilon\rangle$) of 1.3 x 10^{-6} m^2s^{-3} in the Plankton Tower. Turbulent conditions generated at $\langle\varepsilon\rangle$ >3 x 10^{-6} m^2 s^{-3} suppressed the growth of *Microcystis* and for $\langle\varepsilon\rangle$ < 3 x 10^{-7} the fluid flow had a minimal impact on growth. The laboratory results indicated that $\langle\varepsilon\rangle$ in the range from 3 x 10^{-7} to 3 x 10^{-6} m^2 s^{-3} facilitated *Microcystis* growth. Findings from this study can facilitate a greater understanding of physiology and spatial distribution of *Microcystis* in aquatic ecosystems. The results will be instrumental in developing mechanistic models of spatial and temporal variabilities of *Microcystis* that can enhance management of aquatic ecosystems.

4.1. Introduction

The cyanobacterium *Microcystis aeruginosa* (*Microcystis),* is one of the algae groups that is rapidly exploiting a growing number of eutrophic lakes that are fed by excessive urban and agricultural runoff (Kearns and Hunter, 2000). Cyanobacteria are remarkably well adapted to live in a wide array of ecosystems with extreme physical and chemical conditions (Ferris and Hirsch, 1991; Whitton and Potts, 2000; Visser et al., 2005). *Microcystis* naturally form mucilaginous colonies or coenobia (20-400 µm) and can gain positive buoyancy by regulating their gas vacuoles and through synthesis of their carbohydrate content (Reynolds, 2006; Hunter et al., 2008; Šejnohová, 2008; Wang et al., 2010). Under certain environmental conditions *Microcystis* population may bloom, which is to grow at a very rapid rate and reach extremely high cell densities. It is suggested that in the absence of a critical wind speed (such as >3 ms^{-1}) the colonies in a bloom float to the water surface and form a dense layer called scum (Wu and Kong, 2009).

The *Microcystis* blooms and its associated scums may create foul odors and tastes, shade other organisms, severely alter the flow of food and carbon, and deplete oxygen from bottom waters through their decomposition after die-off and cause fish kill, (Paerl et al., 2001; Haven, 2008). *Microcystis* are the leading producers of the toxin microcytins and are a serious health hazard to wildlife and human health globally (Dokulil and Tebner, 2000; Efteland, 2004; Zurawell et al., 2005; Heisler, et al., 2008; Herrero, et al., 2008; Lopez et al., 2008). Harmful algae blooms are becoming rapidly more prevalent due to a combination of eutrophication and climate change (Heisler, et al., 2008; Paerl and Huisman, 2009; O'Neil et al., 2012; Ekvall et at., 2013).

Microcystis scums are commonly associated with warm, calm, and nutrient rich waters (Reynolds, 2006; Carraro et al., 2012). Algae "scum" is at times incorrectly perceived as being caused by a large algal population growth at the surface of water; however, algal scum is merely the accumulation of the algae bloom at the surface of the water in the

absence of sufficient wind energy to keep it distributed within the water column. Algae may have a considerable vertical structure with the highest concentration of algae, such as Cyanobacteria, growing at 2-9 m, depth (Wojciechowsk et al, 2004; Maier et al., 2008; unpublished data). The deep chlorophyll maximum studies and modeling efforts (Cullen, 1982; Robson and Hamilton, 2004; Leon et al, 2011; Carraro et al., 2012; Fernand et al., 2013; Painting and Foster, 2013) recognize the need to integrate physical processes to better understand algal uptake of nutrients, growth, and population density in the water column (Varela et al., 1992).

Microcystis horizontal distribution and patchiness within a water body is driven by advective flow generated by inflow (Qin, 2013) and wind (Hunter et al., 2008; Wu et al., 2010; Carraro et al., 2012; Yajima and Choi, 2013;). *Microcystis* vertical distribution appears to be influenced by mixing conditions in the water column. Depth integrated populations of *Microcystis*, unlike that of the temporary visible surface blooms, have smooth, slow, seasonal (temporal) dynamics, but they show frequent vertical changes that are influenced by local fluid flow conditions (Abbott et al., 1984; Wallace et al., 2000; Pasztaleniec, 2004; Johnk et al., 2008; Moreno-Ostos et al., 2009; Wu and Kong, 2009). Various wind speeds (3-6 ms^{-1}) have been suggested as the critical wind speed needed to generate enough fluid motion to drive *Microcystis* away from the water surface (Wu et al., 2013). On the other hand, in the case of sinking algae, a critical turbulence range, or window, within the water column appears to exist where algae can overcome both mixing and sinking rates and flourish prior to algal bloom (Huisman et al., 1999).

Several experimental studies have demonstrated that fluid motion has effects on algal growth and nutrient uptake rates (e.g. Sullivan et al., 2003; Xiao-li et al., 2004; Peters et al., 2006; Hondzo and Warnaars, 2008). O□Brien et al., (2004) demonstrated the influence of turbulence levels on *Microcystis* colony size. Process-based and three-dimensional (3-D) lake water quality models, have demonstrated that cyanobacteria, *Planktothrix rubescens,* has distinct spatial and temporal distributions that are strongly

influenced by the lake hydrodynamics (Carraro et al., 2012). The current understanding of *Microcystis* bloom formation is limited, and there is a need to better describe and identify the forcing factors and processes influencing *Microcystis* growth and spatial distribution (Regel et al., 2004; Sharma et al., 2009; Wu et al., 2010; Wu et al., 2013).

The motivation for this study was to quantify the influence of fluid motion and corresponding rate of energy dissipation levels on the growth and vertical variability of *Microcystis* under controlled laboratory conditions.

4.2. Materials and methods

4.2.1. Species and cultivation

The *Microcystis* strain was provided by the Department of Fisheries and Allied Aquacultures, Auburn University, Alabama (Wilson, 2011, personal communication). Ten healthy *Microcystis* colonies from original cultures were transferred into sterile culture tubes with 15 mL of modified BG-11 medium media (Sigma -C3061, Sigma-Aldrich, MO) and Milli-Q water (Renaud et al., 2011). All colony transfers were performed under laminar flow hood and sterilized conditions. Culture tubes were incubated at 20 ºC, with an average 140 photosynthetically active radiation (PAR) downwelling cool white fluorescent light on a 14:10 light-dark cycle. After an acclimation period of three weeks, colonies were transferred into stock cultures in 1000 mL Erlenmeyer flasks containing 250 mL of modified BG-11 medium, covered with loose aluminum foil, and incubated under the same conditions. Two weeks prior to each experiment, stock cultures were transferred into a 3000 mL Erlenmeyer flask batch culture containing 2000 mL of modified BG-11 medium. These actively growing batch cultures were used to seed the Plankton Tower columns containing modified BG-11 medium to a cell concentration of about 5×10^4 cells mL^{-1}. Frequently, samples from all cultures were inspected microscopically to detect any contaminations and only healthy cultures were used in the experiments (Fig. 4.1).

Fig. 4.1. Microscopic images of *Microcystis aeruginosa* a) large colonies, b)-c) cell aggregates, and d) unicellular culture (cell diameter about ~5 μm) that was used for the experiments.

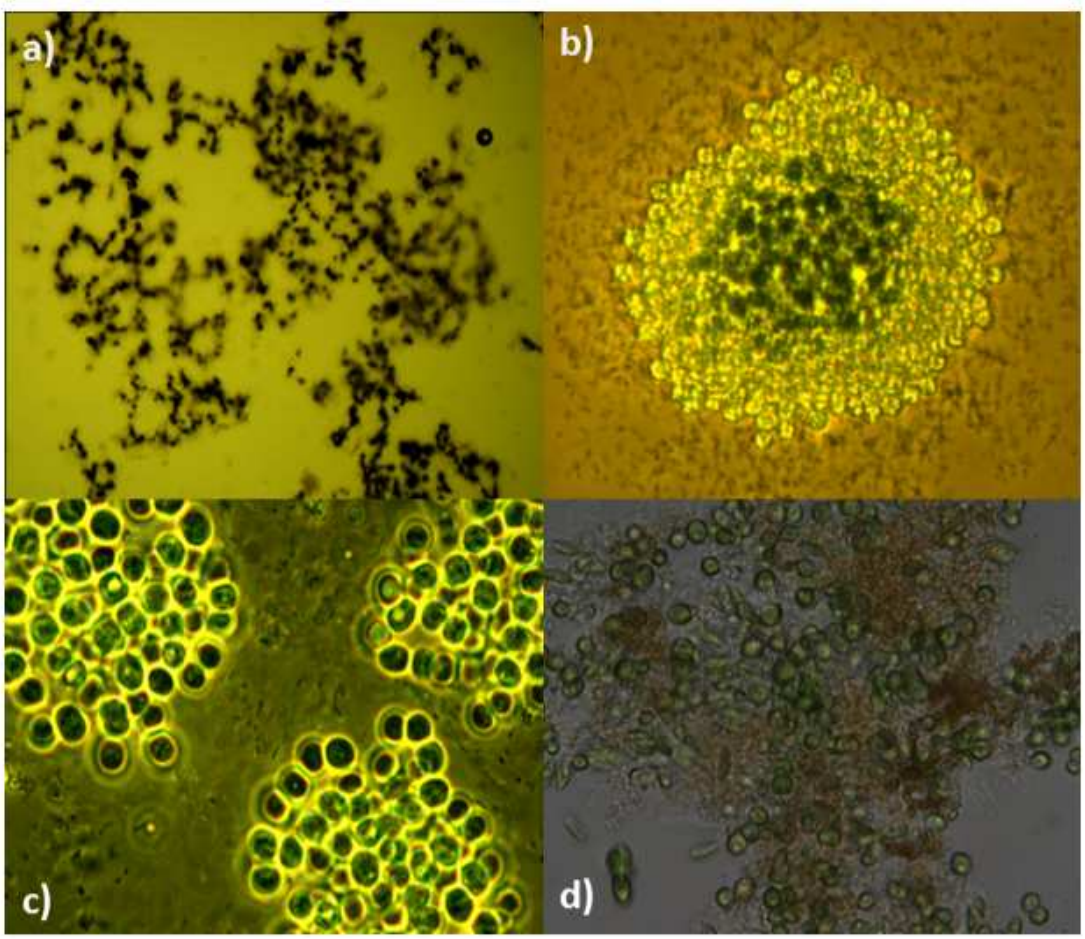

4.2.2. The Plankton Tower bioreactor

The Plankton Tower (PT) bioreactor (1.5 m x 0.6 m x 0.2 m) is a two column (0.2 x 0.2 m) Plexiglass tower that was designed at the Saint Anthony Falls Laboratory, University of Minnesota (Spitael, 2007). The PT has two independent columns that are entirely separated from each other, filled with the same fluid, and are exposed to similar external environmental factors such as temperature and PAR. One of the columns was used as experimental control with no fluid motion in the column and in the second column, fluid motion was systematically controlled. A computer controlled oscillating grid with

variable oscillating frequency was installed at the top of the second column to generate vertical distributed turbulence. The PT was placed in a dark room with controlled air temperature and was illuminated at an averaged PAR of 140 µmol photon $m^{-2}s^{-1}$, using cool fluorescent lights on a 14:10 light-dark cycle (Fig. 4.2). The lights were vertically oriented and mounted at the side of the PT such that algal cells experience uniform exposure to PAR over the entire column. Water temperature was maintained at 21.5 ºC with negligible stratification effects (temperature differences in each column, at different heights, were within 1 ºC). The *Microcystis* cultures were grown in the PT under specified conditions including a control column (without fluid motion) and the column with a variety of turbulence levels that were generated by the oscillating grid setup operated at selected frequencies (*f*). Therefore, the only experimental variable in the PT was fluid motion. All the other environmental conditions (temperature, light, initial nutrient concentrations) that could possibly influence the growth of *Microcystis* in the columns were controlled.

Fig. 4.2. Photograph of the experimental bioreactor (Plankton Tower; 1.5 m x 0.6 m x 0.2 m) with two independent sealed columns that were used for algal growth experiments with one column used as (a) control column without fluid motion and b) turbulent column with fluid motion generated by the oscillating grid. Location of the oscillating grid along with the horizontal (x) and vertical (z) axes are also shown.

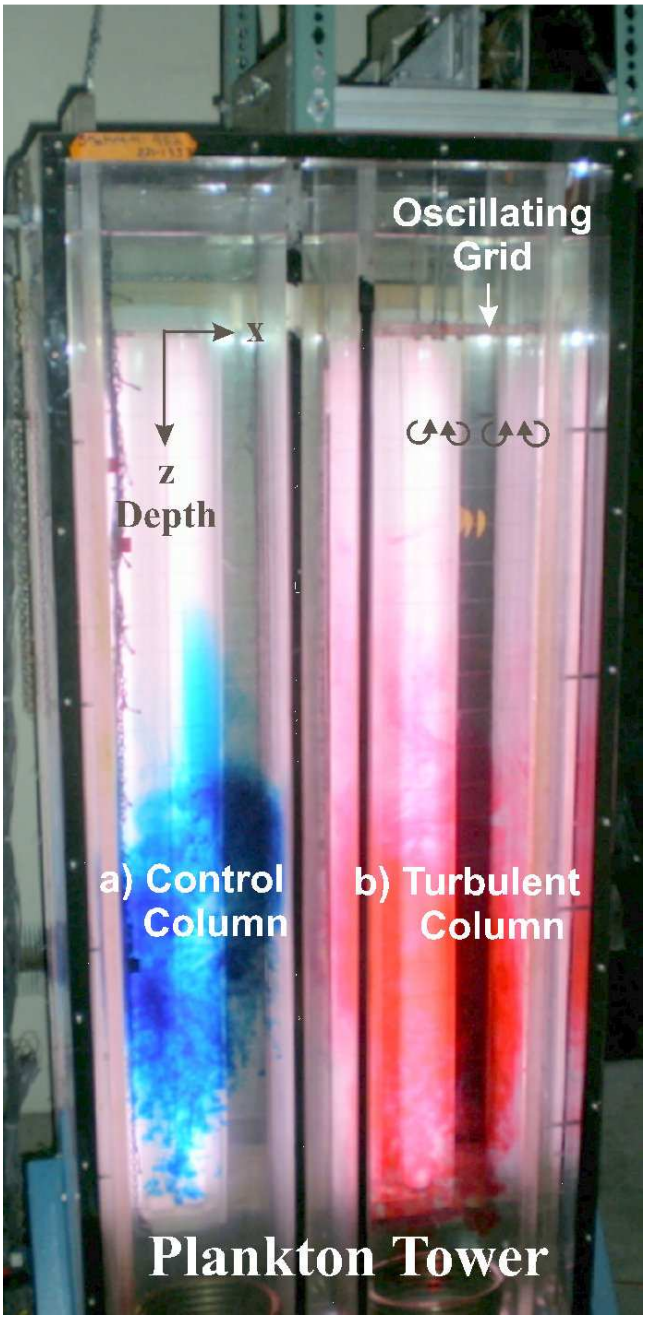

4.2.3. Laboratory measurements

Microcystis cell count (cells mL^{-1}) was conducted using a haemocytometer and chlorophyll *a* (Chl-a) concentration was determined spectrophotometrically using 90% acetone extraction (Clesceri et al., 1995). Vertical cell concentration profiles, C_f (cells mL^{-1}), of each PT columns (stagnant and turbulent) were obtained using a Turner Designs Cyclops-7, an *in vivo* fluorescence cyanobacteria sensor (Sunnyvale, CA). Cyclopes-7 was connected to a computer controlled mechanical traversing system ensuring that profile measurements were taken at specific times and vertical locations with predefined acquisition frequencies and measurement periods.

Microcystis cell concentration is doubled at a constant rate during the exponential phase of its growth cycle where the values of cell concentrations plotted on a natural log scale will produce a straight line. The slope of this line is the algae growth rate (k_g) based on the changes of cell concentrations (cells mL^{-1}) during the exponential growth period and is determined as:

$$k_g = \frac{\ln\left(\frac{\langle C_f \rangle_2}{\langle C_f \rangle_1}\right)}{t_2 - t_1};\ t_2 > t_1 \qquad (1)$$

where $\langle C_f \rangle_1$ and $\langle C_f \rangle_2$ are the column depth-averaged concentrations during the exponential growth phase, and *t* is the time. Samples and data measurements from the PT were taken daily during 13:00 and 16:00 hours. A goodness of fit (r^2), with a minimum value of 0.98, was calculated for each set of depth-averaged concentrations ($\langle C_f \rangle$) selected from the exponential growth period (straight line) for each of *Microcystis* experimental runs.

4.2.4. Calibration of fluorescence sensor

The Cyclops-7 fluorescence sensor was calibrated using the manufacturer recommended setup, by measuring sensor's signal output voltage (mV) in a dilution series of *Microcystis* with known cell (cells mL^{-1}) and Chl-a (μgL^{-1}) concentrations (Fig. 4.3a). The Cyclops-7 measurements of *Microcystis* were confirmed ($r^2 = 0.99$) by comparing the random measurements of Cyclops-7 against the cell count of the same samples using haemocytometer cell count (Fig. 4.3b). The reproducibility of the vertical cell concentrations profiles measured by Cyclops-7 were tested by taking repeated profiles and evaluating the changes in the cell concentrations at each depth. Three profiles were repeated every six minutes and six profiles every 30 minutes with an averaged coefficient of variation (CV) of 4.2% with CV = $\sigma / \overline{X}$ where $\overline{X}$ is the time average cell concentration at each depth and σ is their standard deviation. Culture samples from both the control and column with fluid motion were taken regularly throughout the experiments for cell counts to monitor and confirm the measurements of Cyclops-7.

Fig. 4.3. Measurements by the fluorescence sensor, Cyclops-7 of a series of a) known *Microcystis* sample concentrations that were evaluated against the measured Chl-a (diamonds, μ L^{-1}; $r^2 = 0.95$), and haemocytometer cell counts (triangle, cellsmL^{-1}; $r^2 = 0.99$) for sensor calibrations, and b) of 15 random *Microcystis* samples evaluated for sensor verification ($r^2 = 0.99$) against cell counts of the same samples obtained by using haemocytometer (cells mL^{-1}).

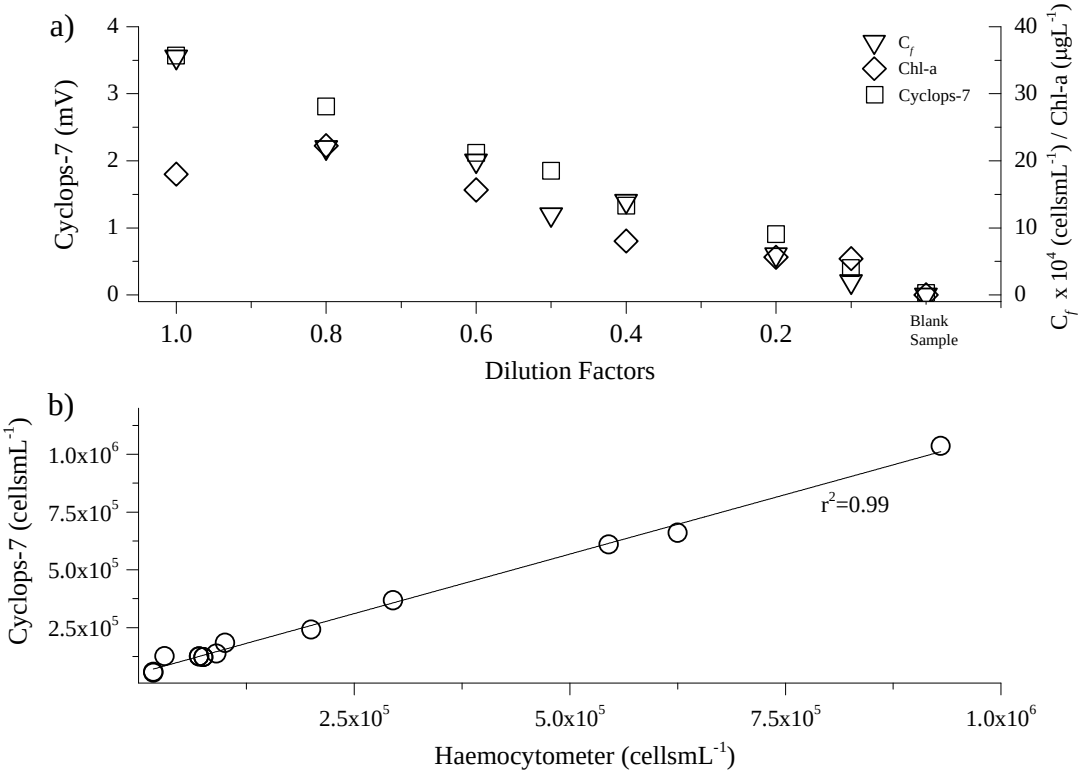

4.2.5. Turbulence generation

In the control column, fluid was stagnant without an oscillating grid setup (f = 0 Hz). In the second column, an oscillating grid with the grid mesh (0.05 m) was set to oscillate at 0.05-0.1 m below the water surface with the stroke (S) of 0.03 m (Fig. 4.2). The oscillating grid was operated at selected frequencies of f = 0.5, 1, 1.5,2, and 3 Hz.

4.2.6. Turbulence measurements and Particle Image Velocimetry

In the experimental set-up, fluid flow velocities were measured using 2-D particle image velocimetry (PIV). PIV is a non-intrusive image based technique able to estimate the change of positions of tracer particles in the fluid, illuminated by a laser sheet, within a prescribed, small, time interval (Adrian 2005). The PIV (TSI, Inc., St. Paul, MN) system consisted of a monochrome CMOS camera, 5.5 μm pixel size, able to capture more than 2000 images (at a rate up to 100 fps) in a field of view of 0.1 x 0.1 m^2 illuminated by a Litron dual cavity laser (LPY 704-100; Rugby, England, capable to deliver up 100mjoule per pulse). The Insight 6 (TSI) software was used to synchronize the laser pulse and the camera acquisition as well as to process the images and compute the instantaneous velocity vectors (u and w). Measurements were taken at two vertical locations, ranging 10-20 mm and 20-30 mm below the origin position of the oscillating grid, respectively. The PIV experiment was conducted with the PT filled with pure water and seeded with hollow glass coated spheres (1.05 g cm^{-3} density). PIV was performed in a baseline set of experiments conducted under the same geometrical, mechanical and environmental conditions of the experiments performed with the algae. PIV measurements were used to describe the turbulence characteristics in the PT experiments and to calculate the energy dissipation rates ε (m^2s^{-3}) using a 2-D approximation (O'Connor and Hondzo, 2008):

$$\varepsilon = 4\nu\left(\left(\frac{\partial u}{\partial x}\right)^2 + \left(\frac{\partial w}{\partial z}\right)^2 + \frac{3}{4}\left(\frac{\partial u}{\partial z}\right)^2 + \frac{3}{4}\left(\frac{\partial w}{\partial x}\right)^2 + \frac{\partial u}{\partial x}\frac{\partial w}{\partial z} + \frac{3}{2}\left(\frac{\partial u}{\partial z}\frac{\partial w}{\partial x}\right)\right) \quad (2)$$

4.2.7. Statistical analysis

Two-sample Student's *t*-test was performed, comparing the average concentration of the daily cell concentration profiles (n=400, where n is the total number of data points) during the exponential growth period from each experimental (f= 0.5, 1, 1.5, 2, and 3 Hz) and its corresponding control condition. In each test, the null hypothesis was that there was no difference in the mean of *Microcystis* daily concentrations between the control and turbulent experimental conditions. Analysis of variance (ANOVA) was preformed to

test the difference between the two groups of *Microcystis* cell concentration profiles selected from the experimental treatments and their corresponding control conditions during their exponential growth period. A two-way ANOVA was also performed with *Microcystis* growth period (8 days) and the daily C_f from each experimental and control conditions as the two factors. The measured *Microcystis* growth period (8 days) was set as the first factor (n=3280, 2 levels) with turbulent experimental condition and the control condition, each as one level. All ANOVA tests were conducted at 95% probability ($p < 0.05$) followed by Tukey's multiple comparison tests to examine the significance of their differences. We also implemented the Student's *t*-test to evaluate the differences between the daily cell concentration profiles from experimental treatments and its corresponding control condition. All statistical analyses were performed using OriginPro9 software (Northampton, MA).

4.3. Results and discussion

4.3.1. Cultures

Every experimental run was started with a *Microcystis* cultures cell concentration of about 7.5×10^4 cells mL^{-1}. A uniform initial *Microcystis* cell concentration among different experimental runs was obtained by starting each experiment with clearly countable single cells (Fig. 4.1d). However, *Microcystis* cultures grow to include double cell and small colonies during the experiment. The exponential growth period (9.0×10^4-1.2×10^6 cells mL^{-1}) generally established within two days and lasted up to 8 days, followed by the stationary period (1.2×10^6- 4×10^6 cells mL^{-1}).

4.3.2. Turbulence characteristics

The generated turbulence levels in the PT produced midrange ε of about 10^{-6} m^2s^{-3}. Mean energy dissipation contours, interpreted as a measure of spatial statistical variability of the turbulent flow in the experimental setup, were estimated for each of 1, 1.5, and 2 Hz oscillating grid frequencies. The rate of energy dissipation is observed to be fairly uniform in the horizontal (x-direction) while exhibiting the expected spatial

decay in the vertical (z-direction) (Fig. 4.4a). Figure 4.4b, provides a spatial sample of the instantaneous velocity vectors showing the vortices that are generated by the oscillating grid, gently propagating in the PT.

Fig. 4.4. Data from 2-D Particle Image Velocimetry were used to estimate a) energy dissipation rate, ε (m^2s^{-3}), contours at 2 Hz oscillating grid frequency, and b) the instantaneous 2-D velocity vectors over the marked square area (40 x 40 mm).

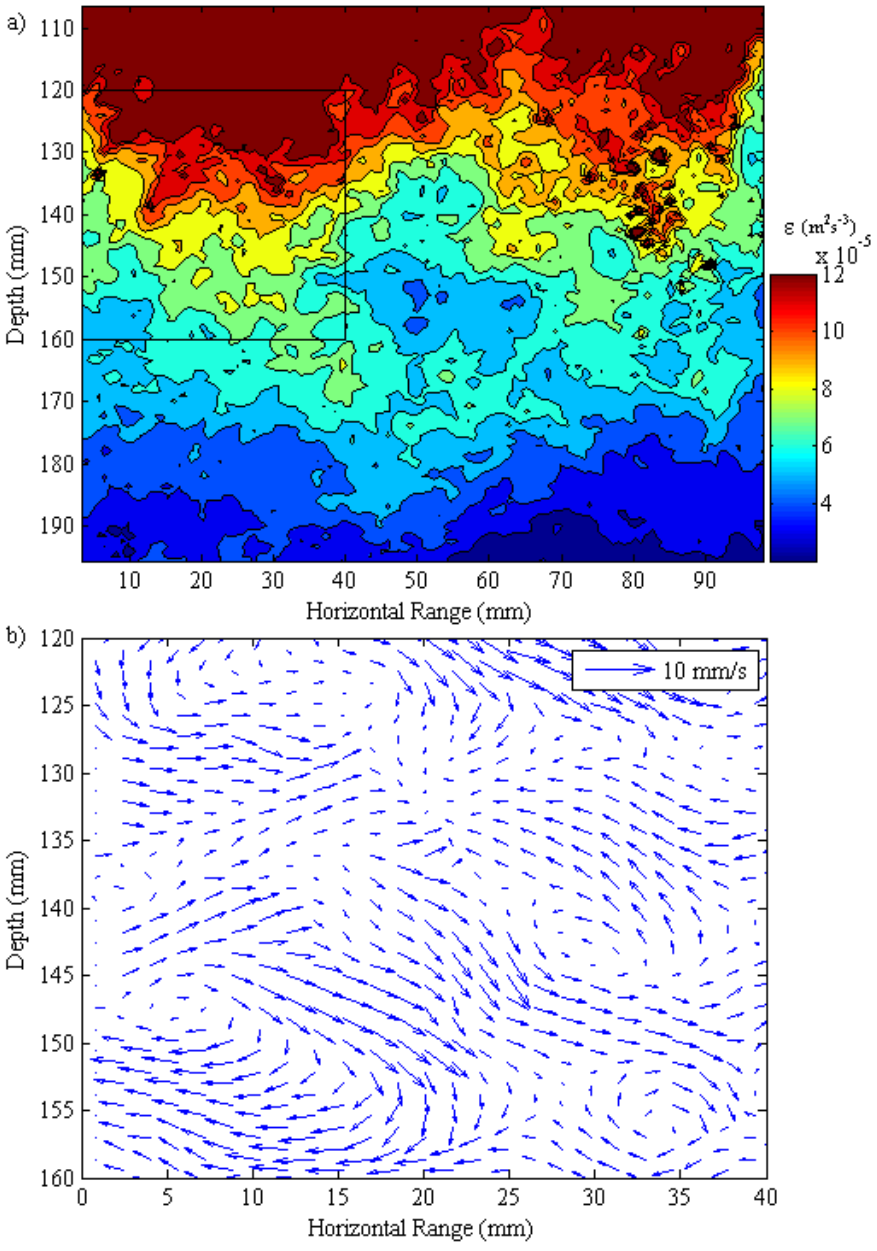

A functional relationship between ε at specified vertical distance from the grid (z) and oscillating grid frequency was proposed by O□Brien et al. (2004), using known oscillating grid turbulence scaling laws (Long 1978, Da Silva and Fernando 1991) combined with a typical expression for energy dissipation in homogeneous turbulence $\varepsilon \sim u^3/l$, with u and l representing the velocity and the length scales of the energy containing eddies. Specifically,

$$\varepsilon = \frac{1}{\beta}\left(\frac{2C_1^2 + C_2^2}{3}\right)^{\frac{3}{2}} \frac{M^{\frac{3}{2}} S^{\frac{9}{2}} f^3}{z^4} = \alpha \frac{f^3}{z^4} \tag{3}$$

where β is 0.1, M is grid mesh size (m), S is stroke length (m), z is distance from the grid (m), f is frequency (Hz) of the oscillating grid, and α is the coefficient (m^6). The values for C_1, C_2 were calculated by $u_{rms} = C_1 S^{3/2} M^{1/2} f z^{-1}$ and $w_{rms} = C_2 S^{3/2} M^{1/2} f z^{-1}$ (Long, 1978; De Silva and Fernando, 1994). The averaged value for α, specific to experimental setup, was estimated to be 2.11 x 10^{-9} (m^6) and equation (3) was used to estimate ε profiles at the selected oscillating grid frequencies of 0.5, 1, 1.5, 2, and 3 Hz. The power law expressing the decrease of ε with vertical distance from the grid (Eq. 3) was verified by direct estimates of the dissipation profiles (Fig. 4.5). The proposed power law depicted fairly well the decrease of ε in the experimental setup.

Fig. 4.5. Averaged energy dissipation rate, ε, profiles created by using the data generated from the 2-D Particle Image Velocimetry for 1 Hz (square), 1.5 Hz (triangle), and 2 Hz (circle) oscillating grid frequency experimental conditions. The solid lines represent the estimated ε using the power-law equation (3).

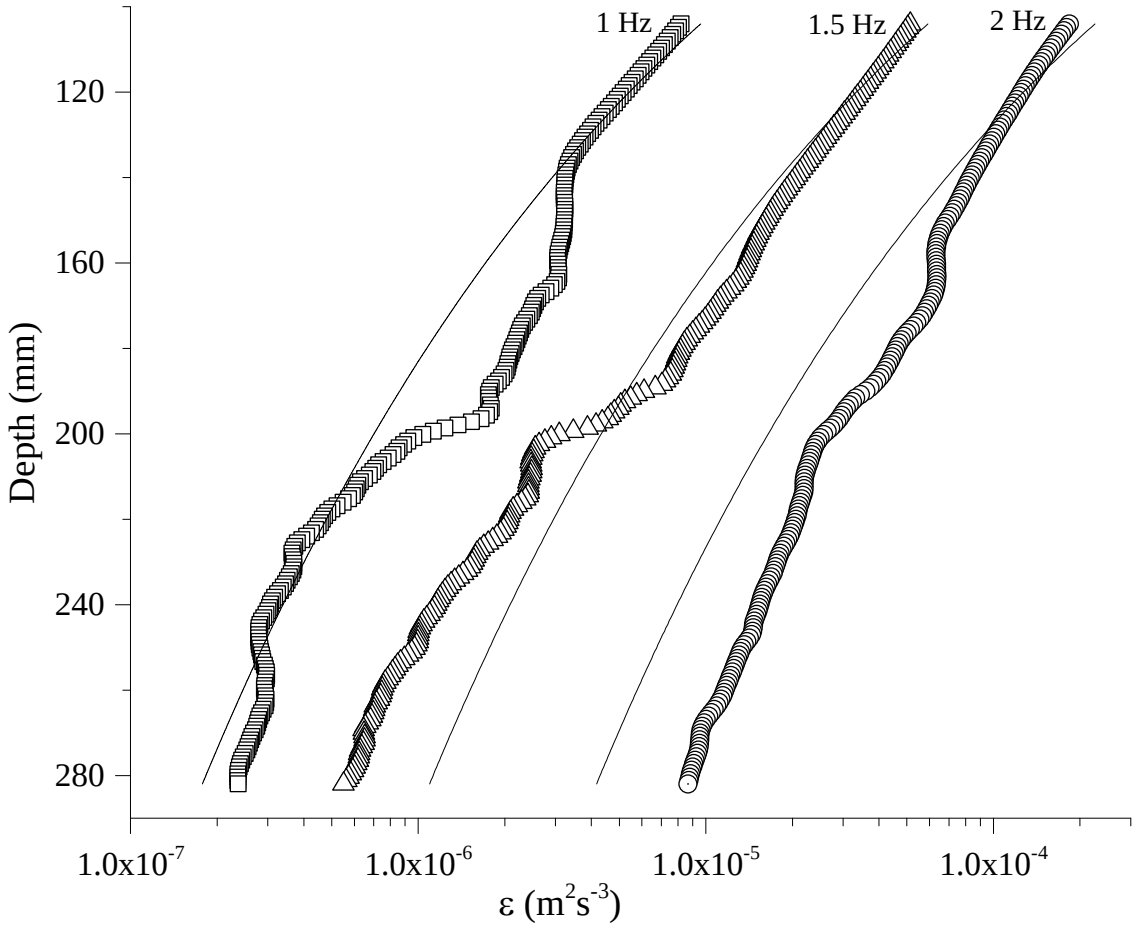

The measured ε for the 2 Hz experiment ranged from 2 x 10^{-3} m^2s^{-3} on the top of the first PIV field of view (z =10 to 20 mm in Fig. 4.5) to 1 x 10^{-5} m^2s^{-3} at the bottom of the second PIV field of view (z = 20 to 30 mm). The calculated ε for *f* = 1.5 Hz experiment was similar to its measured values at the top but became smaller towards large depth with the largest difference (6 x 10^{-6}, m^2s^{-3}) at z = 30 mm. The measured ε for the 1.5 Hz experiment ranged from 6 x 10^{-4} to 5 x 10^{-7} m^2s^{-3}, and the calculated ε values were very similar in the upper window (z = 10 to 20 mm) but became larger than the measured ε in the lower half about 1 x 10^{-6}, m^2s^{-3} at z = 30 mm. The measured and calculated ε for *f* = 1

Hz experiment were very similar and both ranged from 1 x 10^{-5} to 2 x 10^{-7} m^2s^{-3}, except for some deviation in the lower part of the top window (z = 10 to 20 mm) (Fig. 4.5). The minimal deviations between the measured and calculated ε for all three experiments may have been contributed by slow recirculating flow regions, also known as secondary flows in oscillating grid turbulence, that have been observed in this and other experiments (DeSilva and Fernando), 1994. Note that these flows are not accounted for in the grid parameterization scaling laws (thus in equation 3 as well), which assumes turbulence to be statistically homogeneous in the planes parallel to the grid with zero mean flow and zero mean shear. In addition, since those secondary flows are slow as compared to turbulent fluctuating velocities, their effect on the statistical convergence of the dissipation estimate is not negligible, especially in the deep layers far from the grid where dissipation values are very low.

4.3.3. Effects of fluid motion on *Microcyctis* growth rate

Microcystis cell concentration profiles (C_f) were measured daily in the PT under both the control (stagnant fluid) and the turbulent conditions such as the f = 2 Hz vertical concentration profiles (Fig. 4.6). The *Microcystis* cells experienced appreciable growth in the control column and under turbulent conditions in the setup and with their populations significantly (p=0.05) different in each column under each experimental conditions. A two-way ANOVA also revealed (p=0.05) that the population means of the experimental conditions (f= 1, 1.5, 2, and 3 Hz) were significantly different than their corresponding control conditions (Table 4.1). Therefore, the null hypothesis was rejected and the alternative hypothesis was accepted that there were significant differences between *Microcystis* population in the experimental and the control conditions. ANOVA tests revealed that the major source of variability among the C_f was due to the different turbulent conditions.

Fig.4. 6. Examples of the *Microcystis* cell concentration profiles (C_f) measured in the Plankton Tower over eight days with *t* as time, *n* as the day of sampling from the start of the experiment. a) control column (without fluid motion), b) column with oscillating grid at f = 2 Hz, and c) the vertical distribution of energy dissipation (ε) in the column with oscillating grid at f = 2 Hz. The amplitudes of the oscillating grid and stroke distance (*S*) within the column with oscillating grid are also shown in b).

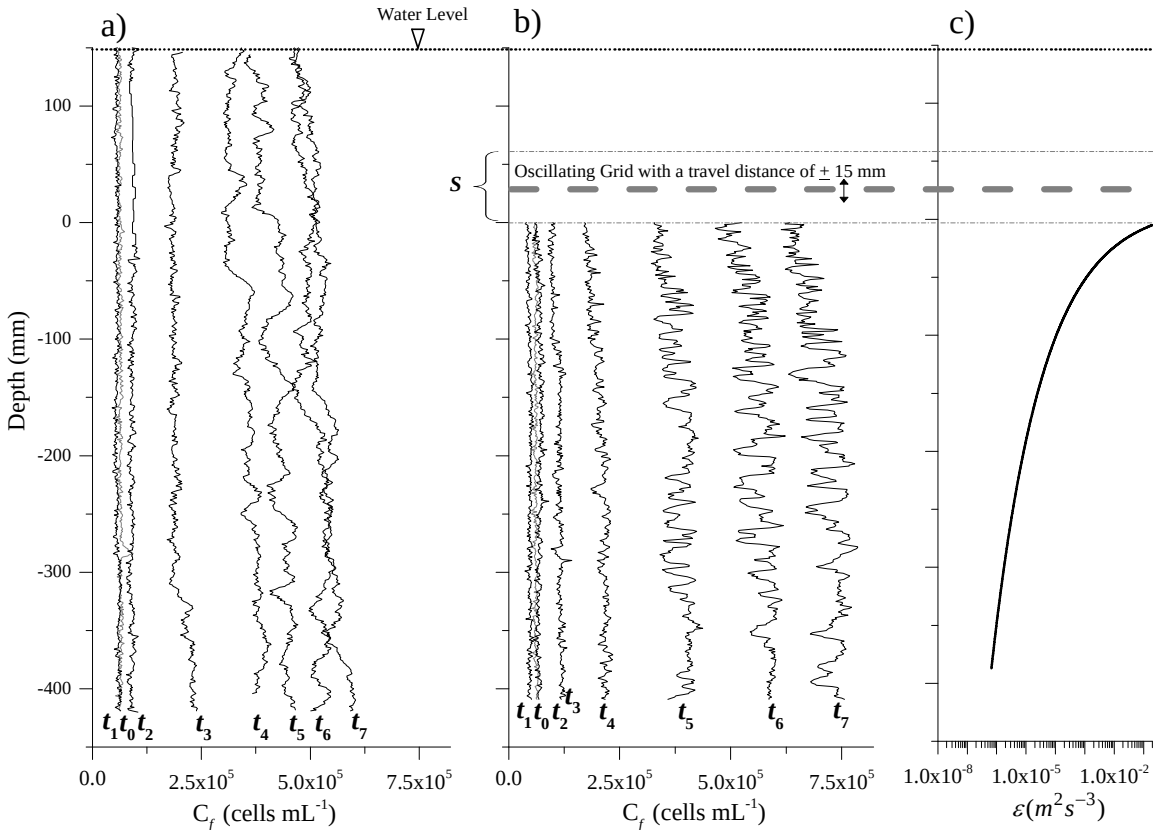

Table 4.1. Results from the experimental conditions in the Plankton Tower where f is the oscillating grid frequency, k_g is the algal growth rate, $k_{gcontrol}$ is the algal growth rate in the control tower (without fluid motion), ε is the rate of energy dissipation averaged over the depth of tower with oscillating grid setup, C_f is *Microcystis* cell concentration profile, and $\overline{C}_f / \overline{C}_{f0}$ is the dimensionless time-averaged cell concentration profile ($\overline{C}_f$) normalized by the their concentration close to the air-water interface in the experimental columns ($\overline{C}_{f0}$) with the coefficient of variation (CV) listed for each of the profiles ($\overline{C}_f / \overline{C}_{f0}$). For ANOVA results: MS is mean square with a degree of freedom of 1 at 95 % probability (p<0.05), and * indicates F value with statistically significant difference between the groups of C_f selected during the exponential growth period from the experimental turbulent and their corresponding control conditions.

f (Hz)	ANOVA		k_g (day^{-1})	$k_{gcontrol}$ (day^{-1})	ε (m^2s^{-3})	$k_g / k_{gcontrol}$	CV of $\overline{C}_f / \overline{C}_{f0}$ (%)
	MS	F value					
0.5	7e-16	3e-12	0.57	0.60	3.6×10^{-8}	0.95	2.4
1	5.02	2325.0*	0.58	0.60	1.5×10^{-7}	0.97	2.4
1.5	1.27	936.3*	0.68	0.59	5.5×10^{-7}	1.15	4.2
2	30.43	6337.2*	0.75	0.57	1.3×10^{-6}	1.32	5.9
3	30.90	11758.4*	0.47	0.64	4.4×10^{-6}	0.73	3.6

To evaluate the effects of fluid motion on *Microcystis* growth rate, the vertical concentration profiles from all experimental conditions were first depth-averaged $\langle C_f \rangle$ and then normalized by the depth-averaged cell concentration of the beginning of each experiment, $\langle C_{fo} \rangle$. These normalized concentrations, $\langle C_f \rangle / \langle C_{fo} \rangle$, depicted that fluid flow in general facilitated the growth (Fig. 4.7). The normalized concentrations, $\langle C_f \rangle / \langle C_{fo} \rangle$, at f = 0.5 Hz was similar to that of f = 1 Hz and is not shown in Fig. 4.7. However, $\langle C_f \rangle / \langle C_{fo} \rangle$ at f = 1 Hz experiment had the longest lag time of the growth cycle whereas the shortest time-lag was evident for the most turbulent conditions at f = 3 Hz. The concentration profiles at f = 1.5 and 2 Hz, had similar mid-range time-lag periods.

Fig.4.7. Semi-logarithmic plots of normalized concentrations of the *Microcystis* for the corresponding control column (f = 0, filled symbols) and the column with oscillating grid at f = 1, 1.5, 2, and 3 Hz, with $\langle C_f \rangle$ as the depth-averaged concentration and $\langle C_{\mathrm{fo}} \rangle$ as the depth-averaged concentration at the beginning (t=0) of each experiment

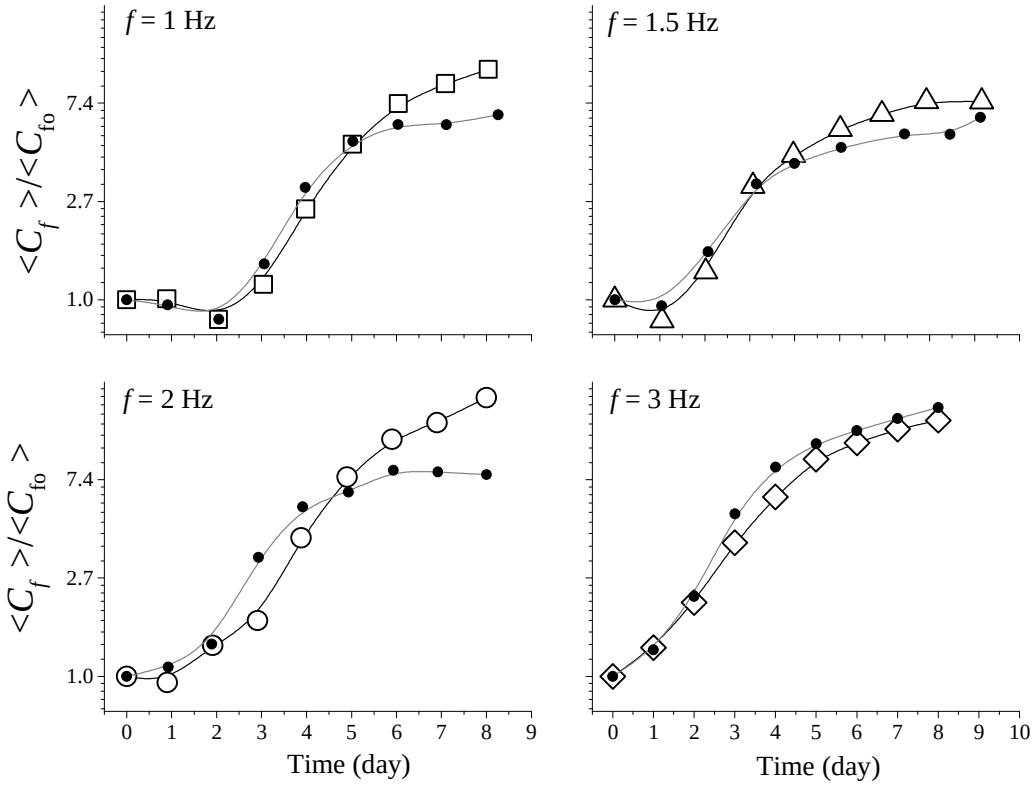

The exponential growth periods for each experimental conditions with oscillating grid operated at f = 0.5, 1, 1.5, 2, and 3 Hz were identified and used to calculate their growth rates, k_g, and their corresponding growth rate under control condition, $k_{gcontrol}$. The depth-averaged concentrations ($\langle C_f \rangle$) selected from the exponential growth period of each of *Microcystis* experimental run, experienced at minimum a goodness of fit of $r^2 = 0.98$. This implies that at least 98% variability of concentrations was explained by the model (Eq. 1) that was used to estimate the growth rate during the exponential growth phase. The measured growth rates were all within the reported range (Shi et al, 2004; Wilson et al., 2006; Park et al., 2009) and were normalized and made dimensionless by taking the

ratio of growth rates under turbulent, k_g, over the control condition, $k_g / k_{gcontrol}$ (Table 4.1). Energy dissipation profiles from each experimental turbulent condition, such as f =2 Hz shown in Fig.4.6, were also depth averaged, $\langle \varepsilon \rangle$ (Table 4.1), and evaluated against the normalized growth rates (Fig. 4.8). There was a minimal (<-5%) change in growth rate for f = 0.5 and 1 Hz conditions ($\langle \varepsilon \rangle \sim 1.5 \times 10^{-7}$-$3.5 \times 10^{-8}$ m^2s^{-3}), with a modest increase (15%) for f = 1.5 Hz ($\langle \varepsilon \rangle = 5.5 \times 10^{-7}$ m^2s^{-3}) and a large increase (32%) at f = 2 Hz ($\langle \varepsilon \rangle = 1.3 \times 10^{-6}$ m^2s^{-3}). A rapid decrease (-27%) in growth rate at f = 3 Hz ($\langle \varepsilon \rangle = 4.4 \times 10^{-6}$ m^2s^{-3}) was evident, which is in agreement with the reports from other studies on *Microcystis* growth rate under turbulent conditions similar to that of 3 Hz but with a stimulated metabolic activity at small scale turbulence generated at 1 and 2 Hz (Regel et al., 2004). The influence of fluid motion on *Microcystis* growth rate is evident by it responses under different experimental turbulent conditions and with a facilitated growth rate corresponding to $\langle \varepsilon \rangle$ values in a range between 3×10^{-7} and 3×10^{-6} m^2s^{-3} (Fig. 4.8). The fluid motions that were measured in the experimental setup encompassed the rate of energy dissipation levels (ε) that were reported in lakes and were similar to the range of ε levels that had corresponded to the Chl-a concentration maximum (Hondzo and Warnaars, 2008).

Fig. 4.8. Normalized *Microcystis* growth rates, $k_g / k_{gcontrol}$ at the corresponding depth-averaged energy dissipation rates, $\langle \varepsilon \rangle$ $(m^2 s^{-3})$, in the experimental column with oscillating grid at f = 0.5, 1, 1.5, 2, and 3 Hz. The graph depicts three growth zones including the non-facilitated, facilitated, and reduced growth regions.

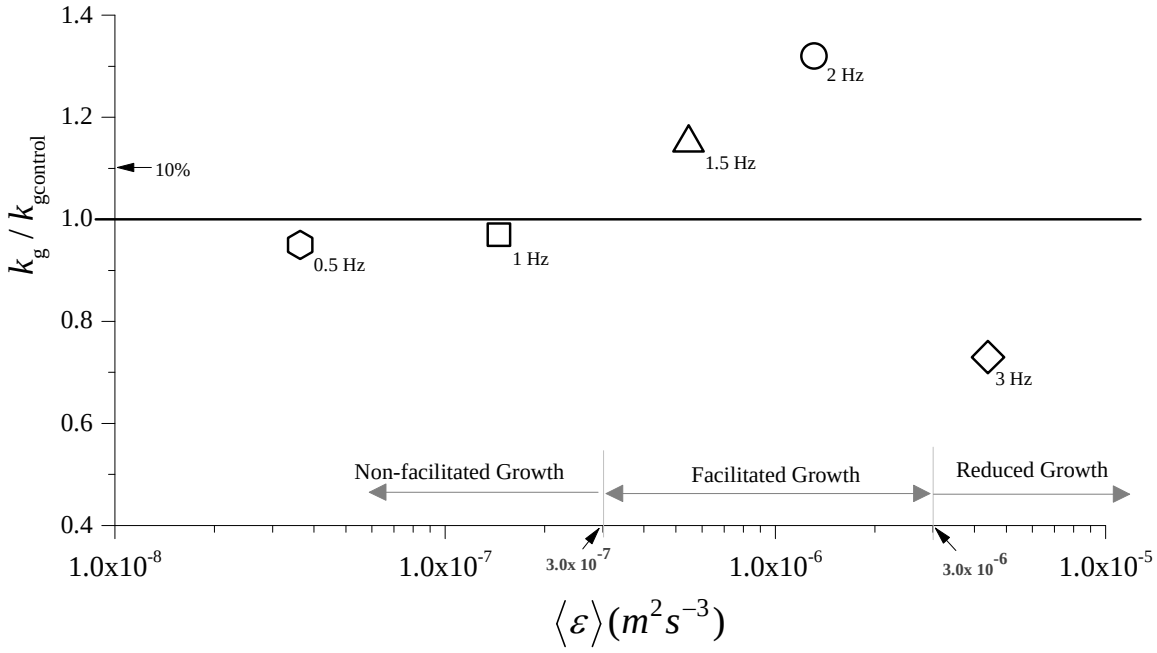

4.3.4. Effects of fluid motion on *Microcyctis* vertical distribution

A time-averaged *Microcystis* cell concentration profile ($\bar{C}_f$) was developed by time averaging vertical cell concentrations from only the exponential growth periods of each experimental condition with f = 0, 0.5, 1, 1.5, 2, and 3 Hz. The time-averaged cell concentration profiles were made dimensionless by dividing the concentrations at each depth by their concentration close to the air-water interface in the experimental columns, $\bar{C}_f / \bar{C}_{f0}$. The normalized time-averaged cell concentration profiles were smoothed by

averaging each profile in 25 mm windows and then analyzed to quantify the influence of fluid motion on *Microcystis* vertical cell concentration variability in the experimental setup.

The fluid motion had a strong influence on *Microcystis* vertical cell concentration profiles (Fig. 4.9). A value of $\bar{C}_f / \bar{C}_{f0} = 1$ indicates no change in cell concentration between that depth and the initial depth of the profile and with no variation in vertical cell concentration. All profiles from the turbulent column (f = 0.5, 1, 1.5, 2, and 3 Hz) showed a decrease in cell concentration in the proximity of oscillating grid (depth < 50 mm), reflecting the mechanical influence of the grid. On the other hand, the control (f = 0 Hz) column showed negligible vertical cell concentration variability. The experimental designed was focused on isolating the influence of turbulence on *Microcystis* vertical cell concentration profiles and growth. Each experiment had a controlled and equal size, geometry, nutrient concentration, and exposure to light as the turbulent water column. The negligible vertical cell concentration variability in the control column is an experimental indication that indeed the potential attractor variables were equally distributed over the experimental control column.

Profiles from the experiments under turbulent conditions showed very different responses. The profiles of f = 0.5 and 1 Hz, were mainly uniform throughout the water column with minor changes ($\bar{C}_f / \bar{C}_{f0} \sim 0.5$) at 200 mm depth. However, profiles for f = 1.5 and 2 Hz had significantly larger maxima ($\bar{C}_f / \bar{C}_{f0}$ = 1.2 and 1.23, respectively) at 250 mm depth. At the highest turbulence level of f = 3 Hz the profile shows a peak at about the same depth as that of f = 1.5 and 2 Hz but less pronounced ($\bar{C}_f / \bar{C}_{f0} = 1.12$).

Fig. 4.9. *Microcystis* vertical distribution of time-averaged profile concentrations ($\bar{C}_f$) from the exponential growth periods and normalized by the concentration at the initial depth ($\bar{C}_{f0}$, with z= 0) in the control column where f = 0 Hz, and in the experimental turbulent column with oscillating grid at f = 0.5, 1, 1.5, 2, and 3 Hz.

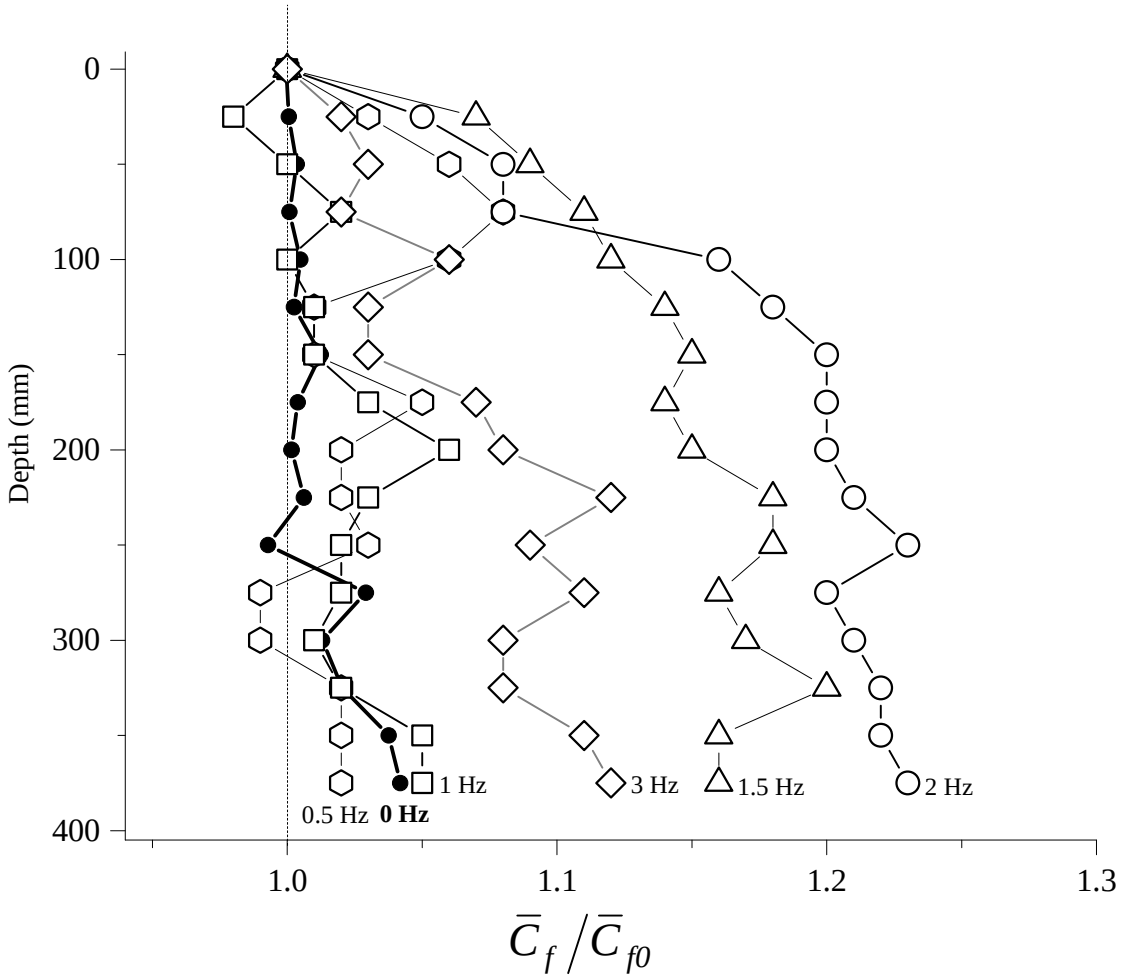

The vertical cell concentration variability is attributed to *Microcystis*' response under different experimental turbulent conditions. Indeed, while a vertically homogeneous profile is observed in the control column (stagnant fluid), a depth-dependent *Microcystis* concentration profile is measured for different grid oscillation frequencies. As both levels of turbulent kinetic energy and dissipation vary with the grid frequency and, locally, with the distance from the grid, a vertical variation in cell concentration indicates

that *Microcystis* statistically respond to turbulence adjusting their position within the water column. In order to statistically quantify the vertical cell concentration variability, data points of all profiles (f = 0, 0.5, 1, 1.5, 2, and 3 Hz) along with their depth-averaged mean value ($\langle X \rangle$) and standard deviation (σ) were analyzed (Fig. 4.10). The data points from the control experiment had the smallest mean value mean and standard deviation of vertical cell concentration ($\bar{C}_f / \bar{C}_{f0}$) followed by the 0.5 and 1 Hz data points. In these three instances the range of $\langle X \rangle \pm \sigma$ is less than 5% ($\bar{C}_f / \bar{C}_{f0} < 0.05$) from the top to the bottom of the column, indicating minimal vertical variation of cell concentration. However, vertical variability of cell concentration increased rapidly at f = 1.5 Hz and continued to increase at f = 2 Hz, followed by a decrease at f = 3 Hz under experimental turbulent conditions (Fig. 4.10).

Fig. 4.10. Normalized *Microcystis* time-averaged vertical concentrations ($\bar{C}_f / \bar{C}_{f0}$) along with their depth-averaged ($\langle X \rangle$, filled square) and standard deviation (σ), and the range of each $\langle X \rangle \pm \sigma$ (offset bars) in the control column where f = 0 Hz, and in the experimental turbulent column with the oscillating grid operating at f = 0.5, 1, 1.5, 2, and 3 Hz.

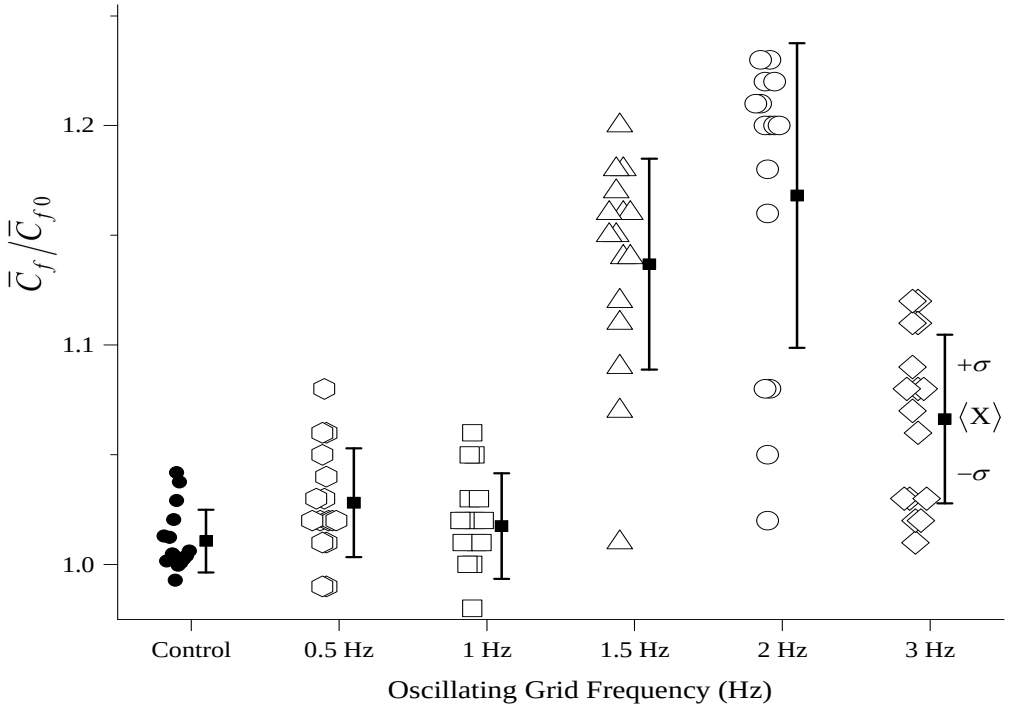

To better focus on the vertical cell concentration fluctuations under each experimental conditions, the coefficient of variation ($CV = \sigma / \langle X \rangle$) of each respective profile was calculated and evaluated against their corresponding $\langle \varepsilon \rangle$ (Fig. 4.11). Smaller CV implies that there was not significant variability in the vertical distribution of algae (homogeneous concentration). Larger CV implies that algae were preferentially concentrated in horizontal layers with the corresponding $\langle \varepsilon \rangle$ that facilitated the growth. *Microcystis* responses, as measured by the CV of $\bar{C}_f / \bar{C}_{f0}$, were similar to that of growth rates to $\langle \varepsilon \rangle$ but with different magnitudes. The CV changed only 2 % from *f* = 0.5 to *f* = 1 Hz, but increase 75% at *f* = 1.5 Hz. At *f* = 2 Hz experimental condition *Microcystis* growth rates is increased 31% but CV of $\bar{C}_f / \bar{C}_{f0}$ is increased 246%, and at *f* = 3 Hz, CV and $k_g / k_{gcontrol}$ are both reduced by 55% and 61% respectively from their values at the *f* = 2 Hz experimental condition. These findings supported our earlier observations that *Microcystis* growth rate and vertical cell concentrations are reduced at f > 2 Hz, remained steady at f = 0.5 and 1 Hz, and were facilitated at f = 1.5 and 2 Hz experimental turbulent conditions. The *Microcystis* vertical cell concentration variability had a stronger response to $\langle \varepsilon \rangle$ as compared to the growth rate, suggesting an increased sensitivity to turbulence. For our experiments, if the *Microcystis* growth rates ($k_g / k_{gcontrol}$) values with changes over 10% are treated as significant, then there appears to be a region of optimal turbulence levels that yields a facilitated growth zone corresponding to $\langle \varepsilon \rangle$ = 3 x 10^{-6} to 3 x 10^{-7} m^2 s^{-3} (Fig. 4.8). Regions with $\langle \varepsilon \rangle$ < 3 x 10^{-7} m^2 s^{-3} had non-facilitated growth and regions of higher turbulence with $\langle \varepsilon \rangle$ > 3 x 10^{-6} m^2 s^{-3} showed significant reduction in growth. We acknowledge that CV is a rather simple estimator of vertical variability of the cell concentration profile. CV emphasizes deviation from homogeneous conditions without specifically distinguishing between the occurrence of marked concentration

layers and gradual variations in the vertical profile. However, it provides a robust measure to associate with depth average dissipation values.

Fig. 4.11. Coefficient of variation, $CV = \sigma / \langle X \rangle$ where $\langle X \rangle$ is depth-averaged and σ standard deviation of normalized *Microcystis* time-averaged vertical concentrations ($\bar{C}_f / \bar{C}_{f0}$), at the corresponding depth-averaged energy dissipation rates, $\langle \varepsilon \rangle$ $(m^2 s^{-3})$, in the control column where *f* = 0 Hz, and in the experimental turbulent column with the oscillating grid operating at *f* = 0.5, 1, 1.5, 2, and 3 Hz.

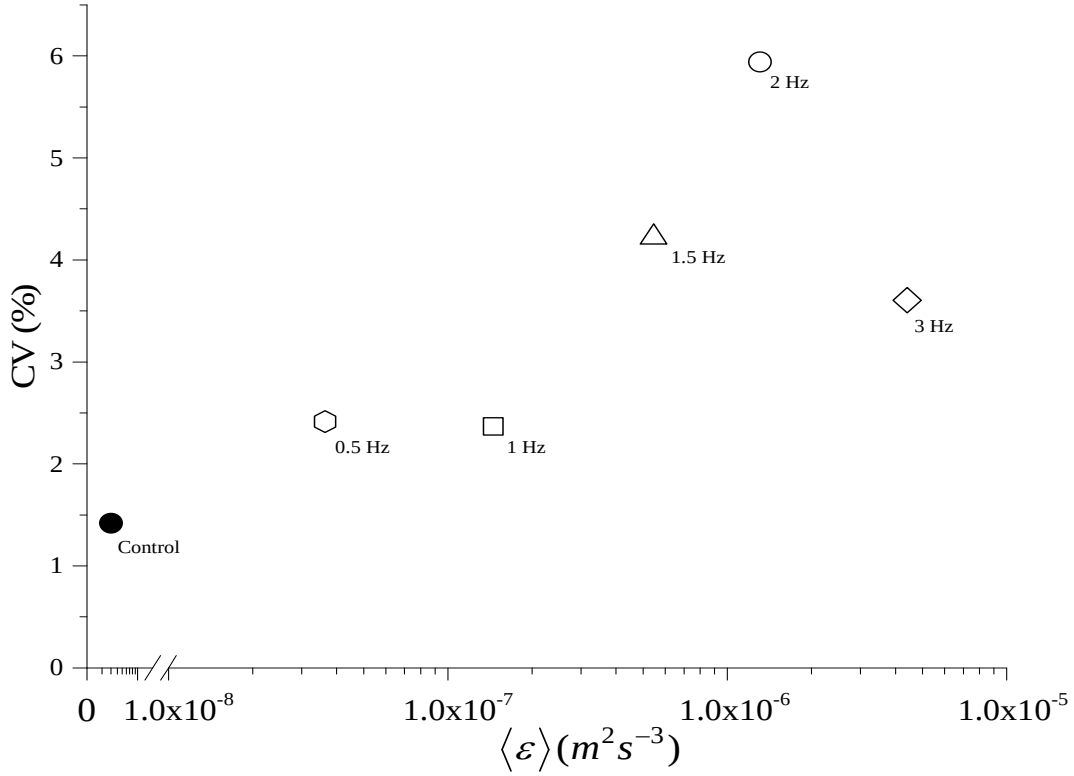

4.4. Conclusions

Laboratory experiments were conducted under controlled and repeatable turbulence conditions to evaluate the effect of fluid motion on the growth and vertical distribution of *Microcystis*. The experiment was designed to quantify the influence of fluid motion on

progressively increasing or decreasing spatial distribution density and growth rate of *Microcystis* from the source of turbulence. A rapid and vertical profile measurement of *Microcystis* cell count was required by the experimental designed. Consequently, we started each experiment with clearly countable unicellular *Microcystis* culture that later in the experiments grow into double cell and small colonies. Nonetheless, this does not change the issue that how the unicellular cultures early in the experiment responded to turbulence is likely to be different than how natural and very large colony forming cultures would. The generated turbulence levels, as measured by 2D PIV, produced midrange rate of energy dissipation (ε) of about 10^{-6} m^2s^{-3} and had negligible mean flow and mean shear, with vortices generated by the oscillating grid and gently propagating in the column. The growth rates ($k_g / k_{gcontrol}$) of *Microcystis* in cultures grown with $\langle\varepsilon\rangle$ from 3.6 x 10^{-8} to 1.5 x 10^{-7} m^2s^{-3}, displayed a minimal change (2%), had a modest increase (15%) at $\langle\varepsilon\rangle$ = 5.5 x 10^{-7} m^2s^{-3}, depicted the largest increase (32%) at $\langle\varepsilon\rangle$ = 1.3 x 10^{-6} m^2s^{-3}, and followed by a 27% decline at $\langle\varepsilon\rangle$ = 4.4 x 10^{-6} m^2s^{-3} (Fig. 4.8). The fluid motion and corresponding turbulence levels also had a strong influence on *Microcystis* vertical distribution where time-averaged vertical cell concentration profiles, $\bar{C}_f / \bar{C}_{f0}$, showed marked individual patterns in response to varying levels of turbulence (Fig. 4.9). Coefficient of variation (CV) of each respective profile was calculated and evaluated against their corresponding $\langle\varepsilon\rangle$ with the highest increase corresponding to $\langle\varepsilon\rangle$ = 1.3 x 10^{-6} m^2s^{-3} (Fig. 4.11). At $\langle\varepsilon\rangle$ = 4.4 x 10^{-6} m^2s^{-3}, fluid motion had a significant effect on both $k_g / k_{gcontrol}$ and CV of $\bar{C}_f / \bar{C}_{f0}$, where it reduced their values by 61% and 55%, respectively (Fig. 4.8 and Fig. 4.11). The results indicate that $\langle\varepsilon\rangle$ in a range of 3 x 10^{-7} to 3 x 10^{-6} m^2s^{-3} generated the largest values for both CV of $\bar{C}_f / \bar{C}_{f0}$ and $k_g / k_{gcontrol}$. The observed energy dissipation rates (ε) were similar to the reported field measurements and to the range of ε that had corresponded to the Chl-a concentration maximum (Hondzo and Warnaars, 2008). The growth and vertical distribution of *Microcystis* are quantified

by fluid flow property (ε) that is predictable in most computational models for water quality modeling in lakes. The results demonstrate the significance and necessity of integration of fluid motion in the models of growth and distribution of *Microcystis* in aquatic environments.

CHAPTER 5

Three Dimensional Prediction of Lake Water Temperature, Dissolved Oxygen, and Fish Habitat under Changing Climate

We applied a three-dimensional model to reveal the influence of local meteorological and global climate conditions on water quality and fish habitat. Water temperature (T) and dissolved oxygen (DO) concentrations were used as key water quality parameters to investigate the temporal and spatial variability of fish habitat dynamics under three climate scenarios of historical normal (HN), future (FU), and future extreme (FE). The analysis demonstrated that the averaged epilimnetic T of the FU and FE climate scenarios were up to 4 °C warmer than the HN scenario during ice-free seasons. The top 0.5 m surface T increased the most and the fastest under the FE scenario. Stratification periods were predicated to expand up to 23% (46 days) and thermocline depth to increase 49% under the FE climate scenario. The averaged DO concentrations were 1 mgL^{-1} less in the FU and FE climate scenarios than the HN scenario during ice-free seasons. However, the onset of anoxia, the depleted DO concentration area, which had started by May 15 under the HN climate scenario was four and two weeks earlier under the FU and FE climate scenarios respectively. In all cases, hypolimnion was mostly anoxic by June 15 and DO concentrations were restored to their maximum levels by fall turnover starting November 10. The good growth, restricted growth and lethal coolwater fish habitats that were based on T and DO thresholds, changed from 2 to 14% of the total lake volume under the three climate scenarios. Compared to the historical normal scenario, the averaged good growth, restricted growth and lethal habitats of future scenarios changed +16%, -18%, and +85% respectively. The majority (70%) of changes from good and restricted growth to lethal habitat took place in the upper 5 m of the water column with significant spatial and temporal consequences. A modest change (8% of total lake volume) of good growth and restricted growth into lethal habitat separated the summer good growth coolwater fish habitat by over 3 weeks.

5.1. Introduction

Local meteorological variables and global climate strongly mediate physical, chemical, and biological conditions in the aquatic ecosystems (Hondzo & Stefan 1993; MacKay et al., 2009; Whitehead et al., 2009). The interactions among aquatic physical, chemical, and biological processes are nonlinear and dynamic, and far from equilibrium. Spatially distributed and dynamic water quality predictors are necessary in order to accurately evaluate the response of aquatic ecosystem under changing climate and corresponding local meteorological conditions (De Stasio et al., 1996; Milly et al., 2008).

A significant effort has been devoted to the prediction of the impact of climate change on fresh water lakes in the past four decades. Climate change is expected to alter lake water temperature (T), increase summer stratification, increase temperature-mediated sediment phosphorus flux, alter dissolved oxygen (DO) dynamics and expand anoxic (DO depleted) zones, and change aquatic habitats such as that of fish (Stefan, Fang & Eaton, 2001; Kling et al 2003; Adrian et al., 2009). Fish habitat regimes are predicted to change their temporal and spatial distributions (Mooij, De Senerpont & Janse 2009; Foley et al., 2012) driven partly by the mixing regime altered by a changing thermal structure. Climate change is also expected to increase stream flow fluctuations leading to lake water level changes and shifting ecosystem states (Coops, Beklioglue & Crisman 2003).

Computer models have been the main tool in analyzing the impact of climate change on lake ecosystems (Menshutkin, Rukhovets & Filatov, 2014). Three dimensional (3D) computer models have the feature of reproducing the ecological processes of the lake in fine temporal and spatial (horizontal and vertical) scales that can enhance our understanding of the interactive feedbacks among physical, chemical, and biological processes. Three dimensional models have been used in climate change assessment of large lakes (Cline, Bennington & Kitchell, 2013). The models are also a good prediction tool for morphologically complex smaller lakes with significant water quality heterogeneity responding dynamically to multiple climatic forces.

We employed a 3D lake water quality model to evaluate the influence of local meteorological and global climate conditions on key environmental parameters that ultimately determine fish habitat and to investigate the temporal and spatial (vertical and horizontal) variability of fish habitat dynamics. Water temperature and DO are considered the most significant water quality parameters that influence fresh water fish habitat (Stefan et al., 2001). Several meteorological parameters can potentially influence lake water quality and fish habitat. Precipitation over a watershed and corresponding surface water runoff to the lake are susceptible to future climatic changes that can significantly alter lake water quality (Coops et al., 2003). Furthermore, wind speed and its pattern above the lake surface generate the force for water column mixing that influence T, DO, primary production, and food web. Climate change is expected to alter the frequency of extreme wind events (Jeppesen et al., 2009) which may increase frequency of sudden episodic water quality changes. Consequently, we selected T, DO, P, and wind speed as the key water quality parameters to evaluate and test them under different climatic scenarios in this study.

The first step of modeling and evaluating the potential climate change impacts on water quality was to select and create a set of historical and future climatic model scenarios. A hybrid of new and existing methods allowed the selection of one climatic historical scenario based on measured meteorological data and two projected future scenarios. We extended a similar approach adopted by Stefan & Fang (1994) and Fang et al. (2012) to investigate the individual and combined influences of select lake water quality parameters on fish habitat by using a 3D model in a morphologically complex lake. We report the findings of historic and climate change scenarios for T and DO, and fish habitat dynamic in a shallow and morphologically complex lake.

5.2. Methods

5.2.1. Study site

Lake Minnetonka (60 km^2), located at 44°54' N; 93°41' W, is a morphologically complex lake (Wetzel, 2001). The lake has 23 bays, 200 km of shoreline, 24 km^2 of littoral area, a maximum depth of 34 m, with a watershed size of 319 km^2 (Fig. 1.1). Lake Minnetonka was inhabited pre European settlement and has been a regional destination offering swimming, boating, and fishing. At least 15 fish species are found in Lake Minnetonka dominated with northern pike (*Esox lucius*), walleye (*Stizostedion vitreum*), and bluegill (*Lepomis macrochirus*). The walleye population is sustained by annual stocking at two bays. However, fish population assessment study results showed different catch average sizes (length) among different bays of the lake indicating the presence of distinct fish habitats within the lake (MNDNR, 2007). The computational domain of the study area included four bays and two stream inflows into the lake. Each bay has a specific individual water quality characteristic representing the strong water quality heterogeneity throughout the whole lake.

5.2.2. Field data

Measured stream and lake water quality data were provided by the Water Quality Department of Minnehaha Creek Watershed District organization (MCWD, MN). All field lake water quality samples were collected from the deepest point of the three bays of Halsted Bay (HB, 10 m), Cooks Bay (CB, 8.5 m), and West Upper Bay (WU, 24 m) within the study area (Fig. 1.1). Each station was sampled biweekly and analyzed for T, DO, conductivity, pH profiles, surface and bottom total phosphorus (TP), soluble reactive phosphorus (PO4), total nitrogen (TN), and a composite top 2-m sample for algae biomass as measured by chlorophyll *a* (Chla). Stream inflow (m^3s^{-1}) data were based on the correlation between daily averaged available measured outflow and precipitation data (1997-2011; R^2= 0.82) where the correlation was then applied to hourly precipitation data of each scenario to generate outflow data. Inflow data from the two creeks were set to equal outflow. The biweekly sampling from Six Mile and Langdon creeks (Fig. 1.1)

included flow, T, DO, Chla, TP, and PO4. Stream water temperatures from nearby (<5 km) streams were used for missing stream water temperature data. Meteorological data, including hourly readings of air temperature (T_a), relative humidity (RH), atmospheric pressure (AP), cloud cover (CC), wind speed (WS), and wind direction (WD), were obtained from the Flying Cloud Airport (44°50′ N, 93°27′ W) about 14.5 km southeast of the lake. Precipitation data were obtained from Mound's weather station (44°56´ N, 93°39´ W) at the northeast of the study area and hourly solar radiation was obtained from Rosemount Experimental Station (44°45′ N,93°04′ W) 45 km southeast of the lake.

5.2.3. Historical and future climate scenarios

Three different types of climate scenarios were selected for the study and designated as historical normal (HN), future (FU), and future extreme (FE) scenarios. The scenarios were based on the T_a and P because they are the two most influential water quality parameters for fresh water fish habitat. The annual T_a average (x axis) of 30 historical years (1981-2010) were plotted against the average annual P (y axis) with the intersection of the axes representing the climate normals (T_a = 7.78 °C and P = 0.78 m) reported for the study area by the National Oceanic and Atmospheric Administration (NOAA, 2012) (Fig. 5.1a). The distance from each of the 30 points to the center was evaluated to identify the year nearest to the climate normal (center) as a surrogate for HN scenario and to identify the year farthest from the center as an extreme year.

To generate future meteorological climate scenarios of FU and FE, we applied the projected mean monthly meteorological change fields to the two sets of base scenarios of HN and extreme year. The change fields method is a hybrid between Global Climate Model (GCM) predicted outputs and the local historical observed metrological data (Smith & Tirpak, 1989). The resolution of the GCM outputs is generally not sufficient to generate locally specific forecasts that reflect the regional dynamics (IPCC, 2008). Various strategies such as statistical down scaling or change field are adopted to transform the available global scale GCM predicted outputs into locally relevant

meteorological data (Fowler, Blenkinsop & Tebaldi 2007). In statistical down scaling a statistical relation between local climate variables (e.g. T_a, P) and large scale predicators (e.g. pressure fields) is established and applied to GCM outputs to generate finer resolution local outputs. In the change factors or change fields (CFs) method, the differences (or ratio for P) between the GCM outputs of a control period (predicted historical climate) and future period (predicted future normal climate) is then applied to the local historical observed metrological data. The CFs (e.g. 2040-2069 minus 1961-1990) selected for this study (Table 5.1) were obtained from International Panel on Climate Change Data Distribution Centre (IPCC DDC, 2012) for the grid point (45° 42' N; 93° 38' W) nearest to the study area. The selected CFs were based on the output of the high resolution Model for Interdisciplinary Research on Climate (MIROC3.2), a Couple General Circulation Model (CGCM), appropriate for use in the study area region (Jiang et al., 2012).

Table 5.1. The set of monthly Change Fields applied to the meteorological data of the normal climate and the extreme climate year within the climate normal period (1981-2010) in order to create the future and future extreme meteorological climate scenarios.

	Air temperature (°C)	Relative Humidity* %	Cloud Cover* (0-1)	Atmospheric Pressure (pa)	Wind Speed (ms^{-1})	Solar Radiation (Wm^{-2})	Precipitation ($mm\ d^{-1}$)
Jan	4.21	-0.47	-0.07	-40.53	0.16	16.53	0.57
Feb	4.61	-4.07	-0.09	50.14	0.22	14.15	0.06
Mar	4.47	-6.94	-0.06	42.03	0.34	16.13	0.10
Apr	3.54	-1.47	-0.02	44.09	0.16	18.64	0.33
May	4.67	0.94	-0.03	-53.70	0.20	31.30	0.04
Jun	3.75	-3.14	-0.04	99.25	0.09	22.88	-0.48
Jul	3.63	-4.17	-0.05	2.12	0.16	23.10	-1.05
Aug	3.52	-2.34	-0.04	7.62	0.10	23.86	-0.20
Sep	3.88	-2.50	-0.06	167.24	0.08	22.71	-0.05
Oct	4.43	-0.77	-0.05	128.29	0.20	22.98	0.82
Nov	4.71	-4.31	-0.09	-7.66	0.43	17.85	0.52
Dec	4.08	-3.83	-0.08	43.47	0.22	14.54	0.11

*calculated values (differences between averaged 2040-2069 and averaged 1961-1990)

The year 2000 with the nearest annual average of T_a and P to climate normals (T_a = 7.78 °C and P = 0.78 m) was designated as the HN scenario for our study (Fig. 5.1a) and was used as a base year to construct FU scenario. The set of CFs (Table 5.1) were applied to the meteorological data of the HN scenario to generate the FU scenario. Extreme climate events, defined as those greater than 90th percentiles (Fowler et al., 2007) could have T_a, and P values that may place them in any of the four quadrants in Fig. 5.1a. We investigated the predicted trend of T_a and P by plotting their bias corrected model (MIROC3.2) historical (1981-2000) and future (2041-2070) annual averages around the climate normals (Fig. 5.1b). The predicted future T_a and P annual averages were generally in the direction of warmer and wetter annual averages, similar to the results of other investigations (ICAT, 2013). Based on these findings, year 2005 which had the longest distance from the climate normals (Fig. 5.1c) and also resided in the warmer and wetter quadrant was considered as the historical extreme year. Year 2005 was then used as a base for future extreme case. The same set of monthly CFs used for developing FU scenario (Table 5.1) was also applied to the metrological data of year 2005 to generate the FE scenario. A drawback of using the CFs method is that it relies on the observed and historical statistical relationships and patterns that may not continue to hold true under future scenarios. The CFs method shifts the historical data into predicted future data. The dynamic Regional Climate Models, on the other hand, generate locally specific predictions that reflect the regional climate dynamics influenced by regional small scale features.

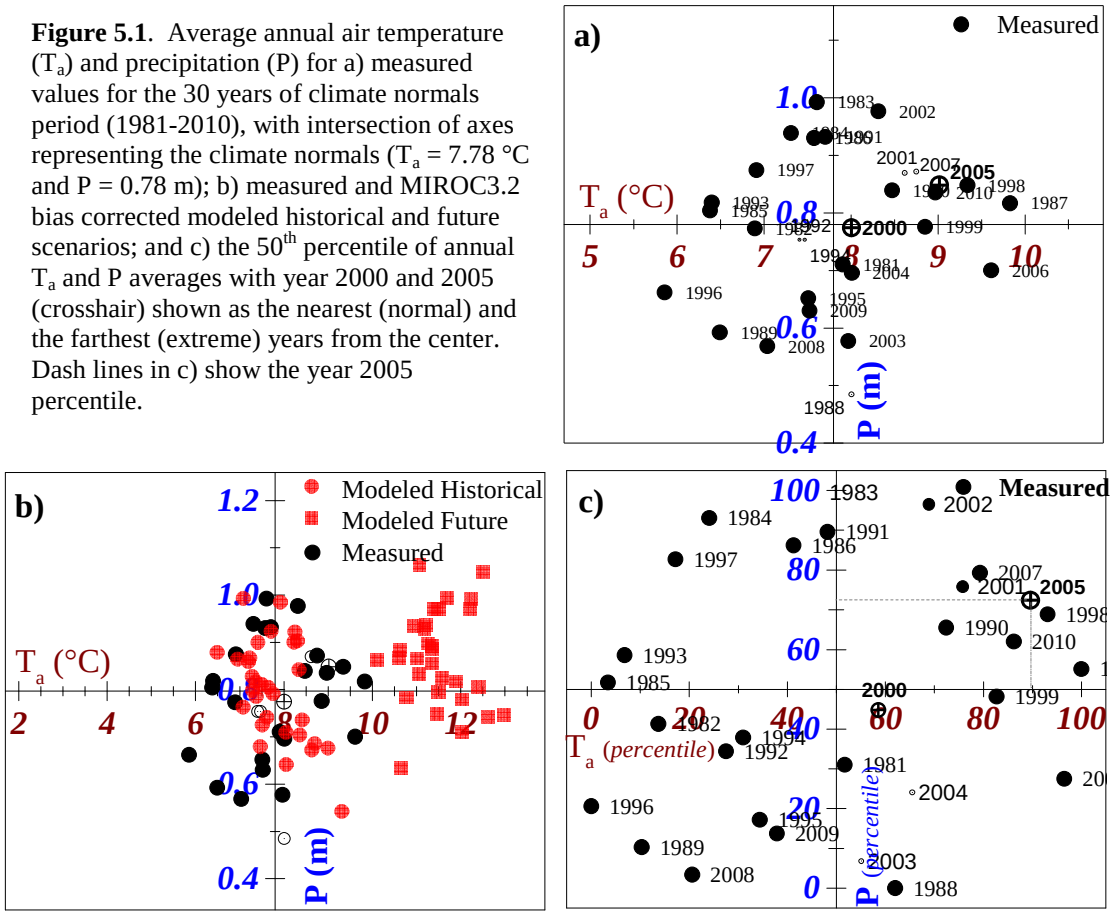

Figure 5.1. Average annual air temperature (T_a) and precipitation (P) for a) measured values for the 30 years of climate normals period (1981-2010), with intersection of axes representing the climate normals (T_a = 7.78 °C and P = 0.78 m); b) measured and MIROC3.2 bias corrected modeled historical and future scenarios; and c) the 50th percentile of annual T_a and P averages with year 2000 and 2005 (crosshair) shown as the nearest (normal) and the farthest (extreme) years from the center. Dash lines in c) show the year 2005 percentile.

5.2.4. Model description

We used the 3D hydrodynamic model ELCOM coupled to the ecological model CAEDYM. ELCOM uses hydrodynamic and thermodynamic models to simulate spatial and temporal variabilities of T and velocity distributions and CAEDYM simulates biogeochemical and chemical water quality variables. Detailed schematic representations of the model processes and descriptions of differential equations are provided by Hodges et al. (2000) for ELCOM and Romero and Imberger, (2003) for CAEDYM. Descriptions of the complete model structure, operations, and documentations are freely available online from the Center for Water Research, University of Western Australia.

5.2.5. Model setup, calibration and validation

The computation domain of the study area was discretized into 200 x 200 x 0.5 m bathymetry grids of 3D Cartesian mesh of computational cells. The model was configured to simulate T, velocities, TP, TN, DO, organic carbon, and one algal group (Cyanobacteria-*Microcystis aeruginosa*). Each simulation began on March 1 and ended on November 30 with time step set to 100 s and output data recorded at 4-h intervals. The period of March 29 to October 20, 2000 and April 25 to October 10 2005 were used for model calibration and validation respectively. The mean difference of water level between the simulated and measured water levels for the model calibration and corroboration periods was mere 0.05m indicating that the model had captured an accurate water budget. Evaluation of agreement (goodness of fit) was conducted by comparing between model predictions and twelve biweekly measured vertical profiles of T and DO from the three sampling locations as measured by R^2 (Fig. 1.6). The model was able to accurately capture the seasonal changes of both T and DO (Fig. 2.4) and it proved that it can reliably be applied to the study area.

A detailed description of evaluation and application of ELCOM-CAEDYM to the study area including model setup, configuration, parameterization, calibration, validatation, and model performance is provided by Missaghi and Hondzo (2010). The details of implementation of sensitivity and uncertainty analyses by two different methods, and the process of model parameter ranking by importance and their influence on the model prediction are provided by Missaghi, Hondzo & Melching 2013. The analyses highlighted the contributions of simulated T, DO, TP, and Chla that resulted in 3, 13, 26, and 58% of total model output variance, respectively.

5.2.6. Model simulations for past and future climate scenarios

The model simulation for the HN scenario was based on the observed reference year 2000 meteorological, stream inflow, and in-lake measured water quality data. To simulate the FU scenario the in-lake water quality, initial conditions, and wind direction were kept the same as in the HN scenario but the newly generated FU metrological data

were used. The stream temperatures time series from the HN scenario were transformed into FU and FE scenarios using their appropriate air temperature. All other inflow scalar variables were kept the same as the reference year 2000, the HN scenario. The same procedure was then applied to create the FE scenario, except year 2005 (historically extreme year) was used as the reference year. The in-lake water quality initial conditions were selected based on the available data and were uniform for all scenarios.

5.2.7. Fish habitat criteria

Suitable fish habitat is determined by a large number of environmental factors. However, T and DO are recognized as the two most significant water quality parameters that influence fish habitat (Hondzo & Stefan, 1996; Cline et al., 2013). For this study, we adopted the mean coolwater fish thermal and DO criteria established by Stefan, Fang & Eaton (2001) (Table 2.3) which includes fish species such as walleye and northern pike. The model was configured to generate the simulated T, DO and other model output state variables in 27 depth layers at 1 m intervals. These outputs were then queried to evaluate each control volume (cell) for the three coolwater fish habitat types of good growth, restricted growth, and lethal.

5.3. Results

The HN, FU, and FE climate model scenarios resulted in distinct T and DO predicted model outputs, reflecting the individual metrological forcing data. Each simulated scenario generated unique thermal structures and DO patterns that ultimately formed varying fish habitats. The 3D modeling analysis revealed both the specific individual and the combined influences of T and DO on the temporal and spatial (horizontal and vertical) distribution of good growth, restricted growth, and lethal habitats.

5.3.1. Model simulations for past and future climate scenarios

The measured meteorological data for the HN (year 2000), and the projected meteorological data of the FU (year 2000 with CFs) and the FE (year 2005 with CFs) scenarios were used as inputs (Fig. 5.2) for the three simulations and the evaluations in

the study. The modeled climate scenarios presented three hydrologically and climatically distinct years as shown by the simulated lake water levels (Fig. 5.3).

Fig. 5.2. Examples of measured and projected (using change fields) air temperature, wind speed, and precipitation time series used for the prediction of ecological changes in the study area as historical normal (HN, black), future (FU, dark gray), and future extreme (FE, light gray) climate scenarios.

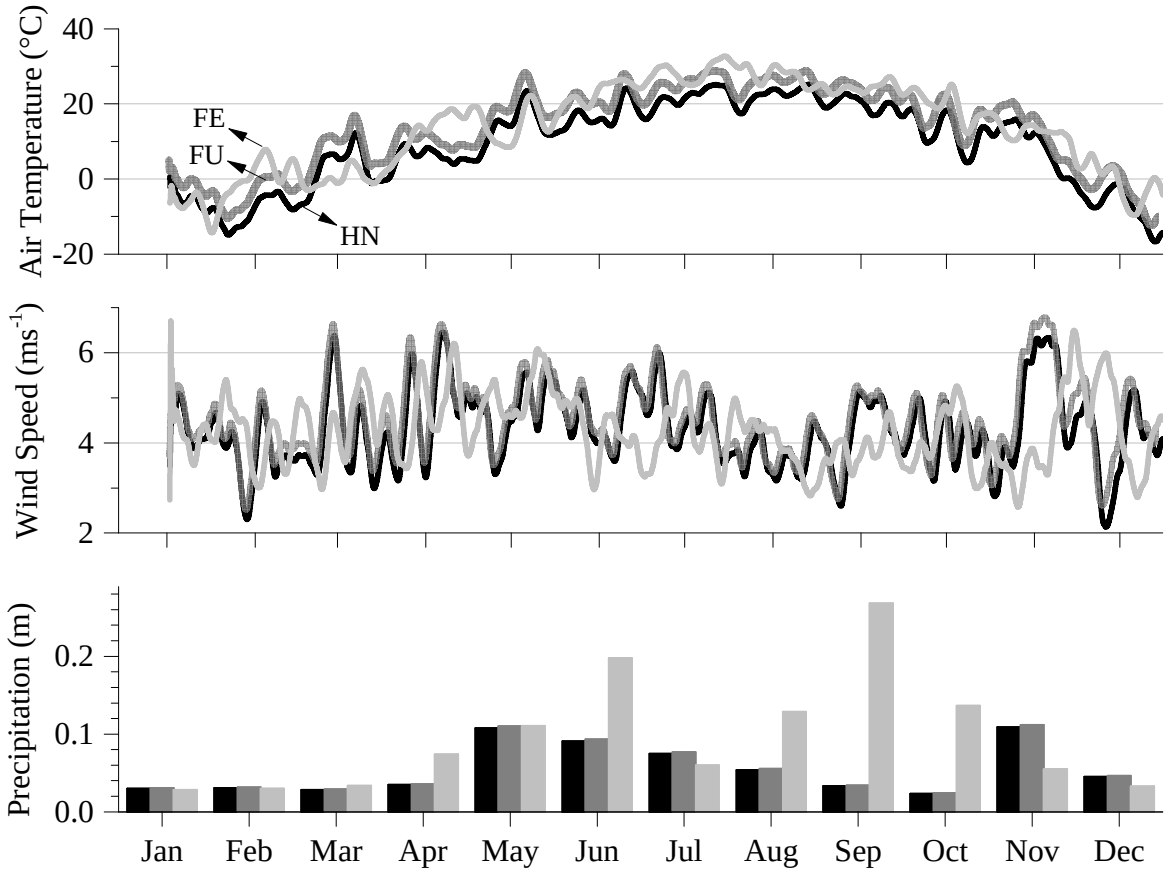

Fig. 5.3. Comparison of lake water levels simulated under historical normal, historical extreme (2005), future, and future extreme climate scenarios for the study area with their monthly total precipitation shown on top.

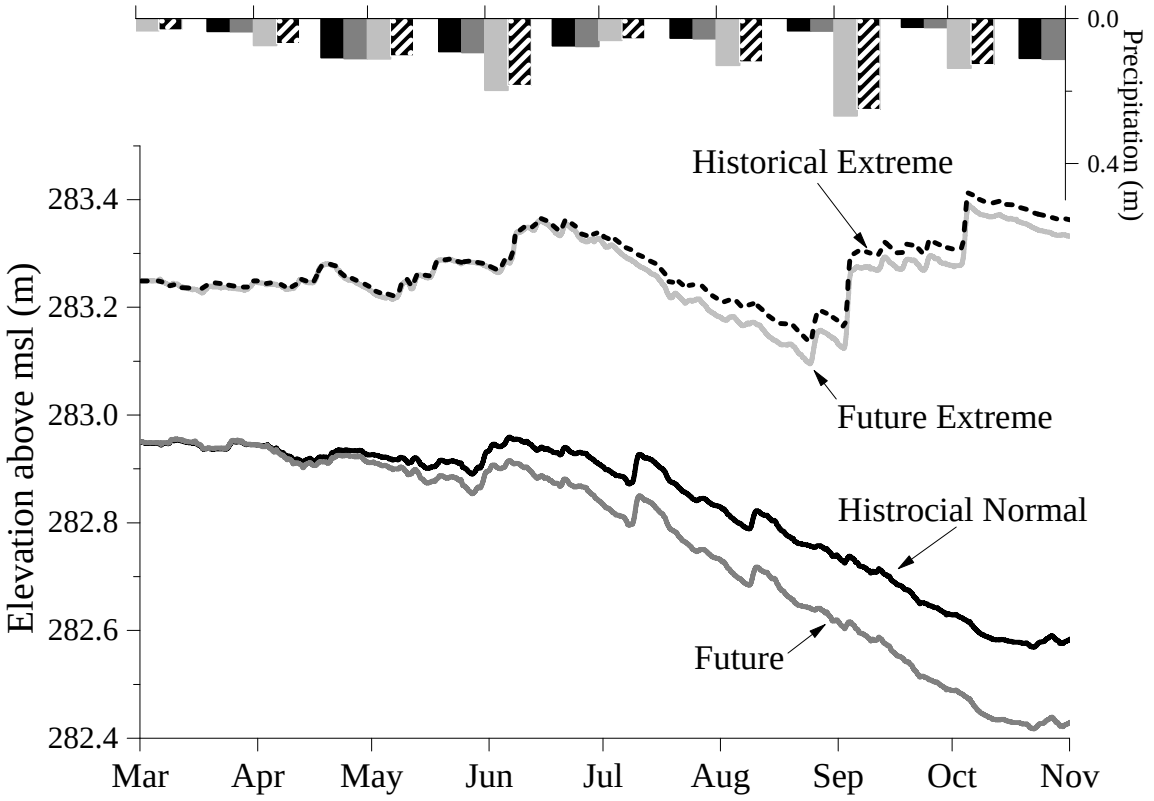

Under all three simulated scenarios, T emerged uniform throughout the water column after spring turnover and followed by surfaced T changes reflecting seasonal pattern of T_a (Fig. 5.4a). A warmer T_a in March and stronger winds in April of FU scenario (Fig. 5.2) caused an increased in hypolimnion T that made it warmer than the other two scenarios throughout the simulation periods (Fig. 5.4b). Beginning November 1, T decreased rapidly followed by fall turnover and water column mixing that yielded a uniform T throughout the water column again in all scenarios.

Fig. 5.4. Comparison of modeled water temperature (°C) and dissolved oxygen (mgL^{-1}) in the study area under a) historical normal , b) future, and c) future extreme climate scenarios. Horizontal and vertical axes of contour plots represent time and depth (m), receptively.

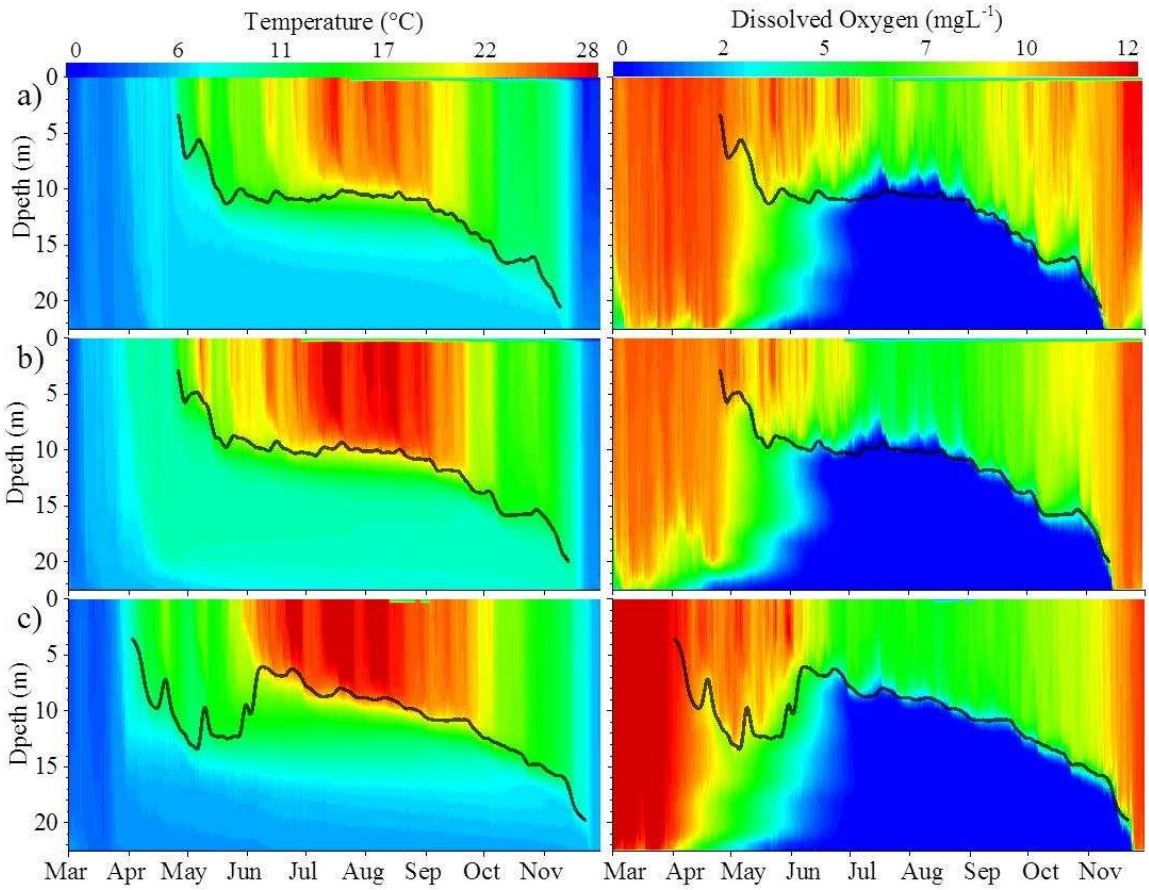

The simulated DO concentrations were at their maximum seasonal concentrations and were uniform throughout the water column immediately after spring turnover under all three scenarios (Fig. 5.4). A warmer hypolimnion in the FU scenario kept the DO concentrations less than in the HN scenario. The warmer FU hypolimnion promoted the onset of anoxia as early as in April 15, a full month earlier than HN and two weeks sooner than the FE scenarios. Nonetheless, hypolimnion was mostly anoxic in all three scenarios by June 15 before the DO concentrations were restored to their maximum levels by fall turnover starting November 10. The seasonally averaged DO profiles of the FU and FE scenarios mimicked each other (Fig. 5.5). For the study area, a season was

defined from the start of the average ice-out day (~April 13) to the end of water quality sampling period marked by fall turnover (November) (MCWD 2009; MCWG, 2013,). For our purposes, we defined the season from April 15 to November 1. The HN seasonally averaged DO profile was generally 1 mgL^{-1} more than both the FU and FE scenarios throughout the water column. The seasonally averaged T in the future scenarios were 4 °C in the eplimnion and 2 °C in the thermocline warmer than in the HN scenario, but the FE scenario had the coldest hypolimnion T. The seasonally averaged DO and T profiles showed a marked increase in T and decrease in DO in the FU and FE scenarios as compared against HN scenario.

Fig. 5.5. Comparison of modeled seasonally averaged of water temperature (°C) and dissolved oxygen (mgL^{-1}) profiles at West Upper Bay of the study area under historical normal , future, and future extreme climate scenarios.

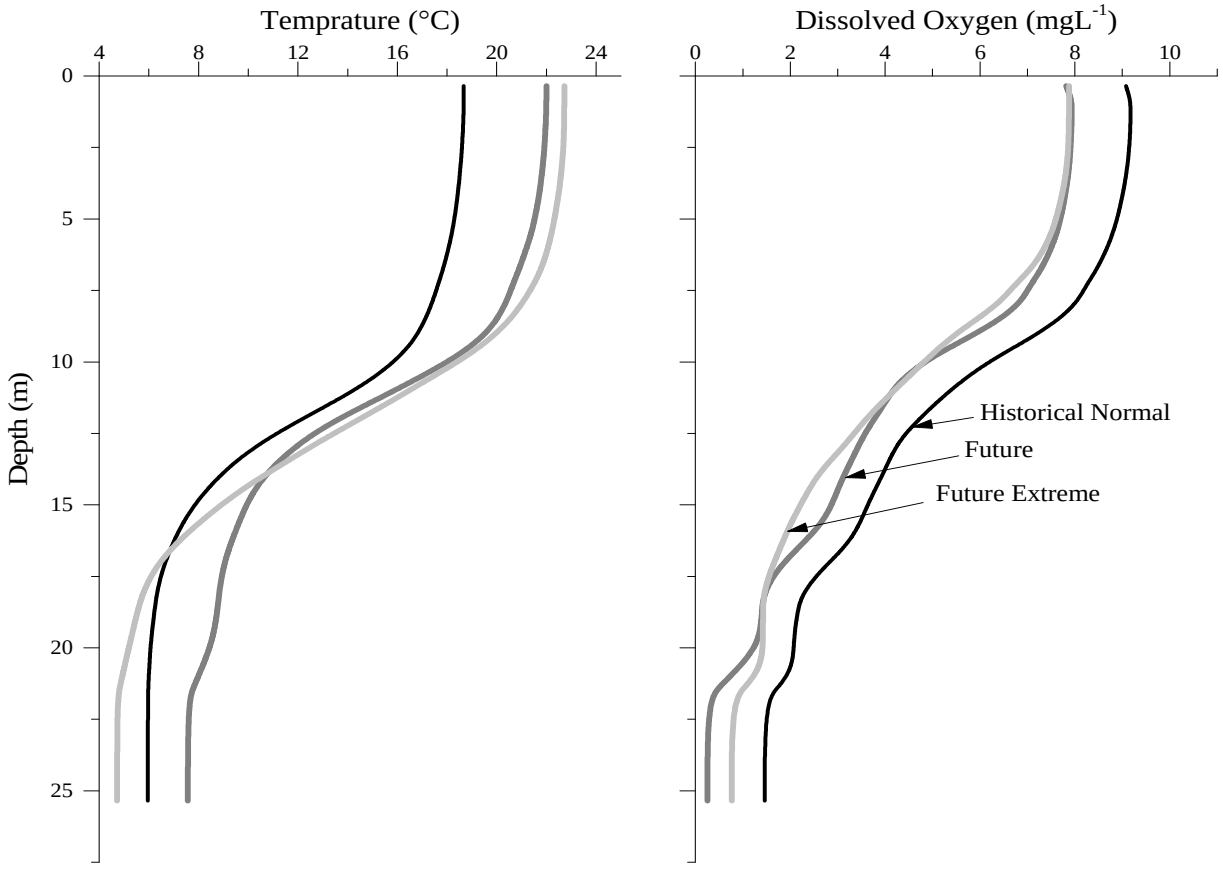

However, each of the HN, FU, and FE scenarios displayed their own distinct maximum (top 0.5 m surface water) and minimum (bottom 1 m depth layer) water temperature (Fig. 5.6). The FE scenario had both the coolest T minimum and highest T maximum. The onset of stratification initiated the formation of thermocline which was calculated by finding the depth layer with the maximum change of T of at least 1°C per 1 m (Wetzel, 2001). A well-defined thermocline started forming in both the HN and FU scenarios by April 26 and followed similar patterns through the simulation periods, except in the months of April and May where the FU scenario thermocline averaged 14% shallower (Table 5.2 and Fig. 5.4). The FE scenario thermocline was formed 3 weeks earlier (April 4) than the HN scenario and had the largest depth fluctuations among all scenario throughout the simulation periods (Fig. 5.4). The FE thermocline was 49% deeper in the months of April and May but was an average of 17% shallower than the HN thermocline for the rest of the simulation period.

Table 5.2. Simulated monthly averaged thermocline depth (m) under historical normal (HN), future (FU), and future extreme (FE) climate scenarios.

	historical normal (m)	**future (m)**	**future extreme (m)**
April	5.5	4.8	8.8
May	8.9	7.7	12.2
June	10.8	10.0	7.2
July	10.6	10.1	8.6
August	10.7	10.5	9.5
September	12.7	12.4	11.2
October	16.2	15.4	13.8
November	19.2	17.8	17.1

Fig. 5.6. Comparison of the surface T, bottom T, and start (circles), end (squares), and duration (vertical lines) of stratification at West Upper Bay modeled under historical normal , future, and future extreme climate scenarios.

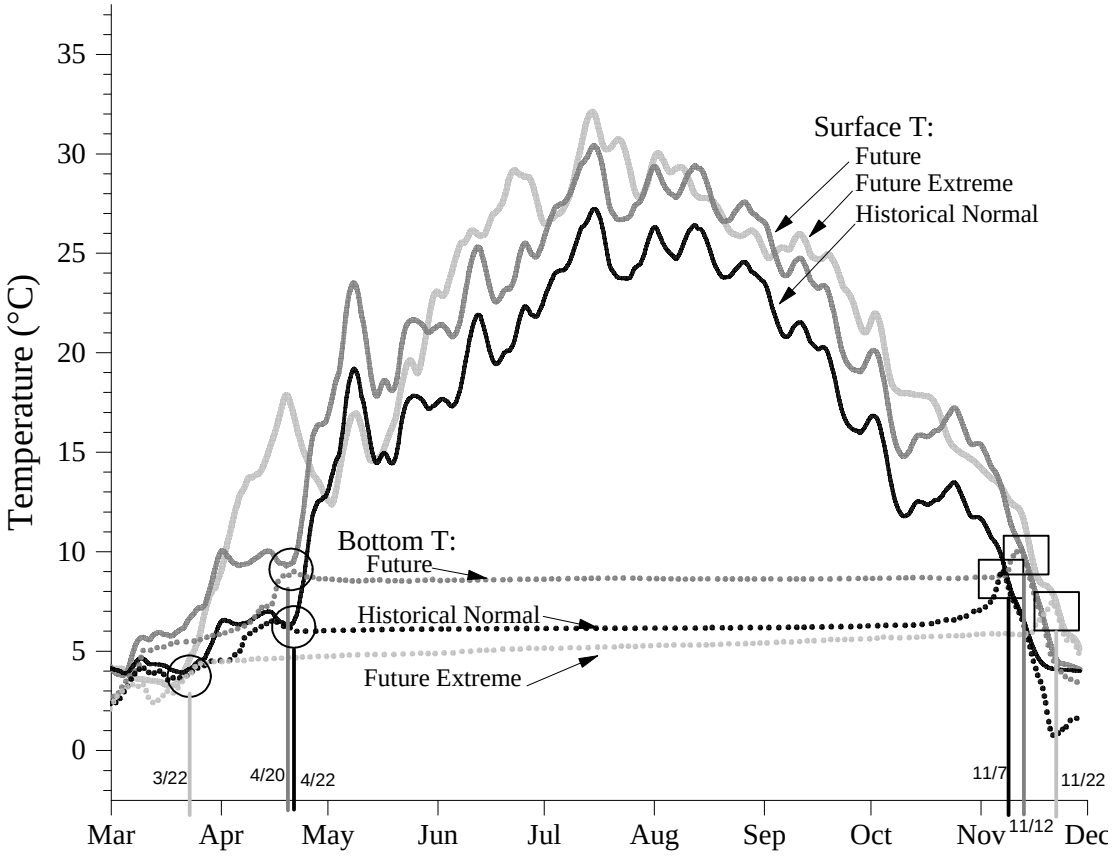

5.3.2. Fish habitat evaluation

Every control volume (cell) of each depth layer model outputs was queried for coolwater fish T and DO criteria for good growth, restricted growth, and lethal habitat under the three HN, FU, and FE scenarios. The number of cells of each type of habitat was computed and normalized by the total volume of the lake and reported as the percentage of the lake volume. The changes in the annual averages within the three fish habitats and between the three scenarios ranged from 2 to 14% of the total lake volume with significant spatial and temporal redistribution (Table 5.3).

Table 5.3. The annual total (percent of the lake volume, %) of good growth, restricted growth, and lethal fish habitats evaluated under simulated historical normal , future, and future extreme climate scenarios in the study area.

Climate Scenarios	Good Growth (%)	Restricted Growth (%)	Lethal (%)
Historical normal	33.3	60.0	6.7
Future	42.4	47.0	10.6
Future extreme	34.8	51.2	14.0

Daily, weekly, and monthly averages of fish habitat criteria of T and DO of every cell for all depth layers were calculated, their fish habitat type evaluated, their sum of percent of the total lake volume computed, and plotted over the simulation periods of the HN, FU, and FE scenarios (Fig. 5.7). The larger time scale of monthly averaged results supported the earlier general findings that under future scenarios the annual percentage of the lake volumes of good growth was increased, restricted growth decreased, and lethal habitat significantly increased. The daily averaged plots of fish habitats with the finest temporal resolution of one day time step, depicted many sudden (1-3 days) episodic fish habitat changes with as much as 80% change in the total lake volume (Fig. 5.7, Jul. 23, lethal habitat in the FE scenario). The impact of undesirable habitat on fish depends on its severity and the duration that fish are exposed to it. Fish may find temporary refuge or survive the stress during the very short and sudden habitat changes. For our purposes, we used a 7-day long (weekly) averaged fish habitat criteria to evaluate the changes in fish habitat. A week long exposure to restricted growth or lethal habitat was deemed sufficient time to use as a metric for our evaluations and to show stress or harm to fish, as used in studies in the US (Fang & Stefan, 2012) and UK, (Elliott & Bell, 2011). Based on the daily and weekly averaged results, we selected five one-week periods to compare the spatial (vertical and horizontal) fish habitat changes under the HN, FU, and FE scenarios. The five periods (shown as thick bars in Fig. 5.7) included four different weeks (June 3-9, June 20-27, July 3-10, and July 29-August 3) with significant (>10 percentage points) and one week (September 1-7) with minimal fish habitat changes.

Fig. 5.7. Percentage of the total lake volume for a) good growth, b) restricted growth, and c) lethal fish habitats based on predicted model variables that are averaged daily, weekly, and monthly modeled under simulated historical normal , future, and future extreme climate scenarios in Lake Minnetonka.

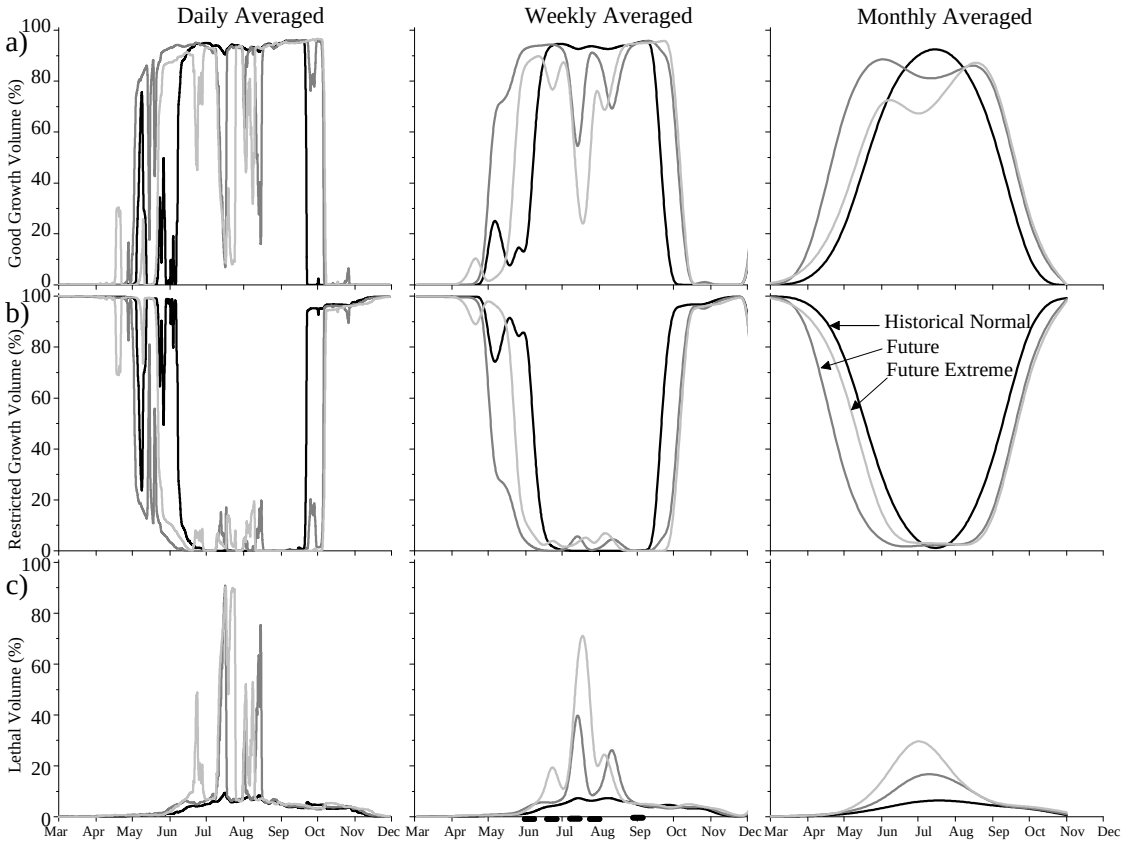

A vertical fish habitat distribution was made by computing the cumulative volume of all depth layers along with the percent of each type of fish habitats within every depth layer and plotting them over depth for all scenarios (Fig. 5.8). Almost all of the cells with lethal habitat in the HN scenario were located below the 10 m depth. Fish habitat changes in the future scenarios from the HN scenario were calculated (Fig. 5.8, Inset) for each depth layers. Under future scenario restricted growth decreased 13, good growth and lethal habitat increased 9 and 14 percentage point of the total lake volume. In the case of the future extreme, good growth changed little but restricted growth decreased 8.8

percentage points, and lethal habitat expanded more than two times (increased from 6.7% to 14%) with 70% of those changes taking place in the top 5 m depth layers.

Fig. 5.8. Hypsographic curves, showing the percentage of total lake volume (x axis) over depth (y axis) for the averaged good growth, restricted growth, and lethal fish habitats under simulated a) historical normal , b) future, and c) future extreme climate scenarios, with the insets showing the changes in percentage points from the historical normal.

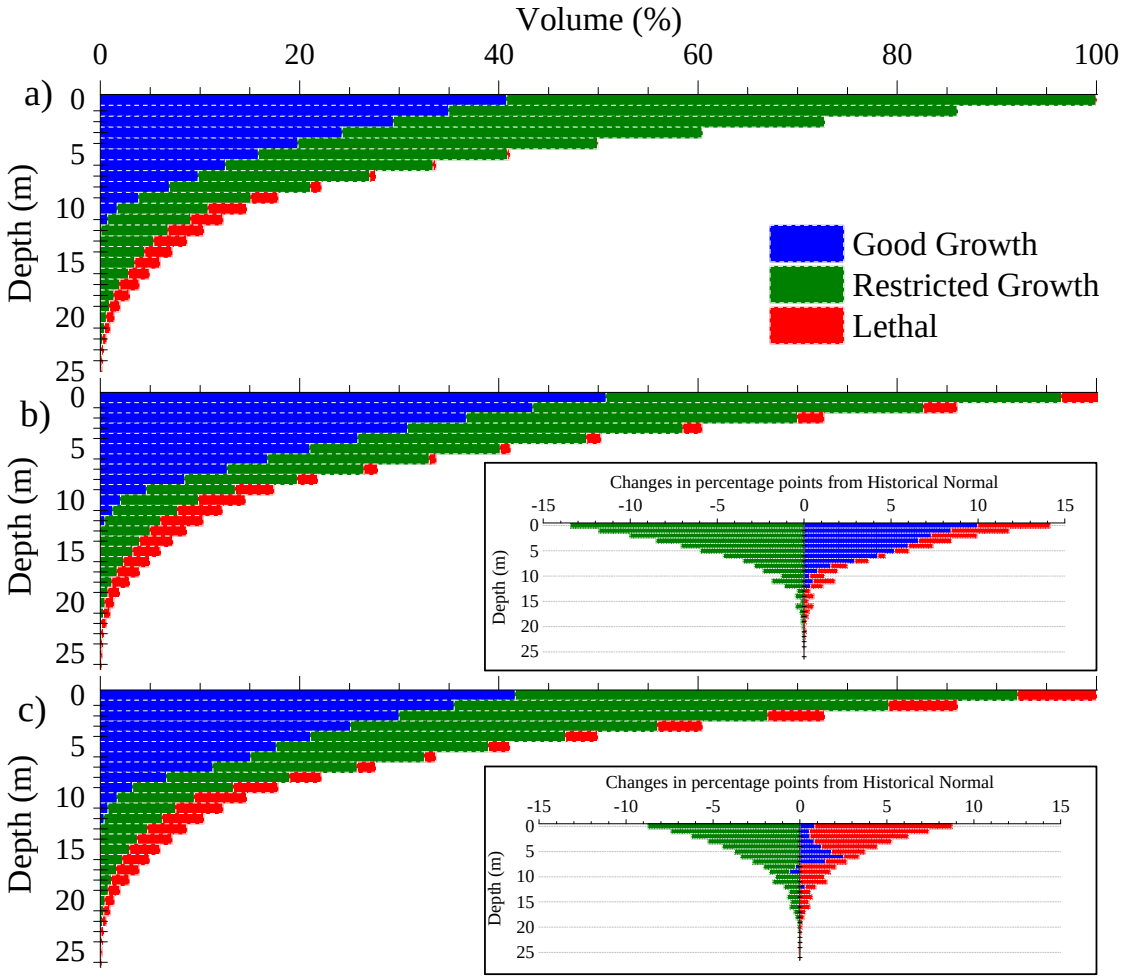

We next focused on the deepest point of the study area (WU) to investigate the fish habitat changes within the water column and throughout the simulation period. Contour plots of the three fish habitats simulated under the historical normal, future, and future extreme scenarios (Fig. 5.9) clearly depicted the changes in fish habitat and correlated well with the findings of the whole lake volume analysis (Fig. 5.8). The period of restricted growth habitat from June 1, to the beginning of the simulation was shortened in both the FU and FE scenarios and replaced by an increase in good growth habitat which expanded earlier into the season by 2 and 3 weeks in the FE and FU respectively. The lethal habitat started on May 12 in the HN, two weeks after (May 26) in the FE scenario, and in both cases quickly expands from the bottom to 10 m depth by June 10. The lethal habitat started earliest in the FU scenario and was at 10 m depth two weeks earlier than both the FE and HN scenarios. Similarly to the whole lake volume analysis (Fig. 5.8) and as depicted in the Fig. 5.9, the majority of changes took place in the upper 5 m of the water column. The timing of changes correlated with the four significant periods identified earlier.

Fig. 5.9. Contour plots of good growth (GG), restricted growth (RG), and lethal (L) fish habitats based on the predicted model variables averaged weekly under simulated a) historical normal , b) future, and c) future extreme climate scenarios at the deepest point (West Upper Bay) of the study area.

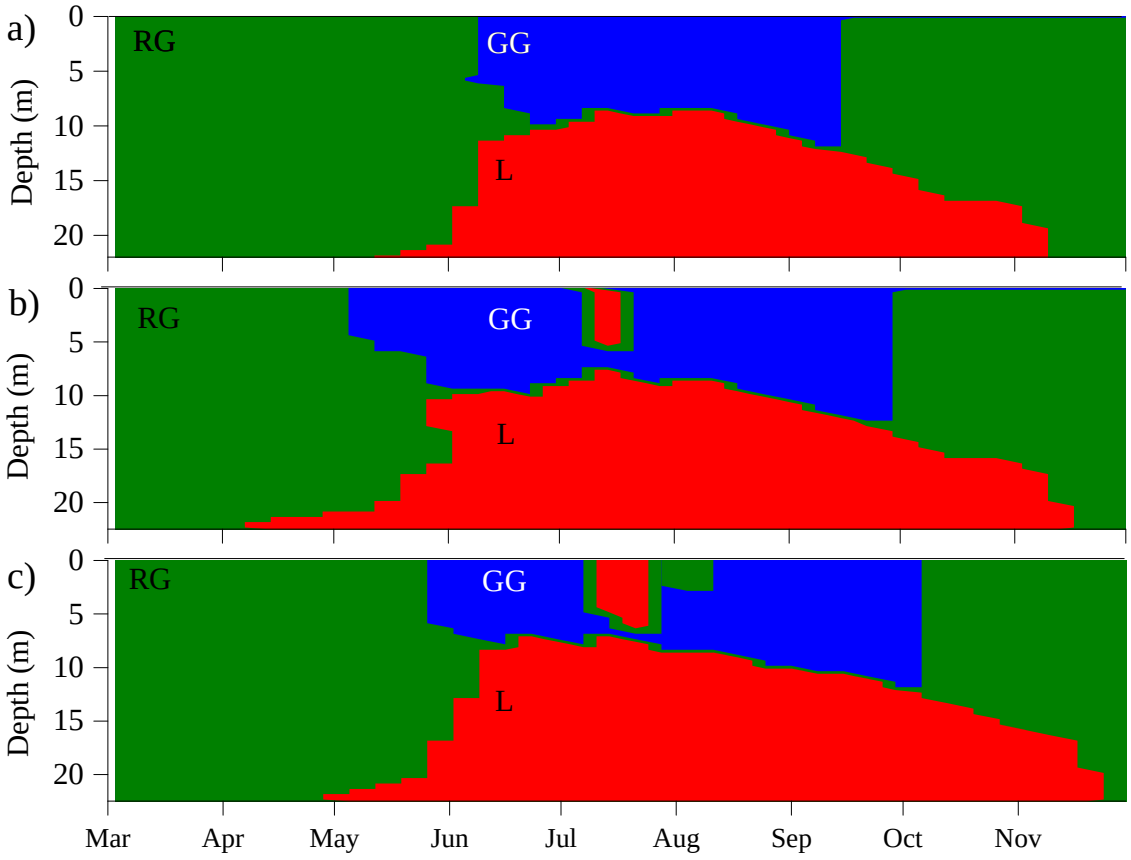

We used the 3D feature of the model to investigate the spatial (horizontal) fish habitat heterogeneity in each of the three different climatic scenarios. We first depth averaged the T and DO of the depth layers covering the entire study area in the top 5 m (depth with most fish habitat changes). The T and DO of each of the cells of this averaged depth layer were then averaged weekly over the entire simulation period and finally evaluated accordingly for the three fish habitat types. The comparison of the surface areas for each of the selected five periods under the simulated HN, FU, and FE scenarios depicted the expansion of lethal habitat in July 7-14 and expansion of good growth habitat earlier in the season in both the FU and FE scenarios (Fig. 5.10). Under the HN scenario the entire surface area (of the top 5 m) of the study area was evaluated as restricted growth habitat

in June 2-7, where average T < 16 °C but is entirely changed to good growth habitat under the FU and FE scenarios. The lethal habitat expanded in the FE scenario from the month of July into earlier in the season (through June 20-27) (Fig. 5.10).

Fig. 5.10. Comparison of the areas of the study area with good growth (blue), restricted growth (green), and lethal (red) coolwater fish habitats based on the predicted model variables averaged weekly for the top 5 meters of water column under simulated a) historical normal, b) future, and c) future extreme scenarios covering the entire study area with all horizontal and vertical axes as distance in km.

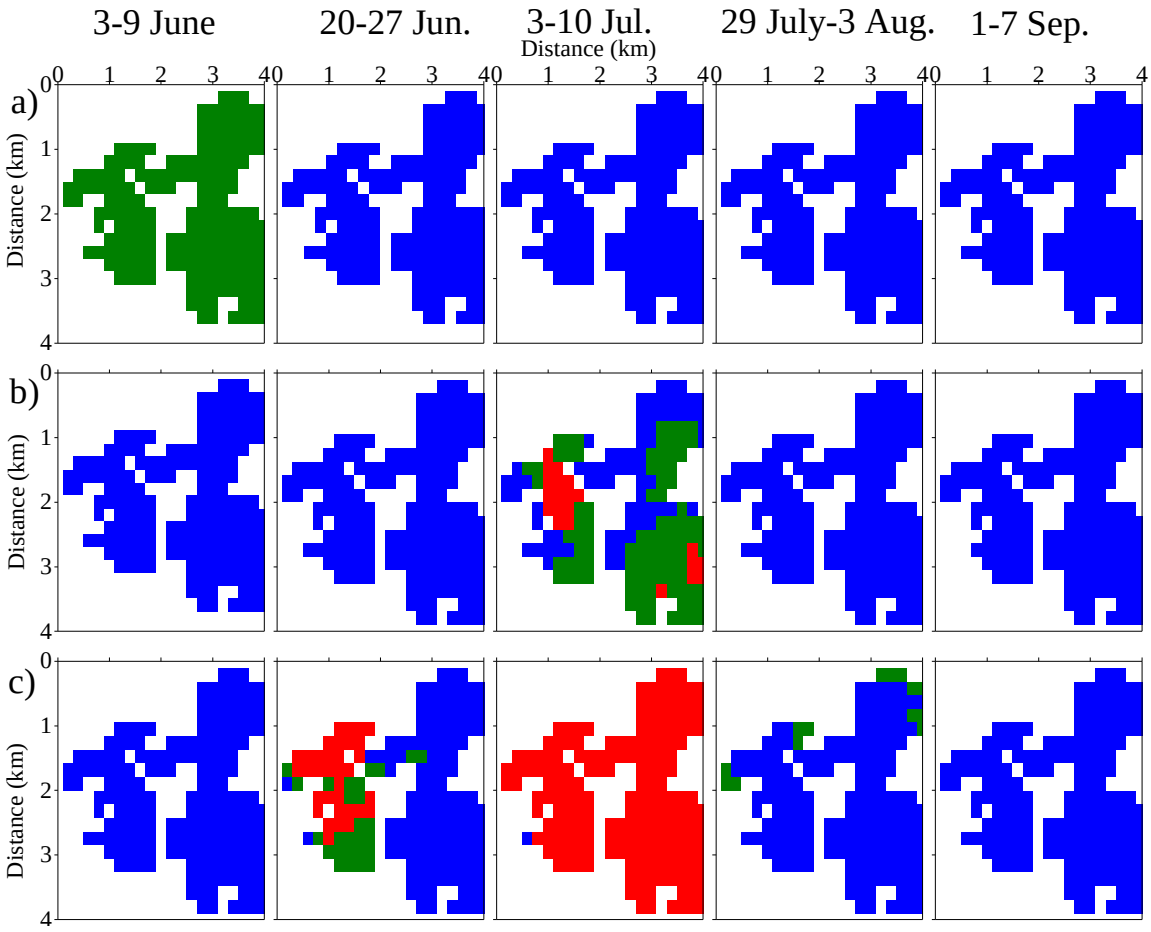

5.4. Discussion

We used a 3D coupled hydrodynamic and ecological model, previously successfully applied to our morphologically complex lake, to simulate one historical and two future climatic scenarios. The results revealed the influence of the specific and combined changes of the metrological forcing data on the key water quality parameters that form the coolwater fish habitat. The selection of the historical normal (HN) scenario based on the most recent climate normals for T_a and P, and the application of CF's to the measured metrological data provided reliable variables for historical and climate change scenarios (Carter, Hulme & Lal, 1999). We were able to generate three hydrologically and climatically distinct and reliable scenarios to use for the simulations where each result showed the influence of their distinct individual meteorological forcing data.

The water level results along with the result of the model goodness of fit, R^2 (Fig. 2.6) proved that the model could reliably be applied to the study area under different climatic scenarios. The measured lake water temperature profiles (vertical) evaluated for the model goodness of fit represented three different distinct bays (horizontal) of the lake and the model was successful in accurately capturing the lake's three dimensional thermo structure and heterogeneity. An extensive sensitivity and uncertainty analysis of the calibrated (year 2000, base reference for FU) and validated (year 2005, used as base reference for FE) simulation results had provided valuable insights in investigating the predicted model outputs (Missaghi et al, 2013) which minimized the model output uncertainty.

Model simulations for past and future climate scenarios

The specific and combined influences of the metrological forcing data of each climatic scenario were well evidenced in the simulation results. With the benefit of the ice-cover during winter, all three scenarios started with similar initial conditions and a uniform T and DO throughout the water column after spring turnover. The water column in the FU scenario began warming up the earliest in the season (March 20) followed by the FE

scenario (April. 1) with the HN scenario at last in April 15. The FE scenario T increased at the fastest rate (6.3 °C per month) before reaching maximum T in July similar to HN and FU scenarios. Considering that the FU forcing data were generated by applying CFs to the HN forcing data, the FU scenario T generally followed similar pattern of that of HN scenario. However, coincidently, the maximum daily surface water temperature for all three scenarios was on July 15 (Fig. 5.6). The onset of stratification also followed similar pattern to T, with the onset of stratification taking place in the FU two days and in the FE a full month earlier than the HN scenario (April 22) (Fig. 5.6). At the end of the season, the stratification periods ended on November 7 for the HN scenario (199 days), lasted to November 12 for the FU scenario (206 days), and ended on Nov. 22 for the FE scenario with 46 days (23% increase) longer than the HN stratification period.

In both future scenarios the epliminion T mimicked the predicted warmer T_a and followed the T_a seasonal changes. The hypolimnion T changes were less responsive to T_a (Fig. 5.6). Our findings were in agreement with previous studies (Trolle et al., 2011; Bayer, Burns & Schallenberg, 2013) and originally reported by Hondzo and Stefan (1993) that T in the epiliminion is very responsive to predicted T_a but not in the hypolimnion. The warmer epilimnion T increases the water column stability which resists mixing and can create cooling of hypolimnion (Livingstone, 2003, Trolle et al., 2011), as observed in the FE scenario which had the warmest eplimnion T and the coolest hypolimnion T. The combined influence of higher wind speed (ave. WS >4.5 ms^{-1}) and rising T in the FE scenario early in the year forced the thermocline deeper than in HN and FU scenarios (Fig. 5.2 and 5.4). But, the thermocline depth rapidly decreased after June where a warmer eplimnion had stabilized the water column (less mixing) followed by persistent low wind conditions (ave. WS <4 ms^{-1}). The predicted thermocline changes in the FE scenario were similar to other studies reported (Bayer et al., 2013). The predicted extended and stronger stratification has significant implications as it can influence timing of fish spawning, reduce the exchange of nutrients between the stratums and interrupt the

transfer of energy and food supply to fish, influence DO concentration dynamics, and alter fish habitats (MacKay et al 2009).

Except with a few deviations, the DO depletion areas (anoxic zone) closely followed the mixing boundaries delineated by thermocline (Fig. 5.4). We had defined thermocline as the maximum T change in areas with of at least 1 °C change of T per m. However, the DO vertical transport has been shown to be suppressed with as little as 0.5 °C change in T per m (Foley et al., 2012) which may explain some of the deviations. The epilimnion DO concentrations were episodic and reflected the influences of physical forcing data of T and wind speed. For example, under the FE scenario, an increased in a 10 day average wind speed from 3.5 ms^{-1} in the 10 days prior to June 24 to an average of 5.23 ms^{-1} in 10 days after (48% increase) caused a sudden deepening of DO rich epliminion and a decrease in the anoxic area (Fig. 5.4c). The DO episodic changes were magnified in the shallow bays (<10 m) where the intermittently mixing of the larger anoxic layer with the epliminion caused DO concentrations of less than 3 mgl^{-1} in the whole water column for short durations (<2 weeks) (not shown here). The short duration changes of DO concentrations in the HN scenario were investigated and shown to be driven in parts by the stream inflow mixing regimes (Missaghi and Hondzo, 2010). Force (inflow and wind) induced mixing of anoxic bottom layers can produce major ecological consequences such as fish kill (Jeppesen et al., 2010).

The thermal structure also plays a major role in the plankton community by shaping plankton species succession dynamics, algae biomass, fish habitat (Elliott & Bell, 2011), and ultimately the aquatic food web (Wetzel 2000; Sastri et al., 2014). The model sensitivity and uncertainty analysis had previously shown that over half (58%) of model output variance was contributed by the algae biomass model predicted variable (Missaghi et al, 2013). The challenge is first to reduce the uncertainty of algae group model output through better field data and greater understanding of the ecological processes that influence algae biomass. The second challenge is to configure algae groups in

simulations not as how they are currently described (model parameters) but how they may adapt and function under future climate scenarios. One potential method of configuring the algae groups would be to include multiple sets of the same algae groups but with varying model parameter values so a proper algae group is provided under each scenario condition.

5.5. Fish habitat evaluation

We used T values and DO concentrations (Table 2.3) to delineate and evaluate coolwater fish habitats as previously established by Stefan et al. 2001 and used by others (e.g. Fang et al., 2012). This and similar approaches (Dillon et al., 2003) have been reliable, effective, and useful in analyzing fish habitat under different climatic scenarios. The influence of T and DO on fish habitat among the scenarios evaluated was significant (Table. 5.3). Under the HN scenario the fish habitat ratio of good growth:restricted growth:lethal equaled to 5:9:1. However, the volumes of good growth habitat increased 9, restricted growth decreased 13, and that of lethal habitat volume increased 4 percentage points under the FU scenario changing the fish habitat ratio to 4:4:1. The volume of lethal habitat more than doubled, but good growth increasing only 1.5 points and restricted growth decreasing 8.8 points yielding a fish habitat ratio of 2:4:1 in the FE scenario. Clearly, the lethal habitat grew to a larger fraction of the total available fish habitat under the FU, and FE scenarios. We were able to analyze the temporal and spatial shift and displacement of fish habitats under future climate change scenarios.

The daily averaged fish habitat time series (Fig. 5.7) with the finest temporal resolution allowed us to identify the important temporal points of environmental stress due to restricted growth or lethal fish habitats. The weekly averaged fish habitat time series offered a time scale with sufficient length to capture the potential stress or harm posed by both restricted growth or lethal habitats and small enough time scale to capture fish habitat dynamics. Most of fish habitat shifts and changes (70%) were concentrated in the top 5 m of the water column (Fig. 5.8) with 5 to 15% of the fish habitats changing within

each depth layer. Only 5% and 1% of fish habitats changed in each depth layer below 5 and 10 m depth, respectively. The climatic changes of the FU and FE scenarios widen the monthly averaged good growth and restricted growth curves and decreased their amplitude (Fig. 5.7). Consequently, the period of the good growth fish habitats was expanded within the simulation period under future scenarios (Fig. 5.9). But the changes in the lethal habitat were focused in one temporal zone (mid Jul.) and their peaks increased significantly under the FU and FE scenarios.

The 3D feature of our model allowed us to analyze the spatial (horizontal) expansion of lethal habitat starting from the mid-season and the contracting good growth fish habitat from the edges (Fig. 5.10). Other studies have also shown that under a warming climate change scenario a reduction of favorable lake fish habitat takes place in edges and near shore habitat (Cline et al., 2013). Areas of the lake with depths shallower than the mixing depth (thermocline) were susceptible to an increase in T and a shift from good growth to restricted growth and lethal habitat (Fig. 5.10). The combination of the lethal habitat increasing in one time period and the good growth fish habitat receding earlier in the year squeezed the good growth area apart for over 3 weeks in July (Fig. 5.9). With good growth fish habitat contracted and separated, the coolwater fish had no potential refuge during the three weeks of good growth fish habitat separation (Fig. 5.10). In our analysis we did not consider fish migration out of the study area and assumed that our study area was physically enclosed similar to an entire lake basin. In case of an enclosed basin with lack of a refuge during the good growth habitat separation, fish cannot physiologically change quick enough to adapt to the shifting and changing of their habitats. Therefore, providing permanent or temporary refuge during good growth habitat separation becomes an important consideration for lake managers. Fish are living organism with an array of behavioral dynamics that may manifest many unknown attributes and establish their own ecological consequences when faced with ecological stresses (Britton et al., 2010), such as developing forging forays into anoxic zones (James et al., 2012). However, a complete separation of good growth habitat with no refuge for

coolwater fish will lead to summer fish kill. If fish cannot adopt new territory by moving outside of their stressed basin then they may become locally extinct and their population shifting to other area lakes or towards higher latitude and altitudes (Jeppesen et al., 2010). The shift and changes of coolwater fish habitat will influence specie competition and prey interactions (Cline et al., 2013) affecting the existing stress of competition or the stress of a newly introduced and better suited specie to the new habitat (Britton et al., 2010).

We successfully applied a 3D coupled hydrodynamic and ecological model to a morphologically complex lake. The success of the model results were supported by prediction of calibration (2000) and validation year (2005) output that accurately captured the thermal structure and DO dynamics of the system. The method of selection of one climatic historical scenario based on measured 30 year normal meteorological data and using two measured historical metrological years (2000 and 2005) as base for predicted future scenarios proved reliable and increased our confidence in the model predicted output results. The results predicted an increase in T values and decrease in DO concentration levels with negative impact on coolwater fish habitat. The results showed that the changes in the lake thermal structure under the future scenarios reflected the influences of a warmer air temperature that along with decreased DO concentration patterns controlled the boundaries of fish habitats. The results of the predicted impact of climate change on fresh-water lakes reported here are supported by other scientific investigations that show, as we found, habitats such that of fish are not stationary (Milly et al., 2008; Fang & Stefan, 2012; Cline et al., 2013). The total change in volume of uninhabitable fish habitat was modest (8 percentage points of total lake volume increase from historical normal to future extreme scenario), but with significant spatial and temporal changes that squeezed feasible good growth fish habitats to the point of separation in July for over 3 weeks. Investigating the potential changes of climate change on fish habitats by solely relying on evaluation of change in volume may miss important temporal and spatial consequences.

Bibliography

Abbott, M.R., Denman, K.L., Powell, T.M., Richerson, P.J., Richards, R.C. and Goldman, C.R., 1984. Mixing and the dynamics of the deep chlorophyll maximum in Lake Tahoe. Limnol.Oceanogr. 29, 862-878.

Adrian, R., O'Reilly, C.M., Zagarese, H., Baines, S.B., Hessen, D.O., Keller, W., Livingstone, D.M., Sommaruga, R., Straile, D. and Van Donk, E., 2009. Lakes as sentinels of climate change. Limnol.Oceanogr. 54, 2283.

Al-Homoud, A. and Hondzo, M., 2008. Enhanced uptake of dissolved oxygen and glucose by Escherichia coli in a turbulent flow. Appl.Microbiol.Biotechnol. 79, 643-655.

Arhonditsis, G.B. and Brett, M.T., 2004. Evaluation of the current state of mechanistic aquatic biogeochemical modeling. Mar.Ecol.Prog.Ser. 271, 13-26.

Arhonditsis, G.B. and Brett, M.T., 2005. Eutrophication model for Lake Washington (USA) Part I. Model description and sensitivity analysis. Ecol.Model. 187, 140-178.

Asaeda, T., Pham, H., Nimal Priyantha, D., Manatunge, J. and Hocking, G., 2001. Control of algal blooms in reservoirs with a curtain: a numerical analysis. Ecol.Eng. 16, 395-404.

Bayer, T.K., Burns, C.W. and Schallenberg, M., 2013. Application of a numerical model to predict impacts of climate change on water temperatures in two deep, oligotrophic lakes in New Zealand. Hydrobiologia. 713, 53-71.

Beck, M.B., 1987. Water quality modeling: a review of the analysis of uncertainty. Water Resour.Res. 23, 1393-1442.

Belmont, M.A., White, J.R. and Reddy, K.R., 2009. Phosphorus sorption and potential phosphorus storage in sediments of Lake Istokpoga and the upper chain of lakes, Florida, USA. J.Environ.Qual. 38, 987-996.

Bergstedt, M.S., Hondzo, M.M. and Cotner, J.B., 2004. Effects of small scale fluid motion on bacterial growth and respiration. Freshwat.Biol. 49, 28-40.

Brett, M.T. and Benjamin, M.M., 2008. A review and reassessment of lake phosphorus retention and the nutrient loading concept. Freshwat.Biol. 53, 194-211.

Britton, J., Cucherousset, J., Davies, G., Godard, M. and Copp, G., 2010. Non-native fishes and climate change: predicting species responses to warming temperatures in a temperate region. Freshwat.Biol. 55, 1130-1141.

Bruce, L.C., Hamilton, D., Imberger, J., Gal, G., Gophen, M., Zohary, T. and Hambright, K.D., 2006. A numerical simulation of the role of zooplankton in C, N and P cycling in Lake Kinneret, Israel. Ecol.Model. 193, 412-436.

Brun, R., Reichert, P. and Kuensch, H.R., 2001. Practical identifiability analysis of large environmental simulation models. Water Resour.Res. 37, 1015-1030.

Brus, D. and Jansen, M., 2004. Uncertainty and sensitivity analysis of spatial predictions of heavy metals in wheat. J.Environ.Qual. 33, 882-890.

Burges, S.J. and Lettenmaier, D.P., 1975. Probabilistic Methods In Stream Quality Management1. JAWRA Journal of the American Water Resources Association. 11, 115-130.

Cacuci D. G., 2003. Sensitivity and Uncertainty Analysis: Theory. 304 CRC Press, Boca Raton, Florida, 304 pp.

Carraro, E., Guyennon, N., Hamilton, D., Valsecchi, L., Manfredi, E.C., Viviano, G., Salerno, F., Tartari, G. and Copetti, D., 2012. Coupling high-resolution measurements to a three-dimensional lake model to assess the spatial and temporal dynamics of the cyanobacterium Planktothrix rubescens in a medium-sized lake. Hydrobiologia. 1-19.

Chadderton, R.A., Miller, A.C. and McDonnell, A.J., 1982. Uncertainty analysis of dissolved oxygen model. Journal of the Environmental Engineering Division. 108, 1003-1013.

Chen, C., Ji, R., Schwab, D.J., Beletsky, D., Fahnenstiel, G.L., Jiang, M., Johengen, T.H., Vanderploeg, H., Eadie, B. and Budd, J.W., 2002. A model study of the coupled biological and physical dynamics in Lake Michigan. Ecol.Model. 152, 145-168.

Christie, G.C. and Regier, H.A., 1988. Measures of optimal thermal habitat and their relationship to yields for four commercial fish species. Can.J.Fish.Aquat.Sci. 45, 301-314.

Christophoridis, C. and Fytianos, K., 2006. Conditions affecting the release of phosphorus from surface lake sediments. J.Environ.Qual. 35, 1181-1192.

Clesceri LS, Greenberg AE, Eaton AD, 1999. Standard methods for the examination of water and wastewater, 20th edn. American Public Health Association, Washington, DC. American Public Health Association, Washington, DC, .

Coops, H., Beklioglu, M. and Crisman, T.L., 2003. The role of water-level fluctuations in shallow lake ecosystems–workshop conclusions. Hydrobiologia. 506, 23-27.

Coutant, C.C., 1985. Striped bass, temperature, and dissolved oxygen: a speculative hypothesis for environmental risk. Trans.Am.Fish.Soc. 114, 31-61.

Cullen, J.J., 1982. The deep chlorophyll maximum: comparing vertical profiles of chlorophyll a. Can.J.Fish.Aquat.Sci. 39, 791-803.

De Silva, I. and Fernando, H., 1994. Oscillating grids as a source of nearly isotropic turbulence. Phys.Fluids. 6, 2455.

De Stasio, B.T., Hill, D.K., Kleinhans, J.M., Nibbelink, N.P. and Magnuson, J.J., 1996. Potential effects of global climate change on small north-temperate lakes: Physics, fish, and plankton. Limnol.Oceanogr. 41, 1136-1149.

Dokulil, M.T. and Teubner, K., 2000. Cyanobacterial dominance in lakes. Hydrobiologia. 438, 1-12.

Durham, W.M., Kessler, J.O. and Stocker, R., 2009. Disruption of vertical motility by shear triggers formation of thin phytoplankton layers. Science. 323, 1067.

Dyble, J., Fahnenstiel, G.L., Litaker, R.W., Millie, D.F. and Tester, P.A., 2008. Microcystin concentrations and genetic diversity of *Microcyctis* in the lower Great Lakes. Environ.Toxicol. 23, 507-516.

Ebert, U., Arrayás, M., Temme, N., Sommeijer, B. and Huisman, J., 2001. Critical conditions for phytoplankton blooms. Bull.Math.Biol. 63, 1095-1124.

Efteland, S.P., 2004. The effects of iron on growth and physiology of the cyanobacterium *Microcyctis* aerugniosa [electronic resource].

Ekvall, M.K., Calle Martin, J., Faassen, E.J., Gustafsson, S., Lürling, M. and Hansson, L., 2013. Synergistic and species-specific effects of climate change and water colour on cyanobacterial toxicity and bloom formation. Freshwat.Biol.

Engstrom, D.R. and Swain, E.B., 1986. The chemistry of lake sediments in time and space. Hydrobiologia. 143, 37-44.

Environmental Protection Agency. US, 2005. **WOW. Water on the Web**. . 2004. Water on the Web - Monitoring Minnesota Lakes on the Internet and Training Water Science Technicians for the Future - A National On-line Curriculum using Advanced Technologies and Real-Time Data.(http://WaterOntheWeb.org). University of Minnesota-D. 2009, .

Fang, X., Stefan, H.G., Eaton, J.G., McCormick, J.H. and Alam, S.R., 2004. Simulation of thermal/dissolved oxygen habitat for fishes in lakes under different climate scenarios Part 1. Cool-water fish in the contiguous US. Ecol.Model. 172, 13-37.

Fang, X., Alam, S.R., Stefan, H.G., Jiang, L., Jacobson, P.C. and Pereira, D.L., 2012. Simulations of water quality and oxythermal cisco habitat in Minnesota lakes under past and future climate scenarios. Water Qual.Res.J.Can. 47, 375-388.

Fang, X. and Stefan, H.G., 2012. Impacts of Climatic Changes on Water Quality and Fish Habitat in Aquatic Systems. In: Anonymous Handbook of Climate Change Mitigation. Springer, pp. 531-569.

Fernand, L., Weston, K., Morris, T., Greenwood, N., Brown, J. and Jickells, T., 2013. The contribution of the deep chlorophyll maximum to primary production in a seasonally stratified shelf sea, the North Sea. Biogeochemistry. 1-14.

Ferris, M.J. and Hirsch, C., 1991. Method for isolation and purification of cyanobacteria. Appl.Environ.Microbiol. 57, 1448.

Foley, B., Jones, I.D., Maberly, S.C. and Rippey, B., 2012. Long-term changes in oxygen depletion in a small temperate lake: effects of climate change and eutrophication. Freshwat.Biol. 57, 278-289.

Fowler, H., Blenkinsop, S. and Tebaldi, C., 2007. Linking climate change modelling to impacts studies: recent advances in downscaling techniques for hydrological modelling. Int.J.Climatol. 27, 1547-1578.

Gaber, N., Guidance on the Development, Evaluation, and Application of Environmental Models. EPA/100/K-09/003, Washington, DC.

Gächter, R. and Müller, B., 2003. Why the phosphorus retention of lakes does not necessarily depend on the oxygen supply to their sediment surface. Limnol.Oceanogr. 929-933.

Gal, G., Hipsey, M., Parparov, A., Wagner, U., Makler, V. and Zohary, T., 2009. Implementation of ecological modeling as an effective management and investigation tool: Lake Kinneret as a case study. Ecol.Model. 220, 1697-1718.

Hamilton, D.P. and Schladow, S.G., 1997. Prediction of water quality in lakes and reservoirs. Part I—Model description. Ecol.Model. 96, 91-110.

Havens, K.E., 2008. Cyanobacteria blooms: effects on aquatic ecosystems. In: H. Kenneth Hudnell(ed.), Cyanobacterial harmful algal blooms: state of the science and research needs. Springer, pp. 733-747.

Heisler, J., Glibert, P.M., Burkholder, J.M., Anderson, D.M., Cochlan, W., Dennison, W.C., Dortch, Q., Gobler, C.J., Heil, C.A. and Humphries, E., 2008. Eutrophication and harmful algal blooms: a scientific consensus. Harmful algae. 8, 3-13.

Henderson-Sellers, B., French, R.H. and McCutcheon, S.C., 1991. Water Quality Modeling: Decision Support Techniques for Lakes and Reservoirs, Volume IV. CRC, .

Hennepin County Department of Environemntal Services, 417 North Fifth Street, Minneapolis, MN 55401-1397, 2003. Lake Minnetonka.

Herrero, A., Flores, E. and Flores, F.G., 2008. The cyanobacteria: molecular biology, genomics, and evolution. Caister Academic Pr, .

Hipsey, M.R., 2008. The CWR Computational Aquatic Ecosystem Dynamics Model CAEDYM. User Manual, Centre for Water Research, The University of Western Australia.

Hipsey, M.R., Gal, G., Antenucci, J.P., Zohary, T., Makler, V. and Imberger, J., 2006. Lake Kinneret water quality management system. Proceedings of the Seventh International Conference on Hydroscience and Engineering.

Hodges, B. and Dallimore, C., 2008. Estuary, Lake and Coastal Ocean Model: ELCOM Science Manual. User Manual, Centre for Water Research, The University of Western Australia. v2. 2, .

Hodges, B.R., 2000. Numerical Techniques in CWR-ELCOM (code release v. 1). CWR Manuscript WP 1422 BH.

Hodges, B., Imberger, J., Laval, B. and Appt, J., 2000. Modeling the hydrodynamics of stratified lakes. Hydroinformatics 2000 Conference. 4, 23-27.

Hondzo, M. and Haider, Z., 2004. Boundary mixing in a small stratified lake. Water Resour.Res. 40, W03101.

Hondzo, M. and Stefan, H.G., 1992. Propagation of uncertainty due to variable meteorological forcing in lake temperature models. Water Resour.Res. 28, 2629-2638.

Hondzo, M. and Stefan, H.G., 1996a. Long-term lake water quality predictors. Water Res. 30, 2835-2852.

Hondzo, M. and Stefan, H.G., 1996b. Dependence of water quality and fish habitat on lake morphometry and meteorology. J.Water Resour.Plann.Manage. 122, 364-373.

Hondzo, M. and Stefan, H.G., 1993. Regional water temperature characteristics of lakes subjected to climate change. Clim.Change. 24, 187-211.

Hondzo, M. and Warnaars, T.A., 2008. Coupled Effects of Small-Scale Turbulence and Phytoplankton Biomass in a Small Stratified Lake. J.Environ.Eng.-ASCE. 134, 954-960.

Huisman, J., Sharples, J., Stroom, J.M., Visser, P.M., Kardinaal, W.E.A., Verspagen, J.M.H. and Sommeijer, B., 2004. Changes in turbulent mixing shift competition for light between phytoplankton species. Ecology. 85, 2960-2970.

Huisman, J., Arrayás, M., Ebert, U. and Sommeijer, B., 2002. How do sinking phytoplankton species manage to persist? Am.Nat. 159, 245-254.

Huisman, J., van Oostveen, P. and Weissing, F.J., 1999. Critical depth and critical turbulence: two different mechanisms for the development of phytoplankton blooms. Limnol.Oceanogr. 44, 1781-1787.

Hunter, P., Tyler, A., Willby, N. and Gilvear, D., 2008. The spatial dynamics of vertical migration by *Microcyctis aeruginosa* in a eutrophic shallow lake: A case study using high spatial resolution time- series airborne remote sensing. Limnol.Oceanogr. 53, 2391-2406.

Hurtado, J.V., 2007. Basin-Scale Hydrodynamics in a Mediterranean reservoir. Implications for the phytoplankton dynamics. Universitat de Girona.

Imberger, J., Loh, I., Hebbert, B. and Patterson, J., 1978. Dynamics of reservoir of medium size. Journal of the Hydraulics Division. 104, 725-743.

Jeppesen, E., Kronvang, B., Meerhoff, M., Søndergaard, M., Hansen, K.M., Andersen, H.E., Lauridsen, T.L., Liboriussen, L., Beklioglu, M. and Özen, A., 2009. Climate change effects on runoff, catchment phosphorus loading and lake ecological state, and potential adaptations. J.Environ.Qual. 38, 1930-1941.

Jeppesen, E., Meerhoff, M., Holmgren, K., González-Bergonzoni, I., Teixeira-de Mello, F., Declerck, S.A., De Meester, L., Søndergaard, M., Lauridsen, T.L. and Bjerring, R., 2010. Impacts of climate warming on lake fish community structure and potential effects on ecosystem function. Hydrobiologia. 646, 73-90.

Jeppesen, E., Soendergaard, M., Jensen, J.P., Havens, K.E., Anneville, O., Carvalho, L., Coveney, M.F., Deneke, R., Dokulil, M.T. and Foy, B., 2005. Lake responses to reduced nutrient loading–an analysis of contemporary long-term data from 35 case studies. Freshwat.Biol. 50, 1747-1771.

Johnk, K.D., Huisman, J., Sharples, J., Sommeijer, B., Visser, P.M. and STROOM, J.M., 2008. Summer heatwaves promote blooms of harmful cyanobacteria. Global Change Biol. 14, 495-512.

Jones, J.R. and Bachmann, R.W., 1976. Prediction of phosphorus and chlorophyll levels in lakes. Journal (Water Pollution Control Federation). 2176-2182.

José R. Romero and Jörg Imberger1, Effect of a flood underflow on reservoir water quality: Data and three-dimensionalmodeling. Arch. Hydrobiol. 157 1 1–25 Stuttgart, April 2003.

Kalff, J., 2002. Limnology: inland water ecosystems. 592Prentice Hall, Upper Saddle River, New Jersey, 592 pp.

Kann, J., 2006. *Microcyctis aeruginosa* occurrence in the Klamath River system of southern Oregon and northern California. Yurok Tribe Environmental and Fisheries Programs. Klamath, CA. .

Kearns, K.D. and Hunter, M.D., 2000. Green algal extracellular products regulate antialgal toxin production in a cyanobacterium. Environ.Microbiol. 2, 291-297.

Kling, G.W., Hayhoe, K., Johnson, L.B., Magnuson, J.J., Polasky, S., Robinson, S.K., Shuter, B.J., Wander, M.M., Wuebbles, D.J. and Zak, D.R., 2003. Confronting climate change in the Great Lakes region.

Kling, G., Hayhoe, K., Johnson, L., Magnuson, J., Polasky, S., Robinson, S., Shuter, B., Wander, M., Wuebbles, D. and Zak, D., Confronting Climate Change in the Great Lakes Region: Impacts on our Communities and Ecosystems; Union of Concerned Scientists: Cambridge, Massachusetts and Ecological Society of America: Washington, DC, 2003. There is no corresponding record for this reference.

Komatsu, E., Fukushima, T. and Shiraishi, H., 2006. Modeling of P-dynamics and algal growth in a stratified reservoir—mechanisms of P-cycle in water and interaction between overlying water and sediment. Ecol.Model. 197, 331-349.

LakeMaster, 2007. Lake Minnetonka. Lake Master, WayPoint Technologies, Inc.,59 East Broadway, Little Falls, Minnesota 56345.

Leon, L.F., Lam, D., Schertzer, W. and Swayne, D., 2005. Lake and climate models linkage: a 3-D hydrodynamic contribution. Advances in Geosciences. 4, 57-62.

Leon, L.F., Smith, R.E.H., Hipsey, M.R., Bocaniov, S.A., Higgins, S.N., Hecky, R.E., Antenucci, J.P., Imberger, J.A. and Guildford, S.J., 2011. Application of a 3D hydrodynamic-biological model for seasonal and spatial dynamics of water quality and phytoplankton in Lake Erie. J.Great Lakes Res. 37, 41-53.

Li, H. and Wu, J., 2006. Uncertainty Analysis in Ecological Studies: An Overview. In: Anonymous Scaling and uncertainty analysis in ecology: methods and applications. Springer Verlag, Netherlands, pp. 45-66.

Lindon, M. and Heiskary, S., 2009. Blue-green algal toxin (microcystin) levels in Minnesota lakes. Lake Reserv.Manage. 25, 240-252.

Lopez, C., Dortch, Q., Jewett, E. and Garrison, D., Scientific Assessment of Freshwater Harmful Algal Blooms. Interagency Working Group on Harmful Algal Blooms, Hypoxia, and Human Health of the Joint Subcommittee on Ocean Science and Technology. Washington, DC. .

Loucks, D.P. and van Beek, E., 2005. Water resources systems planning and management: An introduction to methods, models and applications. Studies and Reports in Hydrology, United Nations Educational, Scientific and Cultural Organization. 680UNESCO). UNESCO Publishing, Paris, France., 680 pp.

Lung, W.S., 2001. Water quality modeling for wasteload allocations and TMDLs. Wiley, John Wiley & Sons, Inc., 605 Third Avenue, New York, NY 10158., .

MacKay, M.D., Neale, P.J., Arp, C.D., De Senerpont Domis, Lisette N, Fang, X., Gal, G., Jöhnk, K.D., Kirillin, G., Lenters, J.D. and Litchman, E., 2009. Modeling lakes and reservoirs in the climate system. Limnol.Oceanogr. 54, 2315.

Maier, R.M., Pepper, I.L. and Gerba, C.P., 2008. Environmental Microbiology. Academic Pr, .

Makler-Pick, V., Gal, G., Gorfine, M., Hipsey, M.R. and Carmel, Y., 2011. Sensitivity analysis for complex ecological models-A new approach. Environmental Modelling & Software. 26, 124-134.

Malits, A., Peters, F., Bayer–Giraldi, M., Marrasé, C., Zoppini, A., Guadayol, O. and Alcaraz, M., 2004. Effects of Small-Scale Turbulence on Bacteria: A Matter of Size. Microb.Ecol. 48, 287-299.

Manache, G. and Melching, C.S., 2008. Identification of reliable regression-and correlation-based sensitivity measures for importance ranking of water-quality model parameters. Environmental Modelling & Software. 23, 549-562.

Marti, C.L. and Imberger, J., 2008. Exchange between littoral and pelagic waters in a stratified lake due to wind-induced motions: Lake Kinneret, Israel. Hydrobiologia. 603, 25-51.

Mazur-Marzec, H., Browarczyk-Matusiak, G., Forycka, K., Kobos, J. and Plinski, M., 2010. Morphological, genetic, chemical and ecophysiological characterisation of two *Microcyctis aeruginosa* isolates from the Vistula Lagoon, southern Baltic. Oceanologia. 52, 127-146.

Megard, R.O., 1970. Nutrient abatement, nutrient abatement, and the photosynthetic system of the phytoplankton. Limnol.Res.Center, Univ.Minn.Interim Rep. 7, 210.

Megard, R.O., 1972. Phytoplankton, photosynthesis, and phosphorus in Lake Minnetonka, Minnesota. Limnol.Oceanogr. 68-87.

Melching, C.S. and Bauwens, W., 2001. Uncertainty in Coupled Nonpoint Source and Stream Water-Quality Models. J.Water Resour.Plann.Manage. 127, 403-413.

Menshutkin, V., Rukhovets, L. and Filatov, N., 2014. Ecosystem modeling of freshwater lakes (review): 2. Models of freshwater lake's ecosystem. Water Resour. 41, 32-45.

Miao, Z., Trevisan, M., Capri, E., Padovani, L. and Del Re, A.A.M., 2004. Uncertainty assessment of the model RICEWQ in northern Italy. J.Environ.Qual. 33, 2217-2228.

Miao, Z., Trevisan, M., Capri, E., Padovani, L. and Del Re, A.A.M., 2004. Uncertainty assessment of the model RICEWQ in northern Italy. J.Environ.Qual. 33, 2217-2228.

Miao, Z., Trevisan, M., Capri, E., Padovani, L. and Del Re, A.A.M., 2004. Uncertainty assessment of the model RICEWQ in northern Italy. J.Environ.Qual. 33, 2217-2228.

Mieleitner, J. and Reichert, P., 2008. Modelling functional groups of phytoplankton in three lakes of different trophic state. Ecol.Model. 211, 279-291.

Milly, P.C.D., Betancourt, J., Falkenmark, M., Hirsch, R.M., Kundzewicz, Z.W., Lettenmaier, D.P. and Stouffer, R.J., Stationarity is dead: whither water management? Earth. 4, 20.

Minnehaha Creek Watershed District, 2006. Lake Minnetonka, Yesterday and Today. 18202 Minnetonka Boulevard Deephaven, MN 55391.

Minnehaha Creek Watershed District (MCWD), 2006 Hydrologic Data Monitoring Report. 18202 Minnetonka Boulevard Deephaven, MN 55391. Prepared by Christianson Y.; Carlson J. and Singh U.

Minnesota Climatology Working Group (MCWG), 2013. Historical Climate Data Retrieval.State Climatology Office.DNR Division of Ecological and Water Resources.

Minnesota Department of Natural Resources (MNDNR), 2000-08. Lake Minnetonka Status of the Fishery. 2009, .

Minnesota Department of Natural Resources (MNDNR), 2007. Lake Minnetonka Status of the Fishery. Minnesota Department of Natural Resources, St. Paul, MN. 2009, .

Missaghi, S. and Hondzo, M., 2010. Evaluation and application of a three-dimensional water quality model in a shallow lake with complex morphometry. Ecol.Model. 221, 1512-1525.

Missaghi, S., Hondzo, M. and Melching, C., 2013. Three-Dimensional Lake Water Quality Modeling: Sensitivity and Uncertainty Analyses. J.Environ.Qual.

Mooij, W., De Senerpont Domis, L. and Janse, J., 2009. Linking species-and ecosystem-level impacts of climate change in lakes with a complex and a minimal model. Ecol.Model. 220, 3011-3020.

Moreno-Ostos, E., Cruz-Pizarro, L., Basanta, A. and George, D.G., 2009. The influence of wind-induced mixing on the vertical distribution of buoyant and sinking phytoplankton species. Aquat.Ecol. 43, 271-284.

Moss, B., Kosten, S., Meerhof, M., Battarbee, R., Jeppesen, E., Mazzeo, N., Havens, K., Lacerot, G., Liu, Z. and De Meester, L., 2011. Allied attack: climate change and eutrophication. Inland waters. 1, 101-105.

Muñoz-Carpena, R., Fox, G.A. and Sabbagh, G.J., 2010. Parameter importance and uncertainty in predicting runoff pesticide reduction with filter strips. J.Environ.Qual. 39, 630-641.

Murchie, S.L., 1985. 210Pb Dating and the Recent Geologic History of Crystal Bay, Lake Minnetonka, Minnesota. Limnol.Oceanogr. 1154-1170.

National Oceanic and Atmospheric Administration (NOAA), 2009. Climate Monitoring Products, US Temperature and Precipitation - 2000 and 2005. (http://www.ncdc.noaa.gov/oa/climate/research/2000/CMB_prod_us_tempandprcp.html). 2000, 1.

O'Brien, K.R., Meyer, D.L., Waite, A.M., Ivey, G.N. and Hamilton, D.P., 2004. Disaggregation of *Microcyctis aeruginosa* colonies under turbulent mixing: laboratory experiments in a grid-stirred tank. Hydrobiologia. 519, 143-152.

O'Neil, J., Davis, T., Burford, M.A. and Gobler, C., 2012. The rise of harmful cyanobacteria blooms: The potential roles of eutrophication and climate change. Harmful Algae. 14, 313-334.

O'Connor, B.L. and Hondzo, M., 2008. Dissolved oxygen transfer to sediments by sweep and eject motions in aquatic environments. Limnol.Oceanogr. 53, 566.

Oliver, R.L., Hamilton, D.P., Brookes, J.D. and Ganf, G.G., 2012. Physiology, blooms and prediction of planktonic cyanobacteria. In: Anonymous Ecology of Cyanobacteria II. Springer, pp. 155-194.

Omlin M., Brun R., Reichert P., 2001. Biogeochemical Model of Lake Zurich: Sensitivity, Identifiability and Uncertainty Analysis. Ecol.Model. 141, 105-123.

Osgood, R.A., 1989. An evaluation of the effects of watershed treatment systems on the summertime phosphorus concentration in Metropolitan area lakes. Metropolitan Council of the Twin Cities Area, .

Paerl, H.W. and Huisman, J., 2009. Climate change: a catalyst for global expansion of harmful cyanobacterial blooms. Environmental Microbiology Reports. 1, 27-37.

Paerl, H.W. and Otten, T.G., 2013. Harmful cyanobacterial blooms: causes, consequences, and controls. Microb.Ecol. 1-16.

Paerl, H.W., Fulton, R.S.,3rd, Moisander, P.H. and Dyble, J., 2001. Harmful freshwater algal blooms, with an emphasis on cyanobacteria. ScientificWorldJournal. 1, 76-113.

Painting, S.J. and Forster, R.M., 2013. Marine Ecosystem Connections: essential indicators of healthy, productive and biologically diverse seas. Biogeochemistry. 1-7.

Park, M.H., Chung, I.M., Ahmad, A., Kim, B.H. and Hwang, S.J., 2009. Growth inhibition of unicellular and colonial *Microcyctis* strains (Cyanophyceae) by compounds isolated from rice (Oryza sativa) hulls. Aquat.Bot. 90, 309-314.

Passalacqua, P., Porté-Agel, F., Foufoula-Georgiou, E. and Paola, C., 2006. Application of dynamic subgrid-scale concepts from large-eddy simulation to modeling landscape evolution. Water Resour.Res. 42, W06D11.

PASZTALENIEC, A., 2004. Vertical distribution of dominant cyanobacteria species in three lakes–evidence of tolerance to different turbulence and oxygen conditions. Pol.J.Ecol. 52, 347-351.

PASZTALENIEC, A., 2004. Vertical distribution of dominant cyanobacteria species in three lakes–evidence of tolerance to different turbulence and oxygen conditions. Pol.J.Ecol. 52, 347-351.

Peters, F., Arin, L., Marrasé, C., Berdalet, E. and Sala, M., 2006. Effects of small-scale turbulence on the growth of two diatoms of different size in a phosphorus-limited medium. J.Mar.Syst. 61, 134-148.

PhycoTech, Algae Analysis. 060001-228, PhycoTech, Inc. 620 Broad Street, Suite 100 St. Joseph, MI 49085, USA.

Power, M.E., Brozovic, N., Bode, C. and Zilberman, D., 2005. Spatially explicit tools for understanding and sustaining inland water ecosystems. Frontiers in Ecology and the Environment. 3, 47-55.

Qin, B., 2013. A large-scale biological control experiment to improve water quality in eutrophic Lake Taihu, China. Lake Reserv.Manage. 29, 33-46.

Radcliffe, D., Freer, J. and Schoumans, O., 2009. Diffuse phosphorus models in the United States and Europe: their usages, scales, and uncertainties. J.Environ.Qual. 38, 1956-1967.

Ramstack, J., Fritz, S., Engstrom, D. and Heiskary, S., 2003. The Application of a Diatom-based Transfer Function to Evaluate Regional Water-Quality Trends in Minnessota Since 1970. J.Paleolimnol. 29, 79-94.

Ravalico, J., Maier, H.R., Dandy, G.C., Norton, J. and Croke, B., 2005. A comparison of sensitivity analysis techniques for complex models for environment management.

Regel, R.H., Brookes, J.D., Ganf, G.G. and Griffiths, R.W., 2004. The influence of experimentally generated turbulence on the Mash01 unicellular *Microcyctis aeruginosa* strain. Hydrobiologia. 517, 107-120.

Renaud, S.L., Pick, F.R. and Fortin, N., 2011. Effect of light intensity on the relative dominance of toxigenic and nontoxigenic strains of *Microcyctis aeruginosa* . Appl.Environ.Microbiol. 77, 7016-7022.

Reynolds, C.S., 2006. Ecology of phytoplankton. Cambridge University Press, 32 Avenue of the Americas New York, NY 10013-2473 USA, .

RILEY, M. and STEFAN, H., 1988. MINLAKE: a dynamic lake water quality simulation model. Ecol.Model. 43, 155-182.

Roberts, J.J., Grecay, P.A., Ludsin, S.A., Pothoven, S.A., Vanderploeg, H.A. and Höök, T.O., 2012. Evidence of hypoxic foraging forays by yellow perch (Perca flavescens) and potential consequences for prey consumption. Freshwat.Biol. 57, 922-937.

Robertson, D.M. and Imberger, J., 1994. Lake number, a quantitative indicator of mixing used to estimate changes in dissolved oxygen. Internationale Revue der gesamten Hydrobiologie und Hydrographie. 79, 159-176.

Robson, B. and Hamilton, D., 2002. Three-dimenstional modelling of a *Microcyctis* bloom event in a Western Australian estuary. 24-27.

Robson, B. and Hamilton, D., 2004. Three-dimensional modelling of a *Microcyctis* bloom event in the Swan River estuary, Western Australia. Ecol.Model. 174, 203-222.

Romero, J.R., Antenucci, J.P. and Imberger, J., 2004. One-and three-dimensional biogeochemical simulations of two differing reservoirs. Ecol.Model. 174, 143-160.

Romero, J.R. and Imberger, J., 2003. Effect of a flood underflow on reservoir water quality: Data and three-dimensional modeling. Archiv fur Hydrobiologie. 157, 1-25.

Romero, J.R., Imberger, J., Antenucci, J.P. and Dallimore, C.J., ARMS (Aquatic Real-time Management System): An Automated Decision Support System for Reservoirs, Estuaries and Coastal Zones. Centre for Water Research, University of Western Australia, Crawley, Western Australia, Australia 6009.

Romero, J., Antenucci, J. and Imberger, J., 2004. One-and three-dimensional biogeochemical simulations of two differing reservoirs. Ecol.Model. 174, 143-160.

Salacinska, K., El Serafy, G.Y., Los, F.J. and Blauw, A., 2009. Sensitivity analysis of the two dimensional application of the Generic Ecological Model (GEM) to algal bloom prediction in the North Sea. Ecol.Model. 221, 178-190.

Saloranta, T.M. and Andersen, T., 2007. MyLake--A multi-year lake simulation model code suitable for uncertainty and sensitivity analysis simulations. Ecol.Model. 207, 45-60.

Saltelli, A., 2002. Sensitivity analysis for importance assessment. Risk Analysis. 22, 579-590.

Saltelli, A., 2008. Global sensitivity analysis: the primer. 292 pagesWiley-Interscience, Great Britain, 292 pages pp.

Saltelli, A., Ratto, M., Tarantola, S. and Campolongo, F., 2006. Sensitivity analysis practices: Strategies for model-based inference. Reliab.Eng.Syst.Saf. 91, 1109-1125.

Saltelli, A., Tarantola, S. and Campolongo, F., 2000. Sensitivity analysis as an ingredient of modeling. Statistical Science. 15, 377-395.

Sastri, A.R., Gauthier, J., Juneau, P. and Beisner, B.E., 2014. Biomass and productivity responses of zooplankton communities to experimental thermocline deepening. Limnol.Oceanogr. 59, 1-16.

Scavia, D. and Fahnenstiel, G.L., 1987. Dynamics of Lake Michigan phytoplankton: mechanisms controlling epilimnetic communities. J.Great Lakes Res. 13, 103-120.

Scavia, D., Moody, J.L., Canale, R.O. and Powers, W.F., 1981. Variance estimates for a dynamic eutrophication model of Saginaw Bay, Lake Huron. Water Resour.Res. 17, 1115-1124.

Scavia, D., Powers, W.F., Canale, R.P. and Moody, J.L., 1981. Comparison of first-order error analysis and Monte Carlo simulation in time-dependent lake eutrophication models. Water Resour.Res. 17, 1051-1059.

Schladow, S.G. and Hamilton, D.P., 1997. Prediction of water quality in lakes and reservoirs: Part II-Model calibration, sensitivity analysis and application. Ecol.Model. 96, 111-123.

Schmolke, A., Thorbek, P., DeAngelis, D.L. and Grimm, V., 2010. Ecological models supporting environmental decision making: a strategy for the future. Trends in Ecology & Evolution.

Šejnohová, L., 2008. *Microcyctis* : New Findings in Peptide Production, Taxonomy and Autecology by Cyanobacterium *Microcyctis* . In: Anonymous Institut of Botany, Czech Academy of Sciences, Masarykova univerzita. Ústav botaniky a zoologie. Brno, Czech Republic., .

Sharma, N.K., Mohan, D. and Rai, A.K., 2009. Predicting Phytoplankton Growth and Dynamics in Relation to Physico-chemical Characteristics of Water Body. Water, Air, & Soil Pollution. 202, 325-333.

Shi, X., Yang, L., Wang, F., Xiao, L., Jiang, L., Kong, Z., Gao, G. and Qin, B., 2004. Growth and phosphate uptake kinetics of *Microcyctis aeruginosa* under various environmental conditions. Journal of Environmental Sciences. 16, 288-292.

Shigesada, N. and Okubo, A., 1981. Analysis of the self-shading effect on algal vertical distribution in natural waters. J.Math.Biol. 12, 311-326.

Smith, J.B. and Tirpak, D.A., 1989. The potential effects of global climate change on the United States: Report to Congress. US Environmental Protection Agency, Office of Policy, Planning, and Evaluation, Office of Research and Development, .

Søndergaard, M., Jensen, J.P. and Jeppesen, E., 2003. Role of sediment and internal loading of phosphorus in shallow lakes. Hydrobiologia. 506, 135-145.

Spillman, C., Imberger, J., Hamilton, D., Hipsey, M. and Romero, J., 2007. Modelling the effects of Po River discharge, internal nutrient cycling and hydrodynamics on biogeochemistry of the Northern Adriatic Sea. J.Mar.Syst. 68, 167-200.

Spitael, M.S., 2007. The effects of physical variables on zooplankton distributions in stratified lakes. Ph.D. thesis, University of Minnesota, Minneosta US.

Stefan, H.G. and Fang, X., 1994. Model simulations of dissolved oxygen characteristics of Minnesota lakes: Past and future. Environ.Manage. 18, 73-92.

Stefan, H.G., Fang, X. and Eaton, J.G., 2001. Simulated fish habitat changes in North American lakes in response to projected climate warming. Trans.Am.Fish.Soc. 130, 459-477.

Stein, G., 1971. Lake Minnetonka: Historical perspectives of an urban lake. University of Minnesota, Minneapolis, MN.

The Intergovernmental Panel on Climate Change Data Distribution Center (DDC), 17 June 2013. http://www.ipcc-data.org/ddc_change_field.html. IPCC. 1/10/2014, 1.

Trolle, D., Skovgaard, H. and Jeppesen, E., 2008. The Water Framework Directive: Setting the phosphorus loading target for a deep lake in Denmark using the 1D lake ecosystem model DYRESM–CAEDYM. Ecol.Model. 219, 138–152.

Trolle, D., Hamilton, D.P., Pilditch, C.A., Duggan, I.C. and Jeppesen, E., 2011. Predicting the effects of climate change on trophic status of three morphologically varying lakes: Implications for lake restoration and management. Environmental Modelling & Software. 26, 354-370.

Turley, M.C. and Ford, E.D., 2009. Definition and calculation of uncertainty in ecological process models. Ecol.Model. 220, 1968-1983.

US Army Corps of Engineers, St. Paul District Hydrology Section, Minnehaha Creek Watershed Planning Study-Phase I. St. Paul District Hydrology Section, 190 East Fifthe Street, St. Paul, MN 55101-1638.

Van Griensven, A. and Meixner, T., 2007. A global and efficient multi-objective auto-calibration and uncertainty estimation method for water quality catchment models. J.Hydroinf. 9, 277-291.

Van Griensven, A., Meixner, T., Grunwald, S., Bishop, T., Diluzio, M. and Srinivasan, R., 2006. A global sensitivity analysis tool for the parameters of multi-variable catchment models. Journal of Hydrology. 324, 10-23.

Varela, R.A., Cruzado, A., Tintore, J. and Garda Ladona, E., 1992. Modelling the deep-chlorophyll maximum: A coupled physical-biological approach. J.Mar.Res. 50, 441-463.

Visser, P., Ibelings, B., Mur, L. and Walsby, A., 2005. The ecophysiology of the harmful cyanobacterium *Microcyctis* . Harmful Cyanobacteria. 109-142.

Wallace, B.B., Bailey, M.C. and Hamilton, D.P., 2000. Simulation of vertical position of buoyancy regulating *Microcyctis aeruginosa* in a shallow eutrophic lake. Aquatic Sciences-Research Across Boundaries. 62, 320-333.

Wang, C., Kong, H., He, S., Zheng, X. and Li, C., 2010. The inverse correlation between growth rate and cell carbohydrate content of *Microcyctis aeruginosa* . J.Appl.Phycol. 22, 105-107.

Wang, P., Shen, H. and Xie, P., 2012. Can Hydrodynamics Change Phosphorus Strategies of Diatoms?-Nutrient Levels and Diatom Blooms in Lotic and Lentic Ecosystems. Microb.Ecol. 63, 369-382.

Wetzel, R., 2001. Limnology, 3 E. Lake and River Ecosystems. 850Academic Press, 525 R Street. Surre 1900. San Dtego, Csllfornta 92101.4495, 1JSA, 850 pp.

Whitehead, P., Wilby, R., Battarbee, R., Kernan, M. and Wade, A.J., 2009. A review of the potential impacts of climate change on surface water quality. Hydrological Sciences Journal. 54, 101-123.

Whitton, B.A. and Potts, M., 2000. The ecology of cyanobacteria: their diversity in time and space. 669Kluwer Academic Publishers, Netherlands, 669 pp.

Wilson, A.E., Wilson, W.A. and Hay, M.E., 2006. Intraspecific variation in growth and morphology of the bloom-forming cyanobacterium, *Microcyctis aeruginosa* . Appl.Environ.Microbiol.

Wojciechowska, W., Poniewozik, M. and Pasztaleniec, A., 2004. Vertical distribution of dominant cyanobacteria species in three lakes-Evidence of tolerance to different turbulence and oxygen conditions. Pol.J.Ecol. 52, 347-351.

Wu, J., Jones, K.B., Li, H. and Loucks, O.L., 2006. Scaling and uncertainty analysis in ecology: methods and applications. 351 pagesSpringer Verlag, Netherlands, 351 pages pp.

Wu, T., Qin, B., Zhu, G., Luo, L., Ding, Y. and Bian, G., 2013. Dynamics of cyanobacterial bloom formation during short-term hydrodynamic fluctuation in a large shallow, eutrophic, and wind-exposed Lake Taihu, China. Environmental Science and Pollution Research. 1-11.

Wu, X. and Kong, F., 2009. Effects of Light and Wind Speed on the Vertical Distribution of *Microcyctis aeruginosa* Colonies of Different Sizes during a Summer Bloom. Int.Rev.Hydrobiol. 94, 258-266.

Wu, X., Kong, F., Chen, Y., Qian, X., Zhang, L., Yu, Y., Zhang, M. and Xing, P., 2010. Horizontal distribution and transport processes of bloom-forming *Microcyctis* in a large shallow lake (Taihu, China). Limnologica-Ecology and Management of Inland Waters. 40, 8-15.

Xiao-li, S., Liu-yan, Y., Feng-ping, W., Lin, X., Li-juan, J., Zhi-ming, K., Guang, G. and Bo-qiang, Q., 2004. Growth and phosphate uptake kinetics of *Microcyctis aeruginosa* under various environmental conditions. Journal of Environmental Sciences. 16, 288-292.

Yajima, H. and Choi, J., 2013. Changes in phytoplankton biomass due to diversion of an inflow into the Urayama Reservoir. Ecol.Eng. 58, 180-191.

Zhang, W. and Arhonditsis, G.B., 2009. A Bayesian hierarchical framework for calibrating aquatic biogeochemical models. Ecol.Model. 220, 2142-2161.

Zurawell, R., Chen, H., Burke, J. and Prepas, E., 2005. Hepatotoxic cyanobacteria: a review of the biological importance of microcystins in freshwater environments. Journal of Toxicology and Environmental Health Part B: Critical Reviews. 8, 1-37.